Sol-Gel Coatings Containing Inorganic and Organic Compounds: Studies using Rutherford Backscattering Spectrometry and UV-VIS Spectroscopy

by

Carol Lynn Schutte

Submitted to the Department of Materials Science and Engineering In Partial Fulfillment of the Requirement for the Degree of Doctor of Philosophy

at the

Massachusetts Institute of Technology

September 1990

© Massachusetts Institute of Technology 1990
All rights reserved

Signature of Author _____
Department of Materials Science and Engineering
August 10, 1990

Certified by _____
George M. Whitesides
Professor of Chemistry, Harvard University
Thesis Supervisor

Certified by _____
Frederick J. McGarry
Professor of Materials Science and Engineering
Thesis Supervisor

Accepted by _____
Linn W. Hobbs, Chairman
Departmental Graduate Committee
Department of Materials Science and Engineering

MASSACHUSETTS INSTITUTE OF TECHNOLOGY
NOV 09 1990
LIBRARIES
ARCHIVES

Sol-Gel Coatings Containing Inorganic and Organic Compounds: Studies using Rutherford Backscattering Spectrometry and UV-VIS Spectroscopy

by

Carol Lynn Schutte

Submitted to the Department of Materials Science and Engineering on August 10, 1990 in partial fulfillment of the requirements for the Degree of Doctor of Philosophy in Materials Science

Abstract

An initial comparison of the depth profile of iron in a multilayer system analyzed by Rutherford Backscattering Spectrometry (RBS) and by Cross-Sectional Transmission Electron Microscopy (XTEM) demonstrated that RBS is suitable for the analysis of multilayer coatings. RBS was applied to the study of the diffusion of cesium in sol-gel films and to the loss of halide from these films on heating. The diffusion and/or infiltration of cesium ion into an SiO_2 gel, at room temperature, depends on the stage of the gel-to-glass transformation of the film. At elevated temperature ($\geq$ 750 °C) however, the rate of detectable diffusion of cesium was independent of the thermal history of the undoped layer over the range of temperatures used in treating these layers (200-800 °C). The rates of loss of halide under air and argon atmospheres were very similar. This result suggests a non-oxidative mechanism for the loss of halide. The relative rate of loss of halide at a particular temperature follows the qualitative order: LiI > LiBr $\simeq$ LiCl > NaI > NaBr > KI $\simeq$ KBr $\simeq$ NaCl. This order correlates with the vapor pressures of the salts and the ΔG of formation of the hydrogen halide from reaction of the halide salt with water, suggesting that volatilization of the salt and/or the hydrogen halide is the mechanism for loss of halide from sol-gel coatings.

A related study examined the thermal and oxidative stability of organic chromophores based on the 2,4-dinitro group, in sol-gel coatings under a variety of coating conditions in both air and argon. The sol-gel matrix has no significant effect on the stability of the chromophore.

Thesis Supervisors: Professor George M. Whitesides

Title: Professor of Chemistry, Harvard University

and

Professor Frederick J. McGarry

Title: Professor of Materials Science and Engineering

We shall not cease from exploration
And the end of all our exploring
will be to arrive where we started
And know the place for the first time.

T. S. Eliot

TABLE OF CONTENTS

Title Page 1

Abstract 2

Table of Contents 4

List of Figures 6

List of Tables 13

Acknowledgements 14

Goals of Thesis 15

Chapter 1: Analysis of Depth Profiles of Sol-Gel Derived Multilayer Coatings by Rutherford Backscattering Spectrometry and by Cross-Sectional Transmission Electron Microscopy 17

Chapter 2: Behavior of Cations - The Diffusion of Cesium Ion in SiO_2 Films Derived From Sol-Gel Precursors 37

Chapter 3: Behavior of Anions - The Loss of Halide from Sol-Gel Films on Heating Does Not Involve Oxidation 65

Chapter 4: Organic Modification of Sol-Gel Materials: An Overview of the Literature 91

Chapter 5: The Thermal and Oxidative Stability of 2,4-Dinitroaniline in Sol-Gel Derived Coatings 104

Appendix 1: Measurement of Indices of Refraction and Thicknesses of SiO_2 Gel Coatings by Optical Ellipsometry 127

Appendix 2: Calculation of the Apparent Diffusion Coefficient of Cesium in SiO_2 Gels 131

Bibliography 135

Biographical Note 140

Recommendations for Future Work 142

List of Figure Captions:

Figure 1: a) Measured and simulated depth profiles of iron for a multilayer coating (derived from alternating coatings of hydrolyzed 1,1'-bis(triethoxysilyl)ferrocene and hydrolyzed TEOS). The depth profile of iron measured by RBS (●) is compared with a simulated depth profile with neither detector resolution nor straggling effects (-), and a simulated depth profile of iron with energy resolution limitation from the detector and energy straggling taken into account (○). Thicknesses of layers are measured at half of the peak height in the RBS depth profile of iron. b) Imaged layers from XTEM analysis for the same multilayer coating as in (a). 22

Figure 2: The depth profiles of iron for a multilayer which has been, heated at 350 °C and 500 °C for one hour each (●), and heated six additional times to 500 °C for six hours each (◇).28

Figure 3: RBS spectrum for a three-layer coating derived from alternating coatings derived from hydrolyzed 1,1'-bis(triethoxysilyl)ferrocene and hydrolyzed TEOS on a silicon substrate. 32

Figure 4: Depth profiles of iron for the multilayer coating (analyzed in Figure 1) with five layers measured from two different regions on the sample, in order to test the reproducibility of data. 34

Figure 5: Scheme describing the coating and thermal treatment of samples used to study the relative rates of diffusion of cesium through undoped SiO_2 coatings that have been thermally treated to different extents along the gel-to-glass transition. The SiO_2 coatings were deposited and heated to either 200, 400, 600, or 800 °C for 2h each. (The temperature-time profiles used are indicated schematically in the Figure in the upper-right corner.) The samples were cooled, and coated with the cesium containing layer. After the layer doped with cesium was applied, the samples were heated and the diffusion of cesium was monitored by RBS. Estimated depth profiles of cesium and oxygen are included to illustrate how the diffusion of cesium into the undoped SiO_2 layer is visualized by RBS analysis. 43

Figure 6: Plot of the index of refraction (n, O) and thickness (d, ▲) obtained from ellipsometry of the SiO_2 films, as a function of the maximum temperature to which they were heated in air. The temperature profile in the heating is summarized in Figure 1. The lines are included only to guide the eye. 46

Figure 7: Loss of weight from TEOS derived SiO_2 as a function of temperature under nitrogen. The temperature of the sample increased at 10 °C/min. 49

Figure 8: IR spectra of an SiO_2 coating on a KBr plate, obtained for samples prepared at: A) room temperature (28 °C), and after heating to: B) 200, C) 400, and D) 600 °C. 50

Figure 9: Representative RBS data for; a) the silicon substrate with no coating; b) a silicon substrate with an SiO_2 film; and c) a silicon substrate with an SiO_2 film under a cesium chloride containing SiO_2 film. 54

Figure 10: Depth profiles for cesium in the two-layer systems summarized in Figure 1. The origin of the distance scale is arbitrarily set at the interface between the original two silicate films: that on the left (-300 - 0 nm) was doped with the cesium; that on the right (0 - 200 nm) was undoped. The top four figures show the intensity of the cesium signal as a function of depth. The temperature at which the undoped layer was heated before applying the cesium-doped layer is indicated on each (200, 400, 600, and 800 °C). Each box contains three traces, corresponding to the temperature at which the two-film system was heated to effect cesium diffusion: no heat (20 °C,○); 750 °C/2h (◇); 800 °C/2h (▲).

The bottom traces are representative oxygen profiles for samples having both silica films, before and after heating as indicated (○,▲). This profile defines the aggregate thickness of the silica layer, and demonstrates that cesium does not diffuse into the silicon substrate under our experimental conditions. 56

Figure 11: Plot of D_{Cs} (cm^2/sec) at 750 and 800 °C for samples previously heated to 200 °C (●), 400 °C (◆), 600 °C (■), and 800 °C (▲). 58

Figure 12: Depth profiles of oxygen (O) and cesium (◇) from unsmoothed data (a: best case and b: worst case). The data in 12a are for the SiO_2 undercoat previously heated to 600 °C, and in 12b are for the SiO_2 undercoat previously heated to 800 °C. Both samples had no thermal treatment after the cesium chloride doped TEOS was applied. 64

Figure 13: Representative depth profiles of iodide and oxygen from Li^+I^- doped SiO_2 and of vanadium and oxygen from $NH_4^+VO_3^-$ doped SiO_2 as a function of temperature of thermal treatment. 70

Figure 14: Plot of the normalized content of sodium halide (I^-, Br^-, and Cl^-), determined by RBS, as a function of thermal treatment (held at each temperature for 3h) under both air and argon. Multiple points indicate measurements from multiple samples. The points are shown displaced from the nominal temperatures to avoid overlap. 72

Figure 15: Plot of the relative loss of Br^- (LiBr ●, KBr △), I^- (LiI ○, KI ◆), Cl^- (LiCl ▲), $\underline{Sb}F_6^-$ ($HSbF_6$ ■), and $\underline{V}O_3^-$ (NH_4VO_3 □) determined by RBS, as a function of temperature of thermal treatment (held at each temperature for 3h) under air and under argon. The points are shown displaced from the nominal temperatures to avoid overlap. 75

Figure 16: Plot of the estimated temperature at which half of the halide would be lost ($T_{1/2}$, °C) following the protocol in the research versus the vapor pressure of the salt at 1000 °C. The error bars represent error in the calculation of the least squares line for each salt. 77

Figure 17: Plot of the derivative of the AES signal intensity versus kinetic energy (eV) of the Auger transition for a NaI/SiO_2 sample before and after thermal treatment. 80

Figure 18: Plot of the estimated temperature at which half of the halide would be lost ($T_{1/2}$, °C) following the protocol in the research versus the ΔG of formation of the hydrogen halide. The error bars represent error in the calculation of the least squares line for each salt. 84

Figure 19: Representative RBS spectrum obtained for a coating of LiI-doped SiO_2 on a silicon substrate. 89

Figure 20: Schematic illustrations of structures that incorporate the arylsiloxane moiety into (or onto) a silicate matrix. The material indicated by ▬ was prepared by hydrolysis of 1. The material indicated by ▭ was prepared by cohydrolysis of 1 and TEOS or by physically mixing 2,4-dinitroaniline with previously hydrolyzed TEOS (mole ratio 1:144 for formulations forming dense SiO_2, 1:31 for porous SiO_2). ▭ is unmodified SiO_2, prepared from TEOS alone, and ▭ is the sapphire substrate (crystalline

Al_2O_3). The porous coating of SiO_2 consists of spherical silica particles.[92] 111

Figure 21: Representative RBS spectra of: the silicon substrate alone; an SiO_2 coating on the silicon substrate; and the sapphire (α-Al_2O_3) substrate alone. 119

Figure 22: Survey transmission UV-VIS spectra of the alumina substrate, the alumina substrate with SiO_2 coatings not containing chromophore, and alumina substrates bearing the chromophore in the configurations shown in Figure 20. 122

Figure 23: UV-VIS spectra and a plot of relative absorbance of 1 (Figure 20, Structure A) as a function of temperature of thermal treatment in air. 124

Figure 24: Relative absorbance at 350 nm of incorporated 2,4-dinitroaniline in sol-gel coatings as a function of temperature of thermal treatment in air and under argon. Samples were held at each temperature for 2 hours. The relative absorbance is the ratio of the measured absorbance to that after an initial treatment at 100°C for 5 min. The symbols denote chromophore: alone (○), over porous SiO_2 (●), with a dense SiO_2 overcoat (△), with a porous SiO_2 overcoat (▲), copolymerized in dense SiO_2 (□), copolymerized in porous SiO_2 (■), physically mixed in dense SiO_2 (◇), and physically mixed in porous SiO_2 (◆). The points are shown displaced from the nominal temperatures to avoid overlap.

The data points represent the average measurement of two samples, the error bars their range. 126

Figure 25: Plot of ln of concentration (atoms/cm^3) versus x^2 (cm^2) for a gel preheated to 800 °C and heated to 750 °C after Cs was applied. 134

List of Tables

Table I. Thicknesses of Layers of a Multilayer Coating as Measured by RBS and XTEM. 25

Acknowledgments: I owe many thanks to many people. These folks are: George Whitesides, Professor McGarry, Professor Greg Ferguson, Professor Mike Rubner, my family, Sharon Melpolder of Eastman Kodak Co., Nancy, Beth, Katie, Tom, and Rena, and the incredibly competent Giselle Weiss. I extend special thanks to Patrick Smith, Dr. Kevin Williams, John Chervinski and Yuan Lu for all of their assistance. Thanks to Rajeeva, Lou, Catherine, Kim, Uwe, and Walter for many inspiring and intellectual discussions while on pilgrimage to Coffee Connection.

I acknowledge financial support from the American Association of University Women through a Dissertation Fellowship (1988-1989).

Professor Roy Gordon and Jianhua Hu assisted in ellipsometric analyses, and E. L. Shaw, MIT, performed the Auger analyses.

Goals of Thesis:

The first part of this thesis addressed the suitability of RBS for the analysis of scl-gel coatings. The comparison of the depth profiles of a multilayer coating using both RBS and XTEM tested the accuracy of the RBS results. Furthermore, this thesis addressed the study of dynamic processes in the sol-gel films using RBS; these processes were the diffusion of cesium in the gel and the loss of halide from the gel. The relative diffusion of cesium as a function of the degree of transformation in the gel-to-glass transition was the focus of the study on the diffusion of cesium. Coatings of TEOS were heated to 200, 400, 600, and 800°C and characterized by IR, TGA, and ellipsometry, to determine their degree of transformation along the gel-to-glass transition. A solution of TEOS doped with cesium chloride was coated over these previously heated gel samples. The depth profile of cesium, measured by RBS, revealed both the room temperature diffusion and/or infiltration and the high temperature (>750 °C) diffusion of cesium into the undoped gel.

In order to determine the mechanism of the loss of halide from halide-doped TEOS coatings, this thesis focused on the relative rate of loss of halides under air and under argon. RBS measurements of the halide contents of iodide, bromide, and chloride (from salts with counterions of lithium, sodium, and potassium), as a function of the thermal history and

atmosphere (oxidative and non-oxidative) of heating, yielded the relative rates of loss of the halides.

The last section of this thesis focused on the study of the relative thermal/oxidative stability of the organic dye 2,4-dinitro aniline in the sol-gel network, incorporated both covalently and non-covalently. The relative stability of the dye, measured by the visible absorption of the dye, was studied under a variety of coating conditions under air and under argon.

Analysis of Depth Profiles of Sol-Gel Derived Multilayer Coatings by Rutherford Backscattering Spectrometry and by Cross-Sectional Transmission Electron Microscopy‡

Abstract: This paper describes the preparation and compositional analysis of multilayer thin-film coatings prepared using sol-gel techniques. Alternate layers were labeled with an iron tag, derived from hydrolyzed 1,1'-bis(triethoxysilyl)ferrocene. Iron-free layers were composed of SiO_2 derived from hydrolyzed tetraethylorthosilicate (TEOS). Analyses of these systems were based on Rutherford Backscattering Spectrometry (RBS) and Cross-Sectional Transmission Electron Microscopy (XTEM). The depth profile of iron, measured by RBS, yielded thicknesses (1,000 - 1,600 Å) for the individual layers that could be verified independently by XTEM.

Introduction: Multilayer ceramic coatings are important in applications in optics[1] and electronics.[2] These and related applications require thin, defect-free layers.[2] Sol-gel technology, combined with spin or dip coating, is an excellent method for the preparation of thin-film and

---

‡ Supported in part by the National Science Foundation (CHE-88-12709). The Cambridge Accelerator for Materials Science was purchased through a DARPA/URI grant and is housed in the Harvard University Materials Research Laboratory, an NSF-funded facility (DMR-86-14003).

multilayer ceramic coatings. The chemical composition of the precursors and the processing conditions control the properties of the final film, and it is relatively straightforward to control the porosity, composition, and index of refraction of these films.[3-8] Multilayers made by the sol-gel route include anti-reflective coatings[9,10,11-15] and wavelength-selective reflectors.[16-18]

In this paper, we address the question of whether thin multilayers (<25 μm thick)[2] of alternating chemical composition of inorganic (SiO_2) and organometallic layers can be produced by the sol-gel route without intermixing of the layers. We present the preparation and characterization of a model multilayer system using sol-gel suspensions derived from solutions of hydrolyzed 1,1'-bis(triethoxysilyl)ferrocene,[19] and from hydrolyzed tetraethylorthosilicate (TEOS). We employed RBS[20] to measure the depth profile of iron in the multilayer system. This technique has previously proven useful in studying the depth profile and diffusion of iron in fused silica glass,[21] and in studying layered systems in combination with TEM.[22] One objective of this work was to demonstrate the usefulness of RBS as a non-destructive technique, complementary to spectroscopic ellipsometry,[23,24] for the analysis of multilayer ceramic coatings.

We verified the accuracy of the thicknesses of iron and iron-free layers, as measured by RBS, by independent examination using cross-sectional transmission electron

microscopy (XTEM). We have also explored the extent of intermixing of the iron-containing layer with the iron-free layer during heating by monitoring the depth profile of iron by RBS as a function of thermal treatment.

The question of diffusion of components in gel structures is of general interest,[25,26] and specifically relevant to thin-film structures requiring abrupt changes in composition.[2] RBS has higher sensitivity to heavy elements than to light ones. The depth resolution of RBS is approximately 21 keV (~ 90 Å) at the surface of the sample due to the limits of the detector for the system we have studied. It is therefore an excellent technique for studying changes in the depth profile of iron as a measure of the diffusion of the iron species.

The limits to the resolution of RBS are set by the detector and by energy straggling. Detectors used for RBS analysis typically are surface-barrier, solid state nuclear particle detectors. When a scattered helium ion passes through the detector, it creates electron-hole pairs in the depletion layer of the inverse Schottky barrier diode. These electron-hole pairs result in a voltage pulse, the height of which is proportional to the energy of the incident helium ion through the number of electron-hole pairs generated. Statistical fluctuations in the number of the electron-hole pairs generated from the scattered helium ions in the detector limit the resolution in the measurement of energy of the incident particle.

Statistical fluctuations in the inelastic interactions between the Helium beam and the electrons in the sample cause energy straggling as the beam particle passes through the sample. The Bohr value of energy straggling,[27] Ω_B^2 (eV^2), is given by eq 1.

$$\Omega_B^2 = 4\pi Z_1^2 e^4 N Z_2 d \qquad (1)$$

Here Z_1 is the atomic number of the ion in the ion beam; e ($[eV\ Å]^{1/2}$), the charge of an electron; N ($Å^{-3}$), the atomic density; Z_2, the atomic number of the atoms in the sample; and d (Å), the thickness. For a sample with a mixture of atoms, as in our sample, the average atomic number (7.25 ± 1.0 based on 70 % ± 9 % $C_{10}H_8FeSi_2O_3$ and 30 % ± 6 % SiO_2), based on a mass average, is used in equation 1. Straggling increases with depth; thus, peaks broaden from straggling with increasing depth into the sample. The theoretical Bohr value for energy straggling for our sample using a helium ion beam is 7.4 keV (30 Å) at 6000 Å.

Results and Discussion: Figure 1 presents three depth profiles of iron. Along with the measured depth profile of iron for a multilayer coating (derived from alternating coatings of hydrolyzed 1,1'-bis(triethoxysilyl)ferrocene and hydrolyzed TEOS) are two additional depth profiles: a simulated depth profile with neither detector resolution nor straggling effects, and a simulated depth profile of iron with energy resolution limitation from the detector (~ 90 Å) and energy straggling (the Bohr value calculated at the depth

Figure 1: a) Measured and simulated depth profiles of iron for a multilayer coating (derived from alternating coatings of hydrolyzed 1,1'-bis(triethoxysilyl)ferrocene and hydrolyzed TEOS). The depth profile of iron measured by RBS (●) is compared with a simulated depth profile with neither detector resolution nor straggling effects (-), and a simulated depth profile of iron with energy resolution limitation from the detector and energy straggling taken into account (○). Thicknesses of layers are measured at half of the peak height in the RBS depth profile of iron. b) Imaged layers from XTEM analysis for the same multilayer coating as in (a).

a)

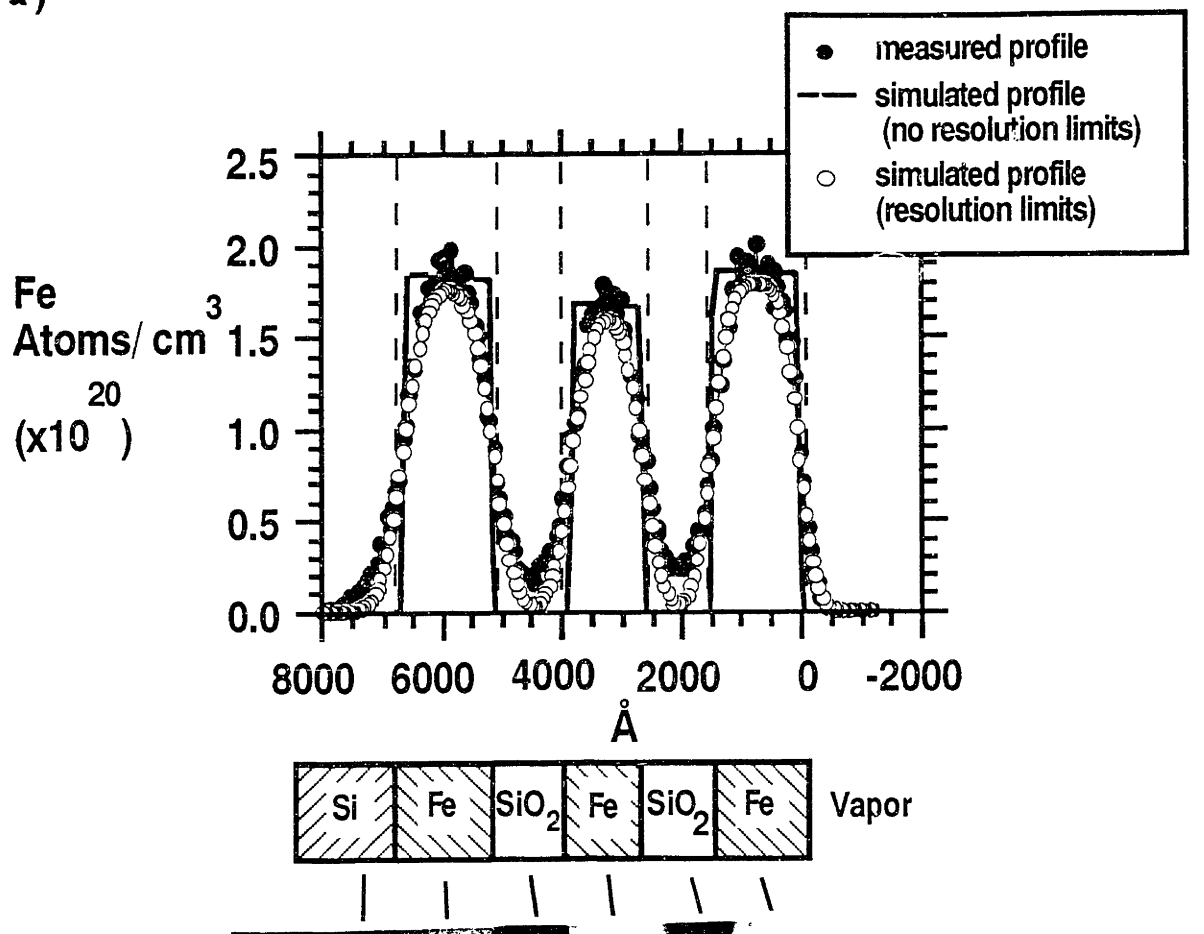
measured profile
simulated profile (no resolution limits)
simulated profile (resolution limits)
Fe Atoms/ cm 3
(x10 20)
2.5
2.0
1.5
1.0
0.5
0.0
8000 6000 4000 2000 0 -2000
Å
Si
Fe
SiO2
Fe
SiO2
Fe
Vapor

b)

of each datum point using eq. 1) taken into account. This figure also presents a cross sectional view by XTEM of the layers of the same sample. We simulated RBS spectra using the program "RUMP"‡ based on values of the measured thicknesses from the RBS analysis and calculated the depth profiles of iron from the RBS spectra using the program "Spectrum Analysis".† The simulated profile of iron without resolution limits has a flat compositional distribution within the iron-containing layers; this profile contrasts with the other two profiles where the detector and straggling effects transform the step-function distribution of iron into peaks resembling gaussian distributions (The areas of these peaks are approximately the same). The simulated profile with limitations of the detector (~ 90 Å) and straggling (calculated from the Bohr value from eq. 1) taken into account is almost superimposable on the experimental data. Thus, it appears that the differential broadening of the deeper peaks is due to energy straggling.

The thicknesses determined from these techniques are compared in Table I, and within experimental error, they are the same. We conclude that RBS is an accurate technique for

---

‡ RUMP is a FORTRAN program written by Larry Doolittle containing algorithms from Chu, W. K.; Mayer, J. W.; Nicolet, M. A. *Backscattering Spectrometry*; Academic Press: New York, 1977.

† SA, written by Patrick M. Smith, Division of Applied Sciences, Harvard University, is a FORTRAN program based on algorithms from Chu, W. K.; Mayer, J. W.; Nicolet, M. A. *Backscattering Spectrometry*; Academic Press: New York, 1977.

the non-destructive analysis of sol-gel derived multilayer coatings.

In the profiles, the iron peaks appear shorter and broader with increasing depth into the sample. Some degree of broadening for deeper layers is expected from energy straggling.[27] Additional broadening could be due to interdiffusion of the iron species with SiO_2 between the deeper layers which have been through more thermal treatments than those layers at the surface. To test this hypothesis, and to test the validity of the simulated spectra in Figure 1, a multilayer coating consisting of three layers was analyzed by RBS, heated six times to 500 °C for six hours each, and analyzed by RBS again. These results are presented in Figure 2. The indistinguishable depth profiles indicate that no detectable (± 200 Å) diffusion occurred during the thermal treatments.

Conclusions: We have prepared multilayers, with modulated composition, derived from the hydrolyzed sol-gel precursors 1,1'-bis(triethoxysilyl)ferrocene and TEOS. These multilayers have sharp interfaces and exhibit no detectable intermixing of the layers after coating.

RBS is a quick and non-destructive tool for the analysis of heavy-atom tagged multilayer systems obtained by sol-gel methods. The iron profile was easily measured by RBS in the ferrocenyl/SiO_2 system for up to five layers (~6,700 Å). Thicknesses were in good agreement with values determined by XTEM. RBS exhibits straggling which broadens the peaks as a

Table I. Thicknesses of Layers of a Multilayer Coating as Measured by RBS and XTEM.

		layer thickness (Å)	
		RBS	XTEM
Vapor			
↑	Fe	1,600 ± 200	1,660 ± 170
	SiO_2	1,050 ± 200	1,070 ± 80
	Fe	1,450 ± 200	1,780 ± 160
	SiO_2	1,200 ± 200	1,130 ± 70
	Fe	1,600 ± 200	1,800 ± 110
Si substrate			

function of depth.

In this system, interdiffusion of species in the iron-containing layer with species in the iron-free layer (SiO_2) after thermal treatment was not detected by RBS.

Experimental Section

Materials: Ferrocene was purchased from Eastman Kodak Company. n-Butyllithium, tetramethylethylenediamine and p-toluene sulfonic acid were purchased from Aldrich. Triethoxychlorosilane was purchased from Petrarch. Hexane was distilled from NaH. n-Butyllithium was titrated with 2,5-dimethoxybenzyl alcohol (Aldrich) immediately before its use.[28] Ethyl ether was purchased from Mallinckrodt. All reagents were used as received unless noted.

1,1'-Bis(triethoxysilyl)ferrocene was synthesized by the procedure of Wrighton and coworkers[19] in 18 % yield; ^{1}HNMR (chloroform-d_1, 250 MHz, 25 ^{o}C) δ1.25 (t, 18H), 3.88 (q, 12H), 4.22 (s, 4H), 4.41 (s, 4H).

Hydrolysis of 1,1'Bis(triethoxysilyl) ferrocene: Distilled water (0.63 mL, 33 mmol), was added to a solution of 1,1'-bis(triethoxysilyl)ferrocene (1.41 g, 2.90 mmol, 16.5 mmoL of SiOR) in ethanol (14 mL) with p-toluenesulfonic acid monohydrate (0.01 g, 0.05 mmol) as catalyst. The solution was allowed to stir overnight prior to coating. "Thick"

Figure 2: The depth profiles of iron for a multilayer which has been, heated at 350 °C and 500 °C for one hour each (●), and heated six additional times to 500 °C for six hours each (◇).

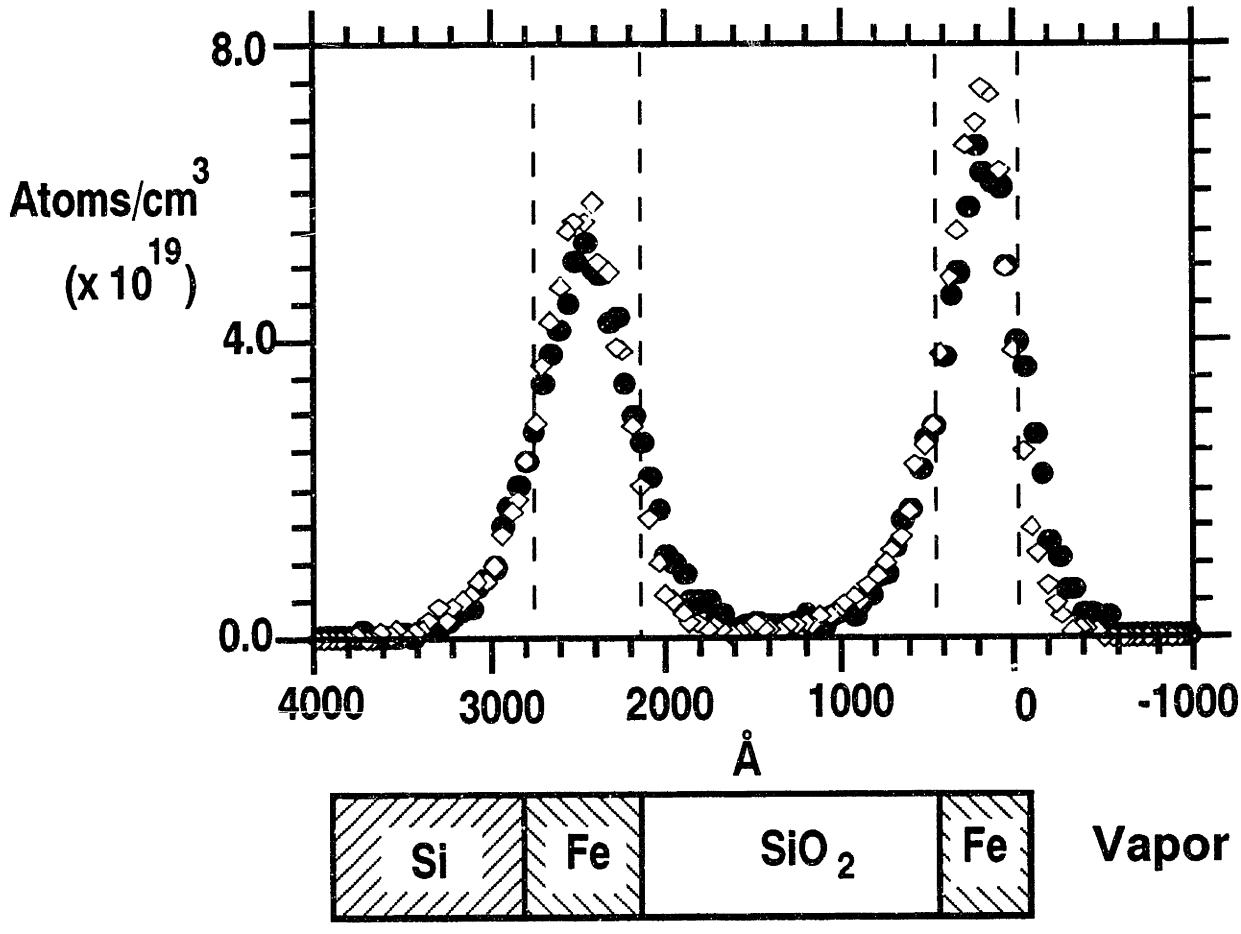
8.0
4.0
0.0
Atoms/cm3
(x 10^19)
4000
3000
2000
1000
0
-1000
Å
Si
Fe
SiO2
Fe
Vapor

coatings (Figure 1) were made from a 10% (weight of 1,1'bis(triethoxysilyl)ferrocene/volume) solution, and "thinner" coatings (Figure 2) were made from a 1% (w/v) solution.

Pre-hydrolyzed TEOS: A solution containing tetraethylorthosilicate (TEOS) (43 mL, 193 mmol of Si), ethanol (43 mL), and aq HCl (14 mL of 0.15 M acid) was heated at 60 °C for 3 h. The solution was cooled and filtered through a 0.2 μm filter, then diluted with additional ethanol (86 mL), and stored in a freezer (-8 °C).

Preparation of Samples: We coated a silicon <100> wafer by pipetting enough solution (~ 3 mL) to cover the wafer, and spinning the substrate at 1500 rpm for 2 min on a Headway Model PWM 101ECR790 spin-coater. The samples were heated in a Fisher Scientific Isotemp Programmable Ashing Furnace Model 497 at 1 °C/min to 350°C, held for 1 h, heated 1°C/min to 500°C, held for 1 h, and cooled at 1 °C/min to 30 °C. Coatings were rinsed with ethyl ether prior to applying the subsequent layer.

RBS Analysis: RBS spectra were obtained using the CAMS (Cambridge Accelerator for Materials Science) facility. The CAMS consists of a tandetron accelerator that supplied a 2-MeV He^+ beam. Backscattered particles were detected at 176°, relative to the incoming beam, with a 150-mm^2 silicon surface barrier detector coupled to a multichannel analyzer and placed about 3 inches from the sample. Typical times for the

acquisition of data were 10-15 min. Depth profiles of iron were calculated using "Spectrum Analysis".‡

Figure 3 shows a representative RBS spectrum[20] of the three-layer coating whose depth profile of iron is presented in Figure 2. At highest energy (~ channels 800-700) in the plot of number of counts versus channel (linearly related to energy) were the signals from iron in the two iron-containing layers. Iron in the layer at the surface came at highest energy. The signal for silicon in the multilayer coating (~ channel 575) was lower in intensity than that for silicon in the substrate (~ channel 475) because it was "diluted" by the other components in the multilayer coating. The oxygen signal (~ channel 350) came at a lower energy than that for silicon because the mass of oxygen is lower than the mass of silicon.

Figure 4 shows the depth profiles of iron measured at two different regions on the sample analyzed in Figure 1. The reproducibility of the data showed that no detectable variation of layer thicknesses existed in the sample within the resolution of RBS.

The diameter of the ion beam was 1 mm. Regions where the beam hit the sample exhibited a shiny spot, as did the silicon substrate with no coating. These spots are attributed

---

‡ SA, written by Patrick M. Smith, Division of Applied Sciences, Harvard University, is a FORTRAN program based on algorithms from Chu, W. K.; Mayer, J. W.; Nicolet, M. A. *Backscattering Spectrometry*; Academic Press: New York, 1977.

Figure 3: RBS spectrum for a three-layer coating derived from alternating coatings derived from hydrolyzed 1,1'-bis(triethoxysilyl)ferrocene and hydrolyzed TEOS on a silicon substrate.

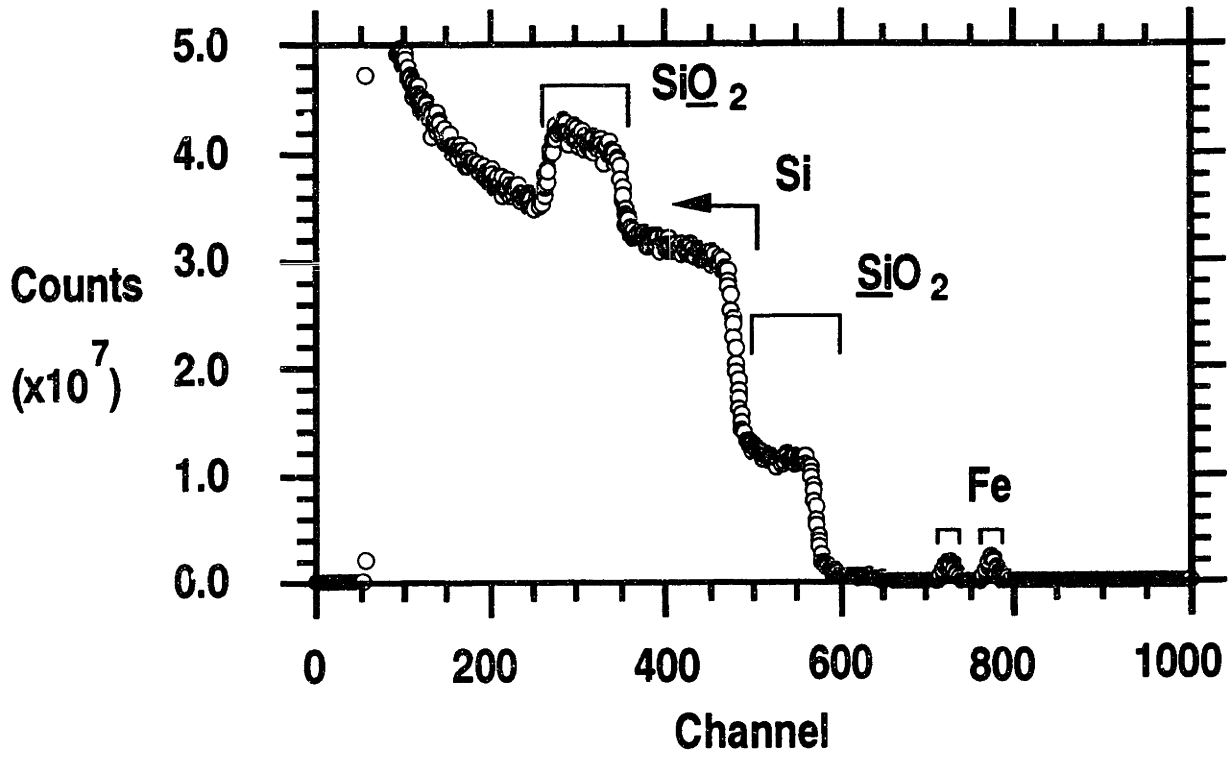
5.0
4.0
3.0
2.0
1.0
0.0
Counts
(x10^7)
SiO2
Si
SiO2
Fe
0
200
400
600
800
1000
Channel

Figure 4: Depth profiles of iron for the multilayer coating (analyzed in Figure 1) with five layers measured from two different regions on the sample, in order to test the reproducibility of data.

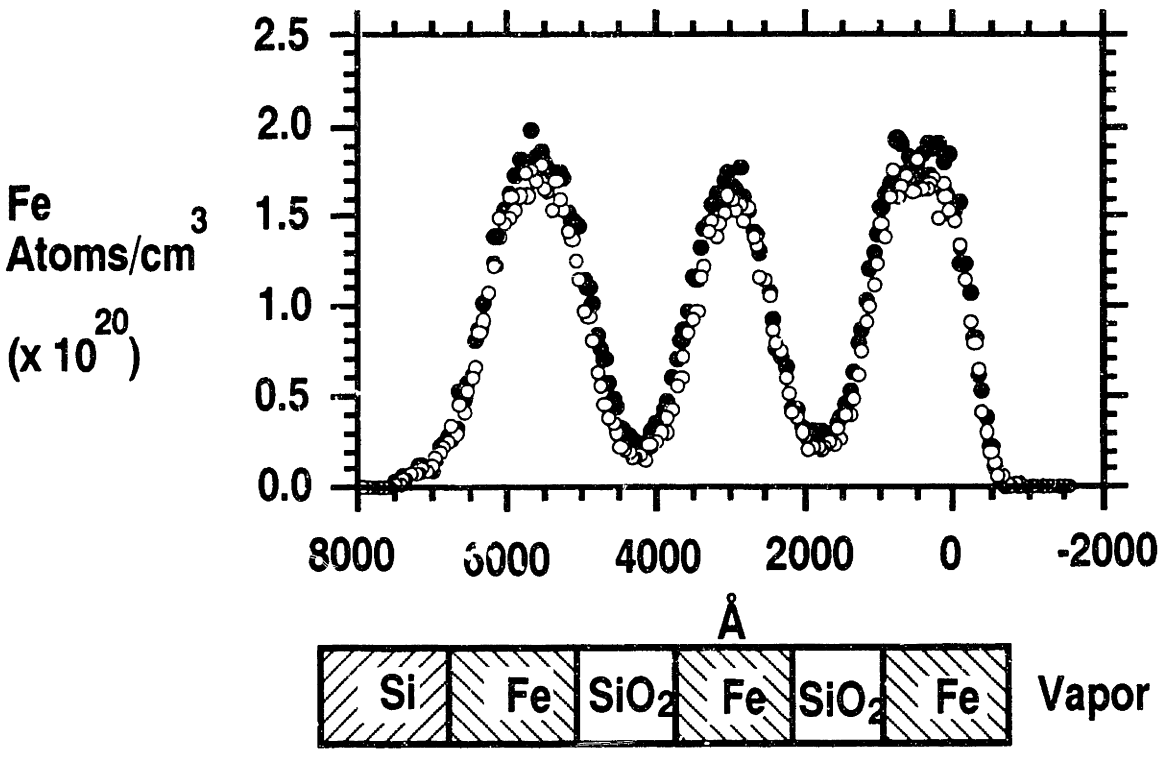
Fe
Atoms/cm3
(x 10^20)
2.5
2.0
1.5
1.0
0.5
0.0
8000
6000
4000
2000
0
-2000
Å
Si
Fe
SiO2
Fe
SiO2
Fe
Vapor

to regions of beam-assisted deposition of hydrocarbons from the vacuum system. No major beam damage to the sample was apparent.

XTEM Analysis:[29] Samples were prepared for XTEM by cutting a coated silicon substrate into 2 pieces (1.5 cm x 1 mm each) and gluing them together, coated face to coated face, with silver epoxy. The sample was thinned by grinding the exposed silicon faces on wet sandpaper until the sample was thin enough to fit into a molybdenum rod (4 cm in length, approximately 2.5 mm diameter) that had a slice removed from the center (through the diameter) through approximately 2 cm of the length. The sample was epoxied into the slice in the molybdenum rod and encircled with a brass sheath that covered about 2 cm of the rod. Approximately 1 mm thick slices were cut from the rod (at the end with the sample) using a Slurry Drill (South Bay Technology Inc. Model 350) equipped with a diamond blade. The center (~ 1 mm) of the slice was thinned to approximately 25 μm with a dimpler (South Bay Technologies Inc. Model 515). Further thinning was achieved using a Gatan Dual Ion Mill (model 600) until the sample had a small hole in it. The thinned sample was analyzed along the edge of the milled hole in a Philips EM 420T Transmission Electron Microscope. One source of error in XTEM analysis is in the uncertainty in the microscope magnification ($\leq$ 5%). We assumed the error was 5%. The thickness values reported in Table I are the average of six measurements taken at different locations in the sample. The error reported in the

table reflects both the variation in the thickness measurement and the error in magnification of the microscope. The layers were analyzed by energy dispersive X-ray analysis in the scanning mode,[20] in the electron microscope, to verify the composition (iron-containing or SiO_2) of the layers.

The Diffusion of Cesium Ion in SiO_2 Films Derived From Sol-Gel Precursors[‡]

Abstract: Hydrolyzed tetraethylorthosilicate (TEOS) forms SiO_2 gel coatings when spun-coated onto silicon substrates. These coatings were heated to different temperatures (200, 400, 600, and 800 °C) to effect different degrees of transformation from gel to glass. The index of refraction of the films increased from 1.42 ± 0.01 at 25 °C to 1.45 ± 0.01 after thermal treatment at 800 °C; thickness of the films decreased by 29.2 ± 6.0%. IR spectroscopic analyses of an SiO_2 gel coating were consistent with the changes expected in the gel-to-glass transition; up to 200 °C, a decrease in the intensities of the H_2O and Si-OH peaks were consistent with loss of water; from 200 to 800 °C, a further decrease in the intensities of the Si-OH peaks was consistent with condensation of the Si-OH to Si-O-Si groups. Gels that had been taken to various stages of their gel-to-glass transition were coated with a second film of sol-gel derived SiO_2 doped with cesium chloride. Diffusion of the cesium ion through the undoped SiO_2 gels was studied by measurement of the depth profile of cesium by Rutherford Backscattering Spectroscopy

‡ Supported in part by the National Science Foundation (CHE-88-12709) The Cambridge Accelerator for Materials Science was purchased and supported (in part) through a DARPA/URI grant and is housed in the Harvard University Materials Science Research Laboratory, an NSF-funded facility (DMR-86-14003).

(RBS). Increasing the temperature at which the undoped layer had been treated before applying the cesium-containing gel decreased the extent of infiltration of cesium into the undoped gel at room temperature. When thermal diffusion of cesium occurred at high temperature ($\geq$ 750 °C), the rate of migration was, however, independent of the thermal history of the undoped layer, at least over the range of temperatures used in treating these layers (200 - 800 °C). This observation indicates that the rate at which the silica film transforms from gel to glass is faster than that at which cesium diffuses, at the high temperatures required for the extent of diffusion of cesium to be detectable by RBS. By 700 °C approximately 90% of the chloride signal has disappeared (by RBS); the counterion of cesium under these conditions was probably either $Si\text{-}O^-$ or $O^=$.

Introduction: The mobility of dopants in SiO_2 films made from sol-gel precursors -- suspensions of silicate particles produced by polymerization involving hydrolysis and condensation reactions of silicon alkoxides[30] -- is important in applications of these films as barriers to oxidation and diffusion,[31-34] and gradient index (GRIN) optical materials.[35-36,26] Studies of diffusion in sol-gel systems have focused on diffusion of liquids into porous gels.[37] The objective of this work was to study the diffusion of cesium ion -- chosen as a representative monovalent cation for its

availability and ease of analysis by Rutherford Backscattering Spectrometry (RBS) -- in SiO_2 films coated on a silicon substrate. The system examined comprised two superimposed layers. The layer adjacent to the silicon substrate originally contained no cesium. It was prepared by coating a sol-gel solution obtained by hydrolysis of tetraethylorthosilicate (TEOS) onto the substrate, and heating the resulting film at temperatures between 200 °C and 800 °C to effect different degrees of transformation from gel to glass.[38] A second film of gel, obtained by addition of cesium chloride to previously hydrolyzed TEOS, was coated onto the first. The two-layer system -- one originally free of cesium and the second containing cesium -- was heated and the depth profile of the cesium determined by RBS. The focus of the investigation was the rate of diffusion of the cesium ion, from the doped into the undoped layer, and the influence of the thermal history and physical state of the undoped layer on the rate of this diffusion. Previous work has illustrated the usefulness of RBS for studies of high-temperature diffusion in glass and ceramic films: TiC in WC,[39] Fe in SiO_2,[40] and Cu in carbon.[41]

Several factors affect the rate of diffusion of cations in conventional SiO_2 glasses: the charge of the cation;[42] the amount of water present in the glass;[43] the mobility of the interdiffusing ion or counter anion;[44] the composition[45] and

free volume[46] of the glass; the presence and nature of other ions.[47,48]

Additional factors affect mobility of ions in SiO_2 made by the sol-gel route, because the structure of the gel changes as it passes through its gel-to-glass transformation.[38] Between 100 - 110 °C, the gel loses surface water; between 100 - 200 °C, it loses physisorbed water; at approximately 400 °C, residual organic groups are lost by oxidation; up to 700 °C, there is a gradual condensation of Si-OH to Si-O-Si groups with loss of water. One goal of our research was to survey the influence of these changes in the chemical composition and physical structure of the gel on the mobility of cesium ion in them.

The choice of monovalent cesium as a probe ion in our studies was a compromise between the atomic number of the diffusing ion and its mobility (Monovalent cations diffuse faster than multivalent cations· therefore we chose Cs^{+} over Ba^{+2} or Ce^{+4} for studies of diffusion).[40] We required a heavy ion in order to be able to measure a signal by RBS without interference from lighter elements in the range of depths $\leq$ ~ 8,000 Å; we also required an ion that was mobile enough to diffuse at an appreciable rate under accessible experimental conditions.[49]

Result and Discussion

Preparation of Samples and Conditions for Studying Diffusion: Figure 5 provides a schematic outline of our experimental protocol. We coated silicon <100> wafers with a sol-gel suspension prepared by hydrolysis of TEOS in the absence of doping agents. The film and substrate were then heated at different temperatures to transform the gel to glass to various degrees.[38] These thermal treatments consisted of heating the sample to either 200, 400, 600, or 800 °C at 1 °C/min, holding it at this temperature for 2 h, and cooling it to 30 °C at 1 °C/min. After heating and cooling, the thickness and index of refraction of the film was measured by optical ellipsometry.

In parallel with these experiments, using the same undoped sol-gel suspension of TEOS, we coated a KBr plate and collected IR spectra at each stage of thermal treatment. The melting point of KBr (mp = 734 °C)[50] made it impossible to obtain an IR spectrum of the coating after thermal treatment at 800 °C.

Thermogravimetric analysis (TGA) of the unheated coating was carried out on a powder obtained by scraping a film from the silicon substrate with a razor blade.

For studies of diffusion, we recoated the undoped, thermally pre-treated SiO_2 film with a sol-gel suspension prepared by addition of CsCl to previously hydrolyzed TEOS.

Figure 5: Scheme describing the coating and thermal treatment of samples used to study the relative rates of diffusion of cesium through undoped SiO_2 coatings that have been thermally treated to different extents along the gel-to-glass transition. The SiO_2 coatings were deposited and heated to either 200, 400, 600, or 800 °C for 2h each. (The temperature-time profiles used are indicated schematically in the Figure in the upper-right corner.) The samples were cooled, and coated with the cesium containing layer. After the layer doped with cesium was applied, the samples were heated and the diffusion of cesium was monitored by RBS. Estimated depth profiles of cesium and oxygen are included to illustrate how the diffusion of cesium into the undoped SiO_2 layer is visualized by RBS analysis.

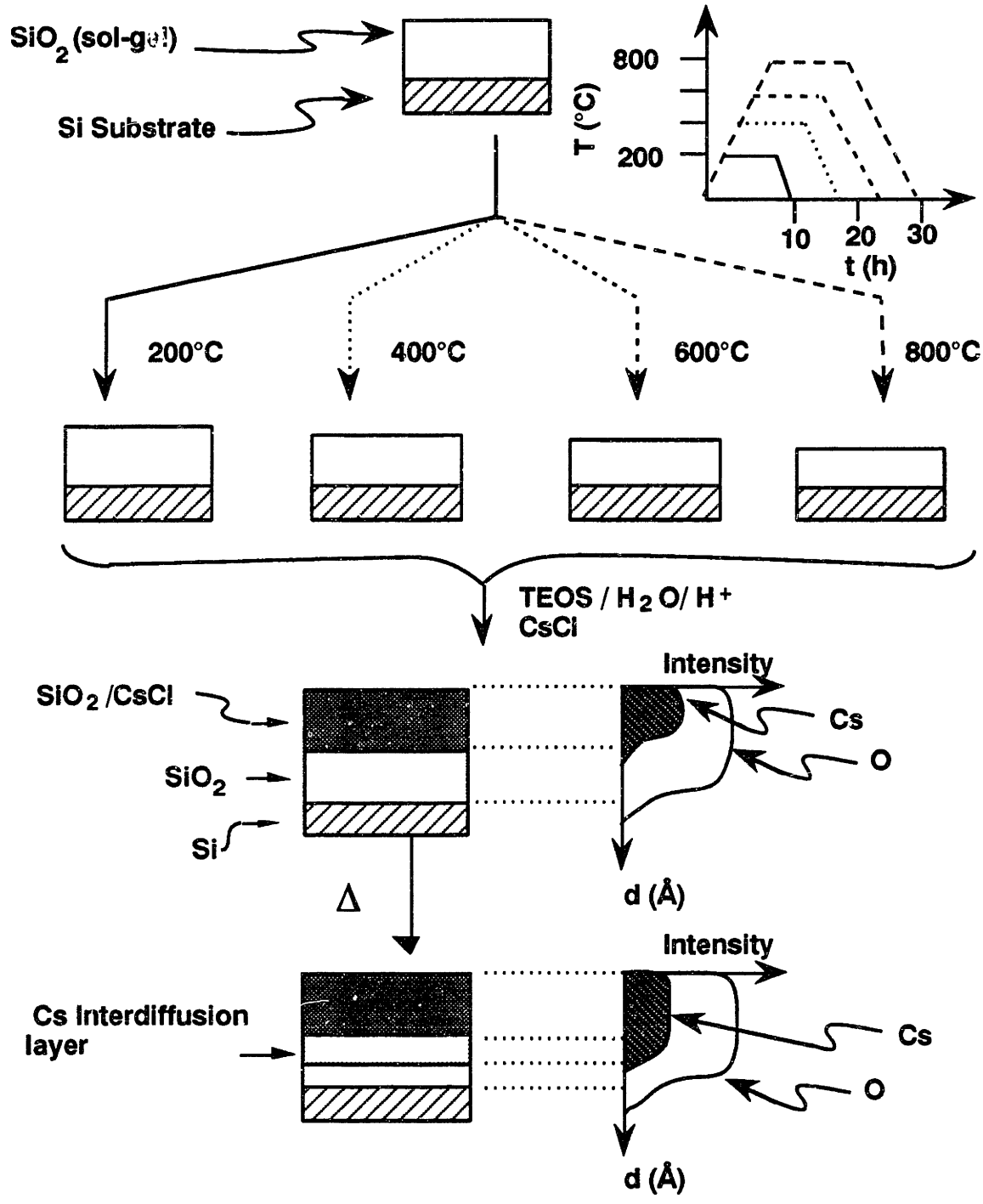
SiO2 (sol-gel)
Si Substrate
800
200
T (°C)
10
20
30
t (h)
200°C
400°C
600°C
800°C
TEOS / H2O/ H+
CsCl
SiO2 /CsCl
SiO2
Si
Intensity
Cs
O
d (Å)
Δ
Cs Interdiffusion layer
Intensity
Cs
O
d (Å)

RBS established the depth profile of cesium. After initial heating of the sample to 300 °C, the signal due to chloride in the RBS profile decreased to 40 mole % relative to cesium; by 700 °C, it was less than 10 %. This observation indicated that chloride ion had volatilized (probably as HCl), and the anionic counterion of the cesium cation had become either OH^- or $O^=$ (from water) or $Si\text{-}O^-$ (from the silicate network).

Characterization of SiO_2 Films

Ellipsometry of the Supported SiO_2 Films as a Function of its Thermal History: Analysis of the undoped SiO_2 coatings by ellipsometry, after heating, gave both their thicknesses and indices of refraction (Figure 6 and Appendix 1). Data in Figure 6 represent the average values of six measurements; the error bars, one standard deviation.

The index of refraction for the SiO_2 gel prepared at 25 °C was 1.42 ± 0.01 (98 ± 1 % dense), and 1.45 ± 0.01 (99 ± 1 % dense) after heating to 800 °C (The index of refraction for dense SiO_2 glass is 1.46).[51] The room temperature values of the index of refraction on our spin-coated samples are consistent with measurements on dense dip-coated samples made from a solution of TEOS prepared by the same procedure that we followed.[9] These latter samples had less than 5 % porosity,[3] a mean pore volume of less than 4 Å (inaccessible to nitrogen),[52] and a surface area of 0.93 cm^2 per cm^2 of

sample.[52] Shear stress increases the density of coatings for formulations designed to give porous coatings,[3] and we expected that shear stress due to spin-coating would contribute to the formation of dense coatings for our samples as well. At 400 °C, the index of refraction of our sample decreased to a minimum of 1.41 ± 0.01 (97 ± 1 % dense). This observation indicates an increase in the sample porosity (a decrease in density) probably due to loss of volatiles from the sample during thermal treatment. At 400 °C, the sample does not densify at a significant rate through viscous flow.

The films decreased in thickness by 29 ± 6 % on heating to the highest temperature studied (800 °C). This decrease in thickness represents a loss of volatiles (water, organics, and possibly low molecular weight silicon containing oligomers), and a decrease in porosity (from 2.2 ± 1.0 % at 25 °C to 1.0 ± 1.0 % at 800 °C). The loss of volatile organosilicon oligomers would allow for the loss of material without a large change in the index of refraction.

Remarkably, the index of refraction changes only slightly, reflecting a change in porosity (density) of 1.5 ± 1 % through the gel-to-glass transformation. The macroscopic density of the film thus does not change significantly with the decrease in film thickness. This observation is also consistent with the volatilization of organosilicon oligomers.

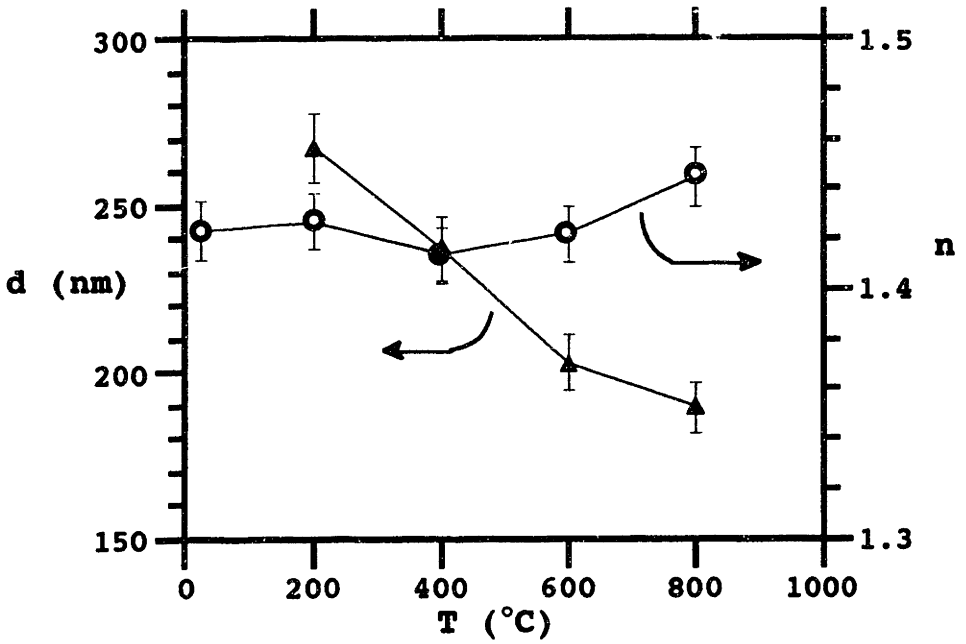

Figure 6: Plot of the index of refraction (n, O) and thickness (d, ▲) obtained from ellipsometry of the SiO_2 films, as a function of the maximum temperature to which they were heated in air. The temperature profile in the heating is summarized in Figure 5. The lines are included only to guide the eye.

Thermogravimetric Analysis (TGA) of the SiO_2 coating: Figure 7 shows the TGA of a gel, heated under nitrogen at 10 °C/min. The sample had lost 6.2 ± 1.5 % of its weight by 200 °C, and an additional 8.5 ± 1.0 % by 800 °C. The rate of loss of weight is faster between 25 and 200 °C than between 200 and 800 °C. These observations correlate with processes important in the gel-to-glass transition: at 400 °C and below, surface and physisorbed water and organic groups are lost; up to 700 °C, a gradual loss of water results from further condensations of the Si-OH groups.[38]

The loss of weight of the sample of 15 ± 2 %, as measured by TGA, is not consistent with a decrease in film thickness of 29 ± 6 % with an accompanying decrease in porosity (or increase in density) of 1.5 ± 1.0 %. These changes in The loss of weight of the sample of 15 ± 2 %, as measured by TGA, is not consistent with a decrease in film thickness of 29 ± 6 % with an accompanying decrease in porosity (or increase in density) of 1.5 ± 1.0 %. These changes in thickness and density would require a loss of weight of 28 ± 6 %.‡

‡ We cannot explain this discrepancy, but speculate that the differences in the conditions under which these samples were heated had a significant effect on these results. In the TGA experiment, the sample form was a powder which was heated under dry nitrogen at 10 °C/min from room temperature to 800 °C. In contrast, the samples analyzed by ellipsometry were films heated in ambient air (approximately 70% humidity at 25 °C) at 1 °C/min, held for 2 h at the holding temperature, and cooled at 1 °C/min to 30 °C.

IR Analysis of SiO_2 Coatings as a Function of Thermal History. Figure 8 presents IR spectra, collected at room temperature and after each thermal cycle, of an SiO_2 coating on a KBr plate. Samples were heated at 1 °C/min, held for 2 h at 200, 400, or 600 °C, and cooled at 1 °C/min.† Below 200 °C the decrease in intensity of the H_2O and Si-OH absorbances are consistent with loss of physisorbed water.[53,54] On heating the sample from 200 °C to 800 °C the decrease in the Si-OH absorbances are consistent with further condensation of Si-OH groups with accompanying loss of H_2O.

---

† We attribute the absorbances at 3600-3400 cm^{-1} to the OH stretching modes of H_2O and SiOH (Maniar, P.; Navrotsky, A.; Rabinovich, E. M.; Wood, D. L.; Kopylov, N. A. *Better Ceramics Through Chemistry III* Materials Research Society Symposium Volume 121; Brinker, C. Jeffrey; Clark, David. E.; Ulrich, Donald R., Eds.; Materials Research Society: Pittsburgh, Pennsylvania, 1988; p. 323-329); at 1620 cm^{-1} to the H_2O bend (Maniar, P. op. cit.); at 1180 cm^{-1} and 1090 cm^{-1} to SiO_2 network vibrations (Wood, D. L.; Rabinovitch, E. M. *J. of Non-Crystalline Solids* **1986**, *82*, 171-176. Wood, D. L.; Potkay, E.; Clark, H. R.; Kometani, T. Y. *Appl. Spect.* **1988**, *42*, 299-304); at 980-950 cm^{-1} to the Si-OH stretch (Walrafen, G. E.; Hokmabadi, M. S.; Holmes, N. C. *J. Chem. Phys.*, **1986**, *85*, 771-776. Walrafen, G. E.; Hokmabadi, M. S.; Holmes, N. C.; Nekllis, W. J.; Henning, S.; *J. Chem. Phys.* **1985**, *82*, 2472-2476); at 800 cm^{-1} to vibrations characteristic of cyclic silica tetrahedra (Tohge, N.; Moore, G. S.; Mackenzie, J. D. *J. of Non-Crystalline Solids* **1984**, *63*, 95-103); at 550 cm^{-1} to the O-Si-O$^-$ bend (Tohge, N. op. cit.); and 440-480 cm^{-1} to O-Si-O bending (Wood, D. L.; Rabinovitch, E. M. op. cit. Wood, D. L.; Potkay, E.; Clark, H. R.; Kometani, T. Y. op. cit.).

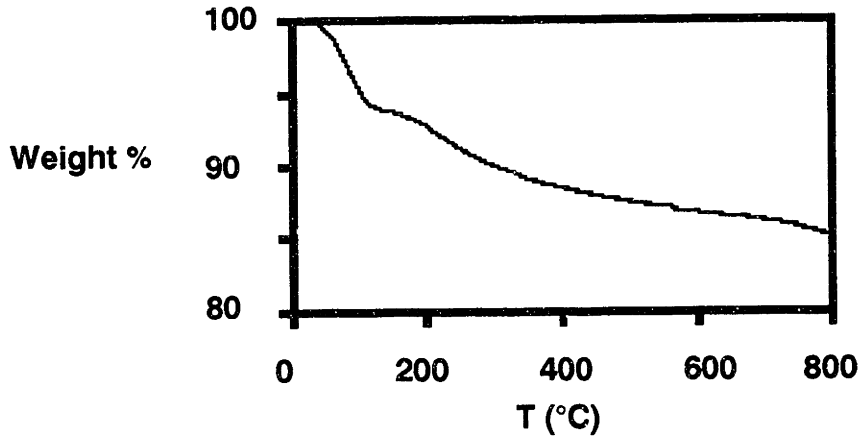

Figure 7: Loss of weight from TEOS derived SiO_2 as a function of temperature under nitrogen. The temperature of the sample increased at 10 °C/min.

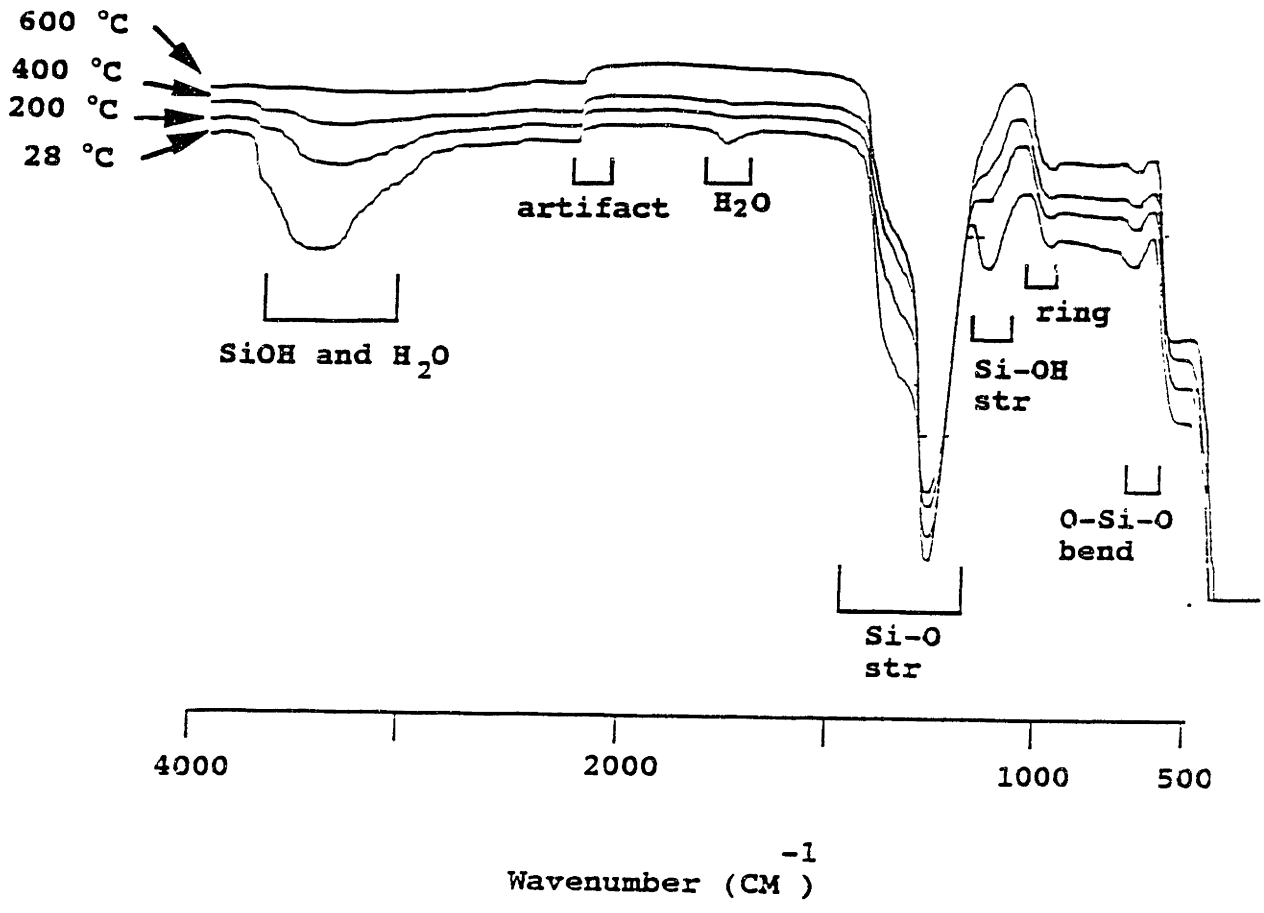

Figure 8: IR spectra of an SiO_2 coating on a KBr plate, obtained for samples prepared at: A) room temperature (28 °C), and after heating to: B) 200, C) 400, and D) 600 °C.

Extent of Diffusion:

Measurement of The Depth Profile of Cesium in SiO_2 by RBS: Our specific goal in this work was to define the mildest heating cycle necessary to transform the undoped gel to a coating that acts as a barrier to diffusion of cesium. More broadly, it is useful to know the rates of diffusion of cations through these sol-gel derived films to define their value for applications as diffusion barriers.

To examine diffusion of cesium, we heated samples to 750 - 800 °C under nitrogen. At these temperature, two processes could, in principle, occur concurrently: transformation (or further transformation, for the undoped SiO_2 layer) of the silica layer from gel to glass, and diffusion of cesium. By studying the relative rates of migration of cesium into gels that had been carried to different stages of the gel-to-glass transformation by prior heating, we hoped to determine, at least qualitatively, whether diffusion or transformation were faster.

We monitored the diffusion of cesium by RBS. For this system (cesium in SiO_2), the depth resolution of RBS is approximately ± 200 Å, and the minimum detectable concentration of cesium is 0.03×10^{20} atoms/cm^3 (approximately 0.03 atom %, assuming a packing density of 10^{22}

atoms/cm^3).[55] Representative plots of RBS data are presented in Figure 9.‡

Figure 10 shows the cesium profile as a function of the temperature in which the sample had been heated; this figure also shows (bottom) the oxygen profile for unheated and heated samples, and provides a direct measure of the total thickness of the two silica films against which the cesium profile can be compared.

To induce diffusion of cesium, the samples were heated under nitrogen using the same profile as shown in Figure 5: heating and cooling rates of 1 °C/min, and two h at the holding temperature (750 or 800 °C). For calibration, one sample in each set was not heated.

We note from the depth profiles of cesium in these samples that the thermal history of the undoped silica layer influences the extent to which cesium infiltrates <u>before</u> heating the two-film sample. For example, at a depth of 180 nm (20 nm above the interface between the undoped silica film and the silicon substrate), the cesium content is approximately 0.1 x 10^{20} atoms/cm^3 for the sample treated initially at 200 °C for 2h; 0.1 x 10^{20} atoms/cm^3 at 400 °C;

---

‡ The chloride signal is small but detectable. We note a progressive decrease in chloride content in the samples with increased thermal treatment. Halide salts could, in principle, be lost from the silica film either as HX or, following oxidation from atmospheric oxygen, as X_2. Experiments are in progress to investigate the mechanism of loss of halide ion from sol-gel coatings on heating.

Figure 9: Representative RBS data for; a) the silicon substrate with no coating; b) a silicon substrate with an SiO_2 film; and c) a silicon substrate with an SiO_2 film under a cesium chloride containing SiO_2 film.

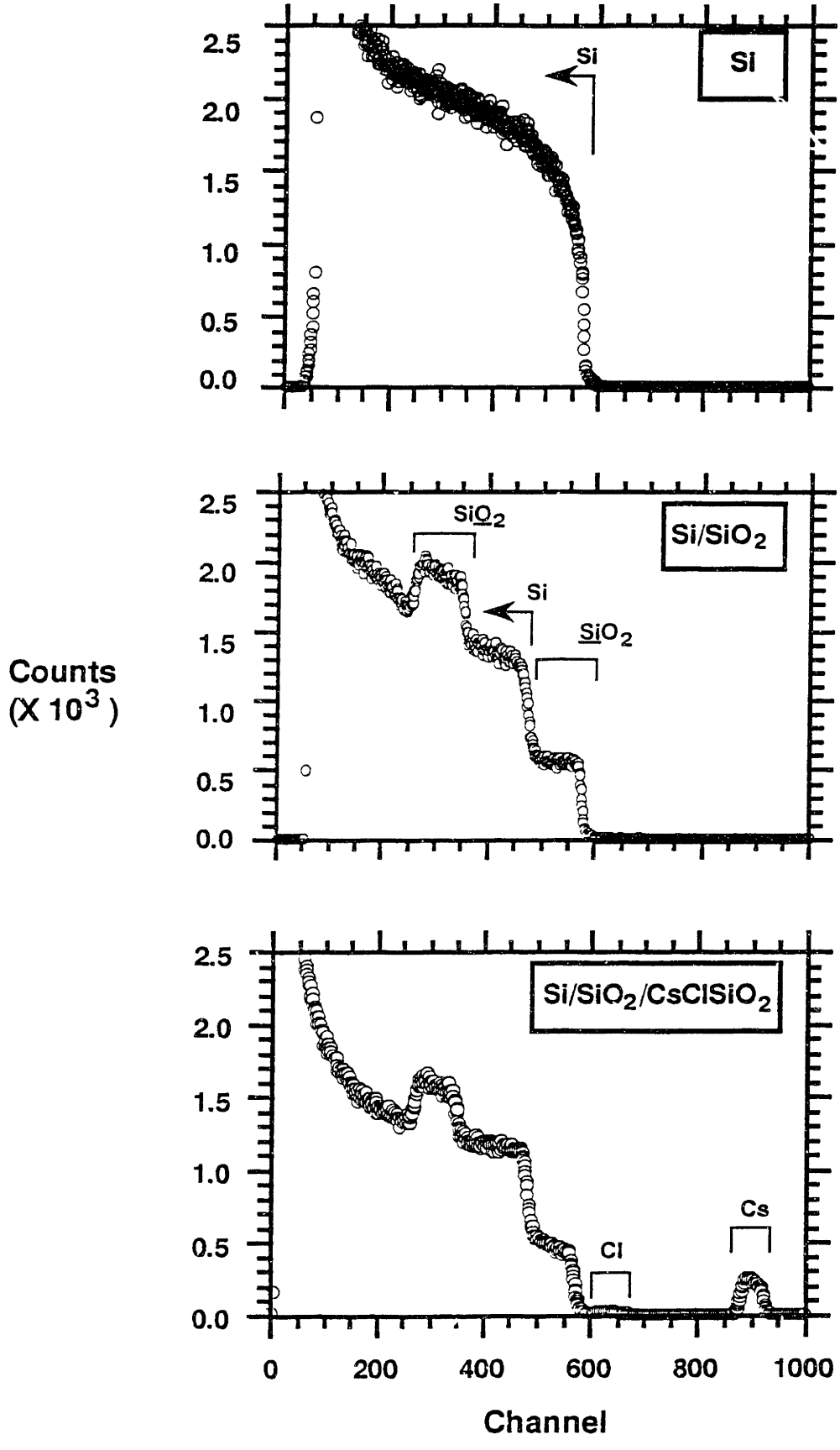
Si
Si
SiO2
Si/SiO2
Si
SiO2
Si/SiO2/CsClSiO2
Cl
Cs
Counts
(X 10^3)
Channel
0.0
0.5
1.0
1.5
2.0
2.5
0
200
400
600
800
1000

Figure 10: Depth profiles for cesium in the two-layer systems summarized in Figure 5. The origin of the distance scale is arbitrarily set at the interface between the original two silicate films: that on the left (-300 - 0 nm) was doped with the cesium; that on the right (0 - 200 nm) was undoped. The top four figures show the intensity of the cesium signal as a function of depth. The temperature at which the undoped layer was heated before applying the cesium-doped layer is indicated on each (200, 400, 600, and 800 °C). Each box contains three traces, corresponding to the temperature at which the two-film system was heated to effect cesium diffusion: no heat (20 °C,○); 750 °C/2h (◇); 800 °C/2h (▲).

The bottom traces are representative oxygen profiles for samples having both silica films, before and after heating as indicated (○,▲). This profile defines the aggregate thickness of the silica layer, and demonstrates that cesium does not diffuse into the silicon substrate under our experimental conditions.

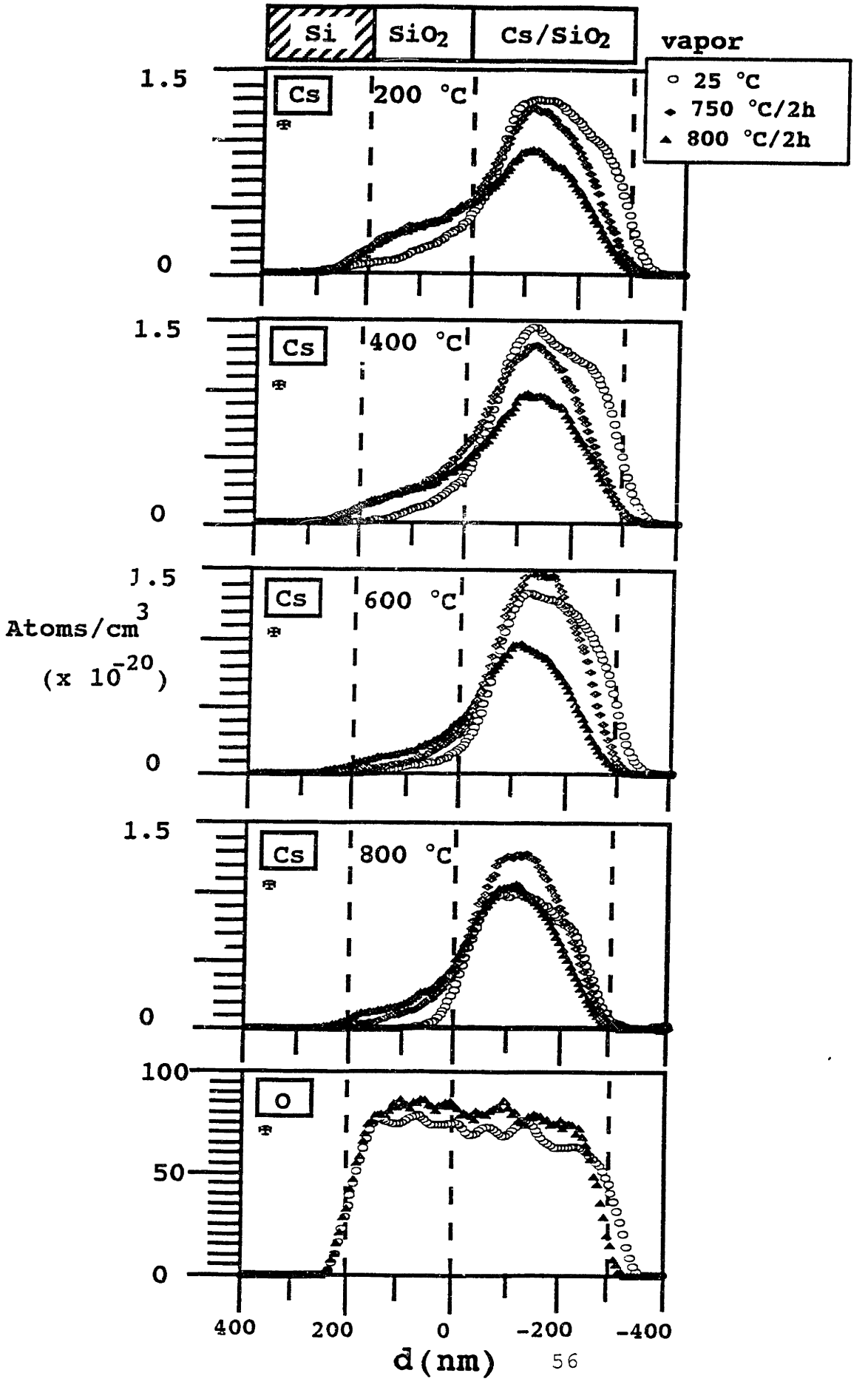
Si
SiO2
Cs/SiO2
vapor
25 °C
750 °C/2h
800 °C/2h
Cs
200 °C
400 °C
600 °C
800 °C
O
1.5
0
100
50
Atoms/cm3
(x 10-20)
400
200
0
-200
-400
d (nm)

and less than 0.05 x 10^{20} atoms/cm^3 for samples taken to both 600 and 800 °C.[55]

Estimation of Apparent Diffusion Coefficient of Cesium in SiO_2 Gels: We estimated the apparent diffusion coefficient, D_{Cs} (cm^2/sec), of cesium in the SiO_2 gel (Appendix 2). Figure 11 presents the calculated diffusion coefficients. Those for the samples that were previously heated to 200 and 400 °C represent an effective diffusion coefficient, reflecting an aggregate of the room temperature infiltration of cesium and the diffusion of cesium at elevated temperature. There is no significant difference in the apparent diffusion coefficients calculated for samples previously heated to 200, 400, 600, and 800 °C; they are all in the order of magnitude of 10^{-15} cm^2/sec.

Conclusions: Increasing the temperature at which the undoped layer was treated before applying the cesium-containing gel decreased the extent of infiltration of cesium into the undoped gel at room temperature. This observation indicates that the physical state of the gel (probably its SiOH content) was important in determining ionic mobility. Cesium diffused at room temperature into undoped films that had been heated to 200 and 400 °C but not into those heated to 600 or 800 °C; diffusion was faster for the film heated only to 200 °C. Thus, it seems to be necessary to heat the undoped film to approximately 600 °C to prevent infiltration

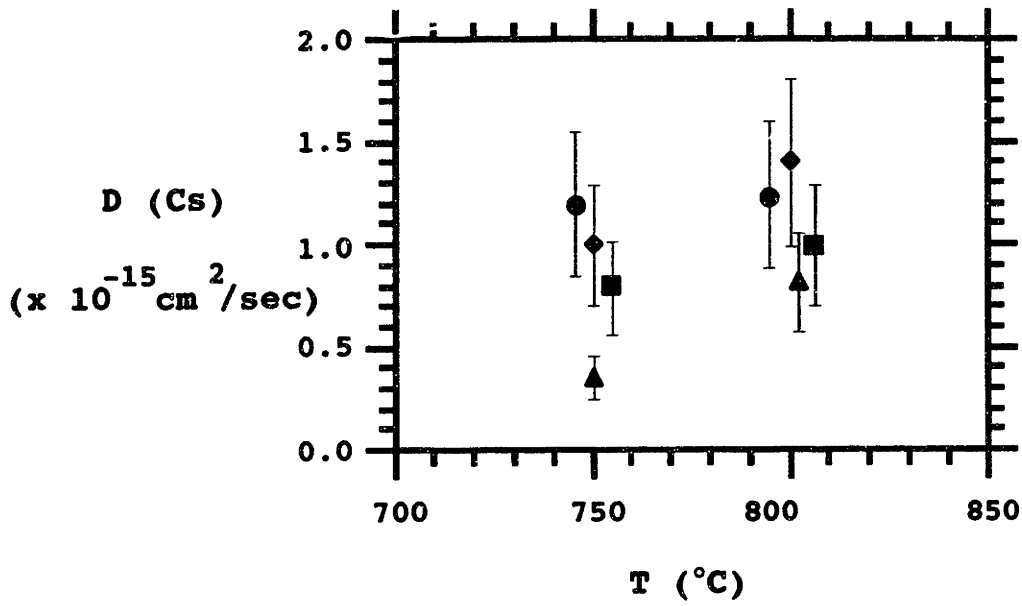

Figure 11: Plot of D_{Cs} (cm^2/sec) at 750 and 800 °C for samples previously heated to 200 °C (●), 400 °C (◆), 600 °C (■), and 800 °C (▲).

of cesium into it when it is overcoated with a cesium chloride-containing gel layer at room temperature.

The rate of diffusion of cesium in the undoped gel correlates qualitatively with the concentration of SiOH groups in this gel, as measured by IR spectroscopy.‡ At room temperature, the gels retain chloride ion, and part of the relatively high room temperature mobility of cesium ion into the undoped gels that have not been heated to temperatures greater than 400 °C may be related to the fact that both cation (cesium) and anion (chloride) exist in this system in diffusible form. Since the chloride ion rapidly disappears (to 37 % of the concentration of cesium by 300 °C and approximately to 10 % by 700 °C) from the gel, we assume the counterion for most of the cesium ion at high temperature is either SiO^- or $O^=$ at temperatures above 300 °C.

When migration of cesium did begin to occur (at high temperatures, 750 °C) the rate of this migration was independent of the thermal history of the undoped layer, at least over the range of temperatures used in treating these

---

‡ The SiOH content in a glass can have a profound influence on its properties. When 0.1 wt % of water is incorporated, the presence of Si-OH groups reduces the viscosity of SiO_2 by three orders of magnitude at 1,000 °C. These non-bridging oxygens interrupt the glass network, allowing it to flow more easily relative to "dense" SiO_2. The Si-OH groups are defects in the SiO_2 network and may bind Cs^+, plausibly as $SiO^- Cs^+$ groups formed by exchange of the Cs^+ ion with the proton in the SiOH group. These anionic sites in the gel may plausibly increase the mobility of cesium. Doremus, Robert H. *Glass Science*; John Wiley and Sons: New York, 1973, p.170-172.

layers (200 - 800 °C). The extent of diffusion of cesium at elevated temperatures did not vary significantly as a function of the temperature of thermal pretreatment of the gel. The diffusion coefficients calculated from these studies are indistinguishable. Thus, when the sample reaches a temperature at which detectable diffusion of cesium occurs (T > 750 °C), the cesium "sees" silica film previously heated to any temperature between 200 and 800 °C as having the same physical state. We infer from this observation that the rate at which the silica film transforms from gel to glass is fast relative to cesium migration, at the high temperatures required for this migration to be detectable by RBS.

Experimental

Materials: We purchased ethyl ether from Mallinckrodt, hexane from Fisher Scientific, cesium chloride and tetraethylorthosilicate (TEOS) from Alfa, and absolute ethanol from USI Chemicals Co. All reagents were used without further purification unless noted.

Preparation of Samples: We coated a silicon <100> wafer by pipetting enough TEOS solution to cover the wafer (3 mL), spinning the substrate at 1500 rpm for 2 min on a Headway Model PWM 101ECR790 spin-coater, pipetting more solution onto the coated substrate, and spinning again. The samples were then heated in a Fisher Scientific Isotemp

Programmable Ashing Furnace Model 497 at 1 °C/min, held for 2 h at either 200, 400, 600, or 800 °C, and cooled at 1 °C/min. Prior to coating and heating the gel layers with CsCl-doped TEOS, the samples were analyzed by ellipsometry.

Ellipsometry of Samples: Ellipsometric measurements were made using a thin film ellipsometer Type 43603-200E manufactured by Rudolf Research, equipped with a He-Ne laser. Thicknesses and indices of refraction were obtained using "A FORTRAN Program for Analysis of Ellipsometric Measurement".‡

IR Analysis of Samples: We performed IR analyses on a Perkin Elmer 598 Infrared Spectrophotometer equipped with a 3600 Data Station. The KBr plate was purchased from Optovac.

TGA: TGA analyses were performed on a powder of the unheated gel, scraped from the Si <100> substrate with a razor blade, using a Seiko 1 TG/DTA 200 equipped with an SSC-5020 Disc station.

RBS Analysis: The depth profiles of cesium were obtained using the Cambridge Accelerator for Materials Science with a 2 MeV He^+ beam. Depth profiles of cesium and oxygen were calculated using "Spectrum Analysis".† The depth profiles presented in Figure 10 were smoothed, and

---

‡ A FORTRAN Program for Analysis of Ellipsometric Measurements was written by Frank L. McCrackin (NBS). McCrackin, F. L.; Passaglia, E.; Stromberg, R. R.; Steinberg, H. L. *J. Res. Natl. Bur. Stand. Sect. A* **1963**, *67*, 363-377.

† Spectrum Analysis, a fortran program based on algorithms from ref. 55, was written by Patrick M. Smith, Division of Applied Physics, Harvard University.

representative profiles from unsmoothed data are presented in Figure 12 for comparison.

Hydrolysis of TEOS: A solution containing TEOS (61 mL, 273 mmol of Si), ethanol (43 mL), doubly distilled water (5 mL) and aq HCl (0.2 mL of 1 M acid) was heated at 60 °C for 1.5 h.[9] After cooling the solution to room temperature, an additional 4.0 mL of doubly distilled water and 12 mL of HCl were added to a 100-mL aliquot of the TEOS solution, and the mixture was stored in a freezer (-8°C), where it was stable (did not gel) for several months. For coating, the solution was diluted by a factor of three with ethanol (0.62 mmol of Si/mL).[9]

Preparation of CsCl-doped TEOS: To a solution of previously hydrolyzed TEOS (10 mL, 6.2 mM in Si) was added a water/ethanol (1.8/5.0 v/v) solution of cesium chloride (0.5 mL, 0.265 mM). The solution was coated immediately.

Figure 12: Depth profiles of oxygen (O) and cesium (◇) from unsmoothed data (a: best case and b: worst case). The data in 12a are for the SiO_2 undercoat previously heated to 600 °C, and in 12b are for the SiO_2 undercoat previously heated to 800 °C. Both samples had no thermal treatment after the cesium chloride doped TEOS was applied.

a)

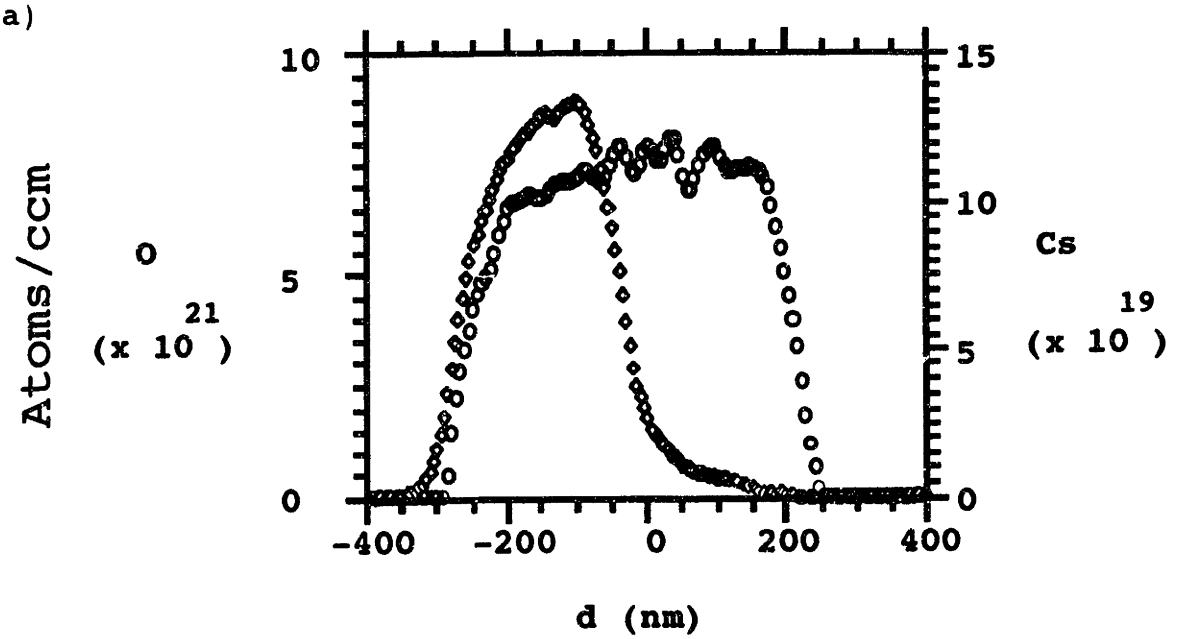
Atoms/ccm
O
(x 10^21)
Cs
(x 10^19)
10
5
0
15
10
5
0
-400
-200
0
200
400
d (nm)

b)

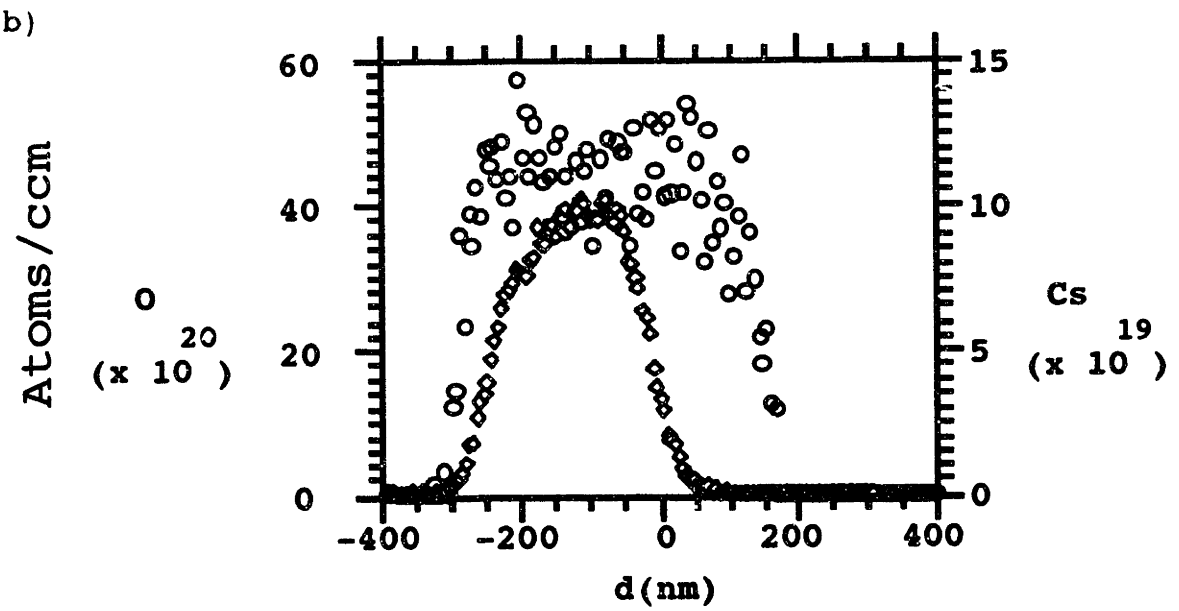
Atoms/ccm
O
(x 10^20)
Cs
(x 10^19)
60
40
20
0
15
10
5
0
-400
-200
0
200
400
d(nm)

The Loss of Halide from Sol-Gel Films on Heating Does Not Involve Oxidation†

Abstract: The loss of halide ion from sol-gel derived films on heating has been studied by RBS. The rates of loss of halide under air and argon atmospheres were very similar. This observation is consistent with a non-oxidative mechanism for the loss of halide. The relative rate of loss of halide at a particular temperature follows the qualitative order: LiI > LiBr ≃ LiCl > NaI > NaBr > KI ≃ KBr ≃ NaCl. This order correlates with the vapor pressures of the salts and with the ΔG of formation of the hydrogen halides, by reaction of metal halide with water, and suggests that volatilization of the salt (MX) and/or the hydrogen halide (HX) is the mechanism for loss of halide ion from sol-gel coatings.

Introduction: Hydrogen halides and halide salts are catalysts used in sol-gel reactions to affect the time required for gelation.[56,57] Little is known about the fate of the ions after gelation, although the halides are known to disappear from the gel during its transformation to glass at high temperatures. The goal of this study was to investigate

---

† Supported in part by the National Science Foundation (CHE-88-12709), the Office of Naval Research, and the Defense Advanced Research Projects Agency (through the University Research Initiative). The Cambridge Accelerator for Materials Science was purchased through a DARPA/URI grant and is housed in the Harvard University Materials Research Laboratory, an NSF-funded facility (DMR-86-14003).

the mechanism of loss of halide ion from sol-gel coatings on heating. We have used Rutherford Backscattering Spectrometry (RBS) to quantify the content of halide ion (and non-halogen anions) in silica films derived from sol-gels as a function of the temperature and atmospheres under which they were heated. We have also used Auger Electron Spectroscopy (AES) for qualitative analysis for the presence of sodium in a NaI-doped SiO_2 sample both before and after thermal treatment.

Mechanisms for the Loss of Halide in Sol-Gel Coatings: Halogen could, in principle, be lost from the silica film either as HX or M^+X^-, or, following oxidation, as X_2 (eqs 1-4; Si_f denotes a representative silicon center in the silicate lattice).

Volatilization of HX

$$Na^+X^- + HOSi \longrightarrow HX\uparrow + NaOSi_f \quad (1)$$

$$Na^+X^- + HOH \longrightarrow HX\uparrow + NaOH \text{ (or } Na_2O) \quad (2)$$

Volatilization of MX

$$Na^+X^- \longrightarrow Na^+X^-\uparrow \quad (3)$$

Oxidation of X^- to X_2

$$2\ Na^+X^- + 1/2\ O_2 \longrightarrow X_2\uparrow + Na_2O \quad (4)$$

It is possible that mass transport of some species (M^+X^-, HX, X^-, X_2, O_2, H_2O) might be rate-limiting. The only plausible oxidant under normal conditions for thermal transformation of

gel to glass is atmospheric oxygen. It should, therefore, be possible to distinguish between mechanisms for loss of halide on heating by examining the rates of loss of anion from the gel during heating for anions differing in the volatility of their conjugate protic acids (eqs 1,2) and their salts (eq 3), and in their susceptibility to oxidation (eq 4).

Results and Discussion

Procedure: We examined the mechanism of loss of halide ion experimentally by determining the quantity and distribution of anions present in silica gels as a function of thermal history, and of the atmosphere (argon or air) under which they had been heated. Heating involved increasing the temperature of the sample linearly to a predetermined value, holding that temperature for 3 h, and then cooling linearly to room temperature. Multiple samples containing the same anion were subjected to one cycle of heating and cooling, analyzed for anion, and then reheated to a higher temperature, cooled and reanalyzed.

The contents and distributions of anions in the silica gel/glass were established by RBS. Figure 13 shows representative distributions for a volatile anion (LiI) and for a less volatile one (NH_4VO_3) as a function of temperature of thermal treatment. Profiles for oxygen (from LiI/SiO_2 and NH_4VO_3/SiO_2) are included for comparison.

RBS detects atoms through elastic collisions of helium ions with their nuclei. The energy of the backscattered

helium ion and the efficiency with which it scatters is directly proportional to the atomic number of the nucleus with which it collides. RBS could not accurately measure the presence of lithium or sodium in these samples because their atomic masses are low.[20,55]

Kinetics of Loss of the Anion: Figure 14 summarizes data showing the relative loss of I^-, Br^-, and Cl^-, with Na^+ as counterion, as a function of temperature under argon and under air. This figure plots the normalized content of halide as a function of temperature of thermal treatment. The normalized content of halide, X_T/X_0, is the ratio of the content of halide after thermal treatment at temperature T (X_T), to the content of halide prior to thermal treatment (X_0). We measured the content of halide by calculating the ratio of the integrated areas of the halide signal to that of a predetermined region of the spectrum from the <100> silicon wafer substrate. We chose the silicon substrate (ρ = 2.33 g/cm^3)[58] as an internal standard.

The data in Figure 14 are scattered; nevertheless, it is clear that the content of iodide decreases faster than that of bromide or chloride. There may also be a small difference in the relative rates of loss of the halides under argon and under air, with rates apparently slightly faster under air (especially at 400 °C).

Figure 13: Representative depth profiles of iodide and oxygen from $Li^{+}I^{-}$ doped SiO_2 and of vanadium and oxygen from $NH_4^{+}VO_3^{-}$ doped SiO_2 as a function of temperature of thermal treatment.

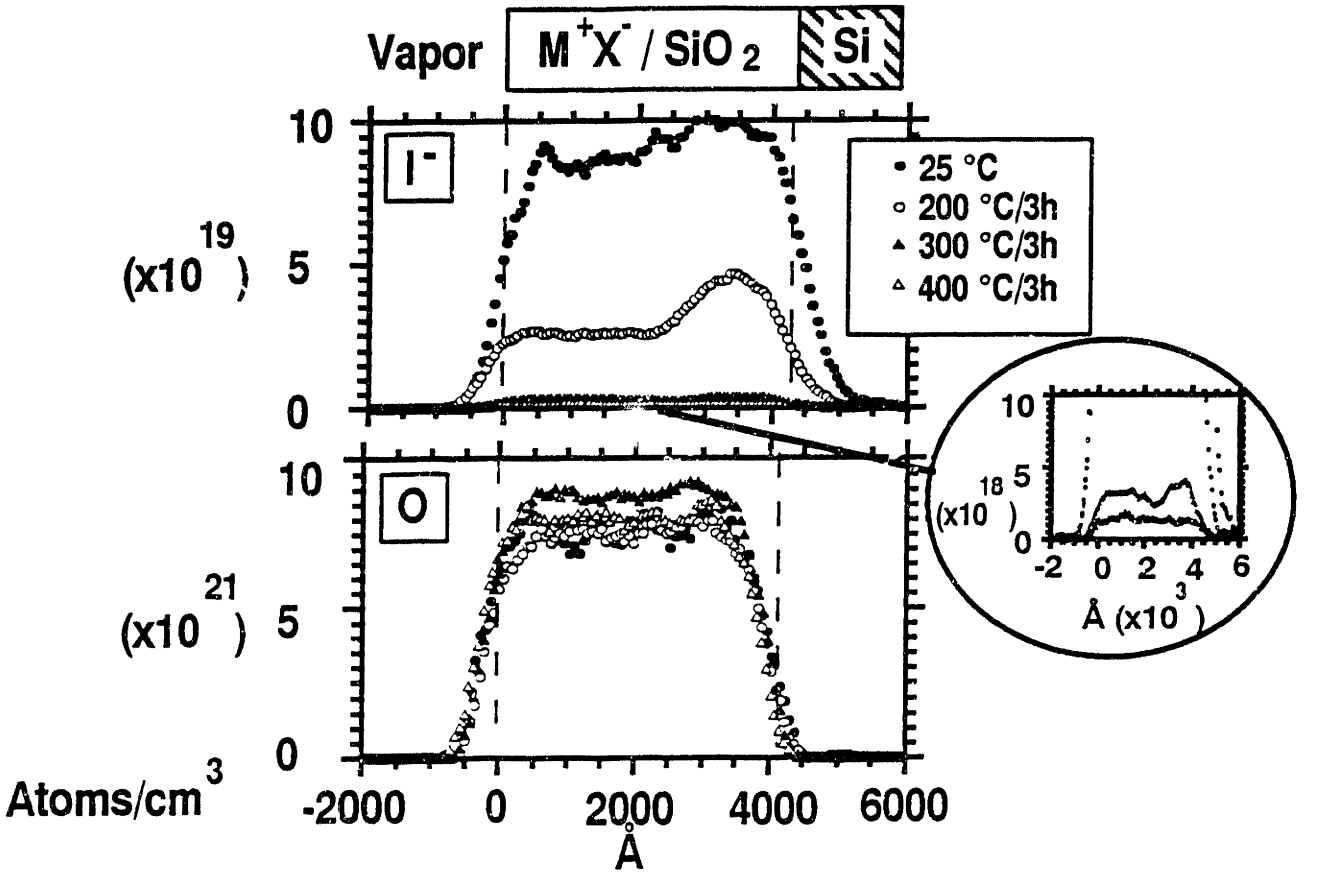
Vapor
M+X- / SiO2
Si
I-
25 °C
200 °C/3h
300 °C/3h
400 °C/3h
(x10^19)
O
(x10^21)
Atoms/cm^3
-2000
0
2000
4000
6000
Å
(x10^18)
Å (x10^3)

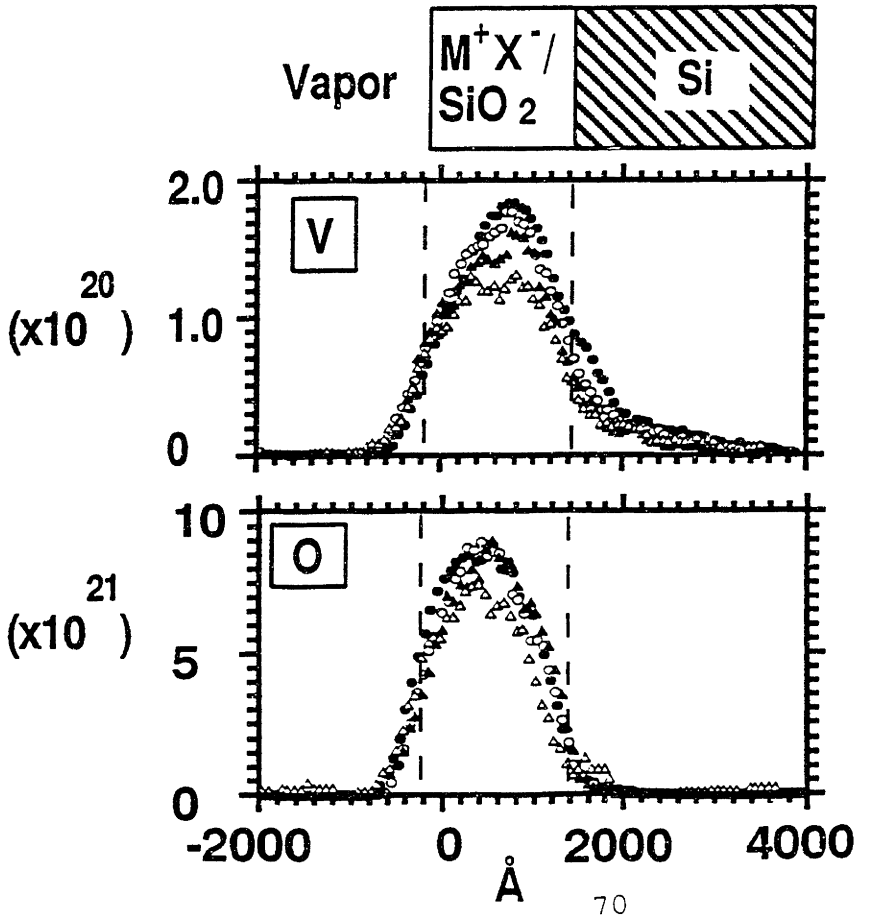
Vapor
M+X- /
SiO2
Si
V
(x10^20)
O
(x10^21)
-2000
0
2000
4000
Å

Figure 14: Plot of the normalized content of sodium halide (I^-, Br^-, and Cl^-), determined by RBS, as a function of thermal treatment (held at each temperature for 3 h) under both air and argon. Multiple points indicate measurements from multiple samples. The points are shown displaced from the nominal temperatures to avoid overlap.

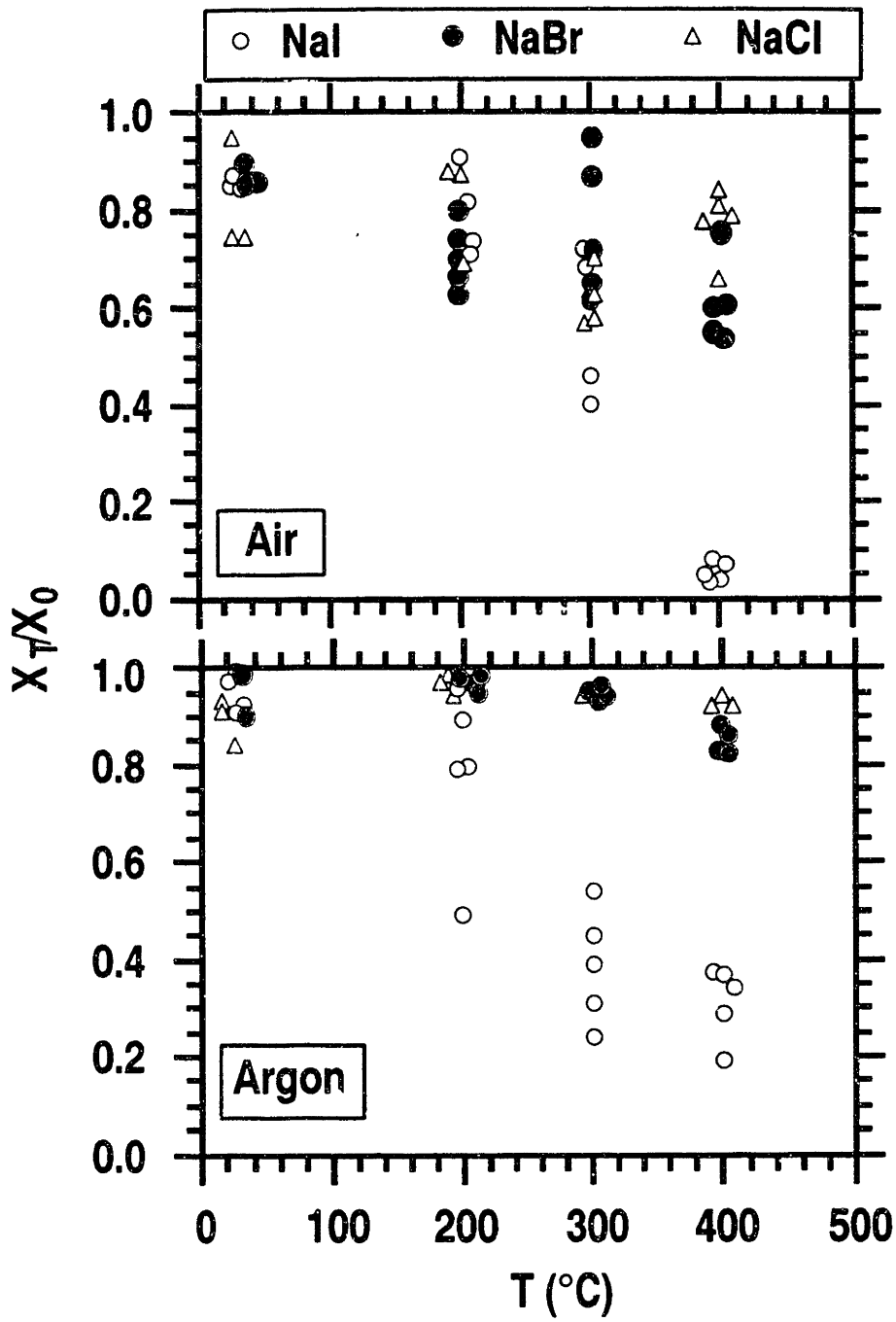
NaI
NaBr
NaCl
Air
Argon
X_T/X_0
T (°C)
0.0
0.2
0.4
0.6
0.8
1.0
0
100
200
300
400
500

We have surveyed several anions using this technique. Results are summarized in Figure 15. The scatter in these data was similar to that in Figure 14. The individual data are omitted; the error bars represent the range of data (highest to lowest), the symbols their mean. Qualitatively, the order of disappearance of these anions is I^- (LiI) > Br^- (LiBr) ≃ Cl^- (LiCl) > I^- (KI) ≃ Br^- (KBr) ≃ SbF_6^- ($HSbF_6$) ≃ VO_3^- (NH_4VO_3). In these data, there is no significant difference in the loss of halide under air and under argon.

Figure 16 presents a plot of the temperature of the half-life for loss of halide under our experimental thermal conditions in air ($T_{1/2}$, °C) versus the vapor pressure of the salt at 1000 °C calculated from literature values.† The value of $T_{1/2}$ was estimated from a straight line, calculated by least squares analysis, through the data in Figures 14 and 15. We omit data for the compounds NH_4VO_3 and $HSbF_6$ because we could find no data on their vapor pressures. The vapor pressures of the salts were calculated at 1000 °C, and not at the lower temperatures of our experiments, because the literature values for the temperature dependence of the vapor pressures were not valid for low temperatures (< ~ 1000 °C). Thus, the data in Figure 16 have no quantitative significance. They do, however, show a rough correlation

† The vapor pressures (mm Hg) of halide salts at 1000°C, based on calculations from literature values (*Handbook of Chemistry and Physics, 64th ed.*; Weast, Robert C., Ed.; CRC Press: Cleveland, Ohio, 1983-84, pp D-215-217), are LiI (131 mm) > LiBr (64 mm) > KI (43 mm) > LiCl (35 mm) ~ NaI (40 mm) > NaBr (21 mm) ~ KBr (23 mm) > NaCl (9 mm).

Figure 15: Plot of the relative loss of Br^- (LiBr ●, KBr △), I^- (LiI ○, KI ◆), Cl^- (LiCl ▲), $\underline{Sb}F_6^-$ ($HSbF_6$ ■), and $\underline{V}O_3^-$ (NH_4VO_3 □) determined by RBS, as a function of temperature of thermal treatment (held at each temperature for 3 h) under air and under argon. The points are shown displaced from the nominal temperatures to avoid overlap.

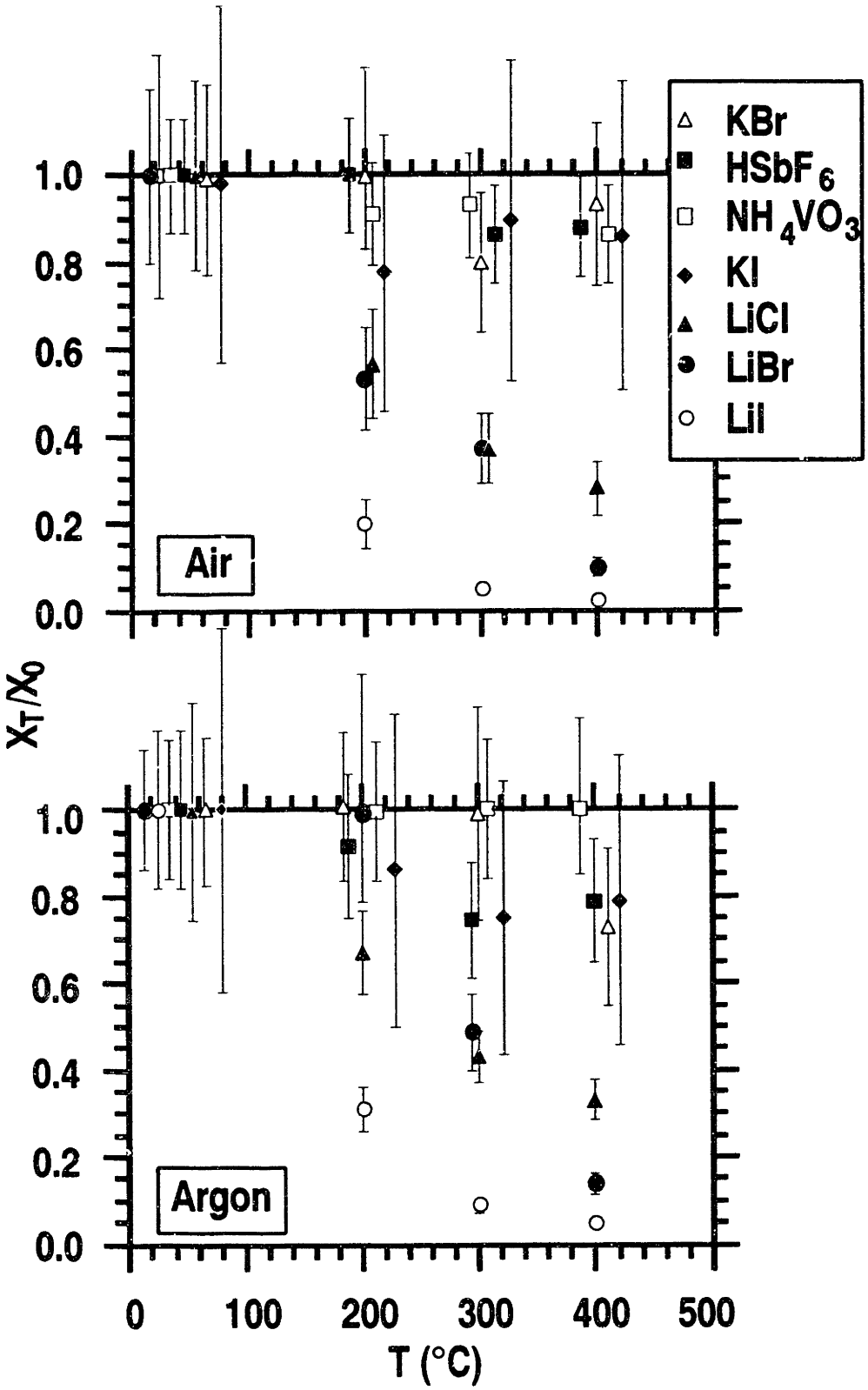
KBr
HSbF6
NH4VO3
KI
LiCl
LiBr
LiI
Air
Argon
1.0
0.8
0.6
0.4
0.2
0.0
XT/X0
0
100
200
300
400
500
T (°C)

Figure 16: Plot of the estimated temperature at which half of the halide would be lost ($T_{1/2}$, °C) following the protocol in the research versus the vapor pressure of the salt at 1000 °C. The error bars represent error in the calculation of the least squares line for each salt.

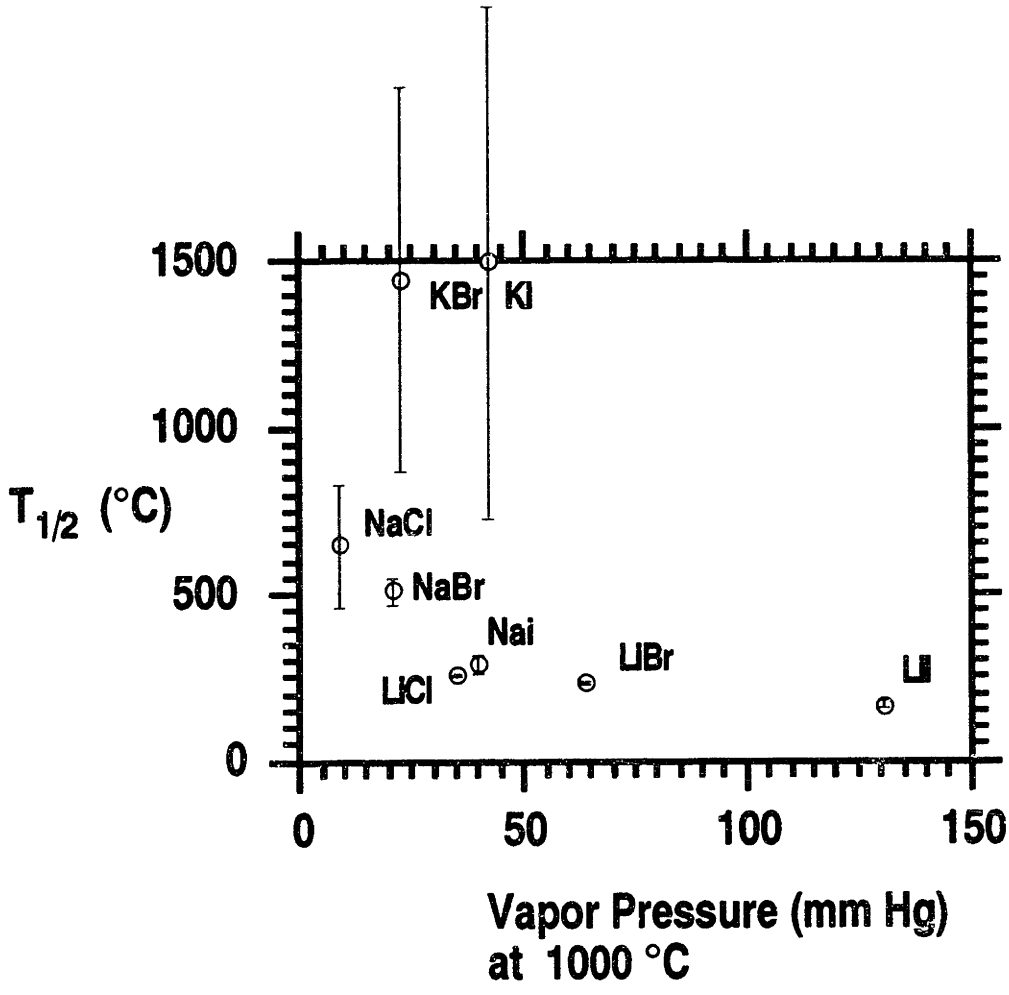
1500
1000
500
0
$T_{1/2}$ (°C)
KBr
KI
NaCl
NaBr
NaI
LiCl
LiBr
LiI
0
50
100
150
Vapor Pressure (mm Hg)
at 1000 °C

between the relative rate of loss of halide and the vapor pressure of the salt.

If the mechanism for the loss of the halide salt is the vaporization of the salt, then the cation must volatilize with the anion. Figure 17 presents the results of Auger analyses of the NaI doped SiO_2 sample before any thermal treatment and after the series of thermal treatments in air. The samples were sputtered to remove any surface impurities, analyzed for the relative content of Na, Si, O, I, and a survey spectra was taken. Figure 17 shows the derivatives of the Auger signal intensities from the survey spectra which show the presence of Si, C (in the unheated sample, presumably from the presence of alkoxides in the gel), O and I (which we cannot distinguish between because the energies are too close), and Na. The normalized content of sodium, the ratio of the content of sodium to the content of silicon, after thermal treatment, decreased to approximately 20% of its original content.[59] This result is consistent with the decrease in the content of iodide estimated by RBS to be approximately 10% under the same conditions.

Examination of the surface of the sample by AES (scanning mode) showed heterogeneities -- precipitates rich in iodide in an iodide-poor sol-gel matrix. These precipitates (most diameters $\leq 2\mu m$) are small compared to the regions examined by both RBS and AES (analytical mode).

Figure 17: Plot of the derivative of the AES signal intensity versus kinetic energy (eV) of the Auger transition for a NaI/SiO_2 sample before and after thermal treatment.

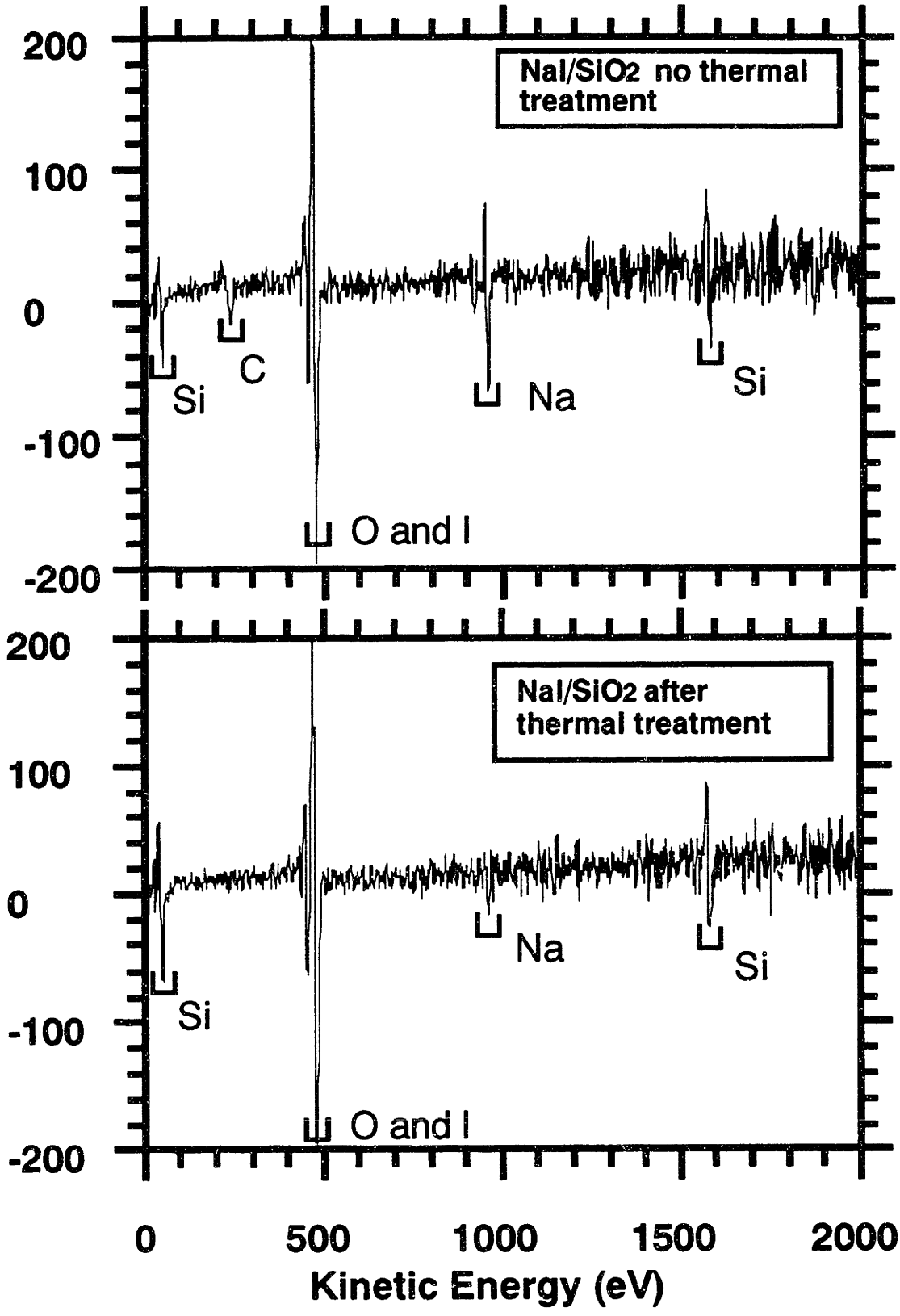
NaI/SiO2 no thermal treatment
NaI/SiO2 after thermal treatment
Si
C
Na
Si
O and I
200
100
0
-100
-200
0
500
1000
1500
2000
Kinetic Energy (eV)

The data presented in this paper for NaI are compatible with, but do not demand, a mechanism for loss of halide by volatilization of NaI. Because AES is a surface sensitive technique, it would not distinguish loss of Na^+ from the surface by volatilization, migration into the bulk, or segregation into phase-seperated regions. Previous work on CsCl-doped SiO_2 revealed the loss of Cl^- without the loss of Cs^+.† This observation suggests loss of HX by hydrolysis of MX.

Figure 18 presents a plot of $T_{1/2}$ versus the ΔG for formation of HX by reaction of MX with water (eq 6), calculated from literature values.‡

$$MX_c + H_2O_l \longrightarrow HX_v + MOH_c \quad (5)$$

$$\Delta G_{HX} = \Delta G_{HX_v} + \Delta G_{NaOH_c} - \Delta G_{MX_c} - \Delta G_{H_2O_l} \quad (6)$$

These data show a rough correlation between the value of the ΔG of formation of the hydrogen halide and the rate of loss of the halide from the silicate matrix.

---

† After initial heating of the sample to 300 °C, the signal due to chloride in the RBS profile decreased to 40 mol% relative to cesium; by 700 °C, it was less than 10%. This observation indicated that chloride ion had volatilized, probably as HCl (Chapter 2).

‡ The ΔG of formation of hydrogen halide from the metal halide, based on calculations from literature values (*Handbook of Chemistry and Physics, 64th ed.*; Weast, R. C., Ed.; CRC Press: Cleveland, Ohio, 1983-84, pp D-50-93) and using crystalline metal halide, crystalline metal hydroxides, gaseous acid halides, and liquid water as the standard states. These values are LiI (16.78) < LiBr (20.79) ~ LiCl (20.87) < NaI (34.76) ~ NaCl (35.04) ~ NaBr (36.67) < KI (44.14) ~ KBr (44.34) in units of kcal/mole at 25 °C.

Conclusions: The depth profile of iodide as a function of temperature in Figure 13 shows an uneven distribution of iodide in the sample after treatments at T = 200 °C/3 h. The composition of the iodide is lower near the surface than near the silicon substrate. This observation suggests that mass transport -- either of the salt diffusing out of the sample or of a reagent (O_2, H_2O) diffusion into the sample -- may be significant under these conditions. At higher temperatures, ther is little evidence for a concentration gradient in the samples. The thicknesses of ther other samples were too narrow to distinguish if there were a concentration gradient.

The difference in the rate of loss of halide under air or argon atmospheres is small enough to be of only marginal significance. The observation that the rate of loss is the same in oxidizing and non-oxidizing environments is inconsistent with oxidation as a step in the mechanism for the loss of halide. The relative rate of loss of the halides correlates with the vapor pressures of halide salts (Figure 16)[58] and with the ΔG of formation of the hydrogen halides from metal halide and water (Figure 18). This observation suggests that the loss of halide proceeds by volatilization of the metal halide itself and/or by hydrolysis of the metal halide to the hydrogen halide, and that the rate of diffusion of the volatile species from the gel matrix may contribute to the overall rate under some conditions.

Figure 18: Plot of the estimated temperature at which half of the halide would be lost ($T_{1/2}$, °C) following the protocol in the research versus the ΔG of formation of the hydrogen halide.† The error bars represent error in the calculation of the least squares line for each salt.

† The ΔG of formation of hydrogen halide from the metal halide, based on calculations from literature values (*Handbook of Chemistry and Physics, 64th ed.*; Weast, R. C., Ed.; CRC Press: Cleveland, Ohio, 1983-84, pp D-50-93) and using crystalline metal halide, crystalline metal hydroxides, gaseous acid halides, and liquid water as the standard states. These values are LiI (16.78) < LiBr (20.79) ~ LiCl (20.87) < NaI (24.76) ~ NaCl (35.04) ~ NaBr (36.67) < KI (44.14) ~ KBr (44.34) in units of kcal/mol.

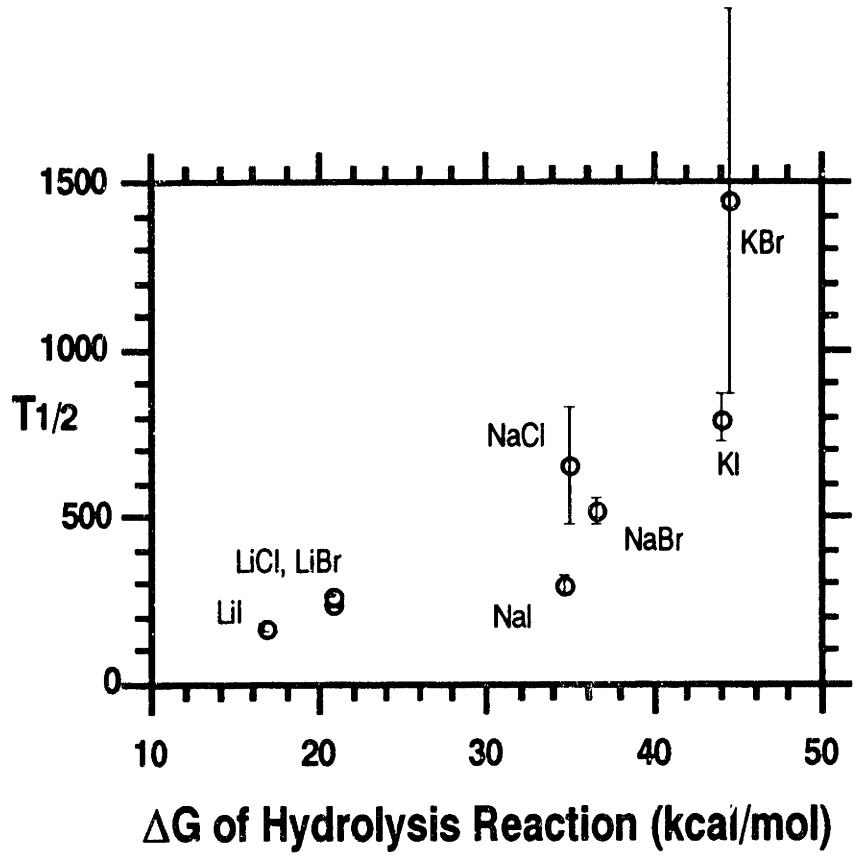
1500
1000
T1/2
500
0
10
20
30
40
50
KBr
KI
NaCl
NaBr
NaI
LiCl, LiBr
LiI
ΔG of Hydrolysis Reaction (kcal/mol)

The decrease in the relative content of sodium, as measured by AES, after thermal treatment is consistent with volatilization of the salt as one mechanism of loss, but is subject to other interpretations. It was not possible to measure the concentration of the ion in the bulk sample, since AES is a surface sensitive technique and RBS cannot distinguish sodium ion against a silicon background. The observed loss of sodium may thus represent either volatilization of NaI or migration of sodium ion away from the surface and into the bulk of the silica or into precipitates of iodide-rich material. In the case of a similar gel containing CsCl[†] , the chloride clearly volatilizes independently of the cesium ion, which remained in the gel.

[†] After initial heating of the sample to 300 °C, the signal due to chloride in the RBS profile decreased to 40 mol% relative to cesium; by 700 °C, it was less than 10%. This observation indicated that chloride ion had volatilized, probably as HCl (Chapter 2).

Experimental

Chemicals: Sodium iodide, sodium bromide, and ammonium vanadate were purchased from Fisher Scientific Co. Tetraethylorthosilicate (TEOS), lithium iodide, lithium chloride, and hydrogen hexafluoroantimoniate (V) were purchased from Alfa, and absolute ethanol from USI Chemicals Co. Sodium chloride was purchased from Mallinckrodt. Potassium bromide and potassium iodide were purchased from Merck. Lithium bromide was purchased from Bradford Scientific, Inc. All reagents were used without purification.

RBS Analysis: The depth profiles of I, V, and O were obtained using the Cambridge Accelerator for Materials Science with a 2 MeV He^+ beam with a diameter of 1 mm. Backscattered particles were detected at 176°, relative to the incoming ion beam, with a 150-mm^2 silicon surface barrier detector placed approximately three inches from the sample and coupled to a multichannel analyzer. Depth profiles of I, V, and O were calculated using the program "Spectrum Analysis"† as were the integrals of their signals.

Figure 18 shows a representative spectrum of a LiI-doped SiO_2 coating on a silicon substrate. The signal for iodide was at highest energy (~ channel 800-730). The signal for silicon in the SiO_2 coating (~ channel 500-430) was lower in intensity than for that in the substrate (~ channel 430)

---

† "Spectrum Analysis", written by Patrick M. Smith, Division of Applied Sciences, Harvard University, is a FORTRAN program based on algorithms from ref.55.

because it was "diluted" by the other components (O, Li^+, and I^-) in the coating.

AES Analysis: AES analyses were performed on a Perkin Elmer Model 660 Auger Spectrometer equipped with an Apollo Workstation 3500 housed at the Center for Materials Science and Engineering and the Cambridge Surface Facility at MIT. Samples were sputtered with 2 keV argon ions (condenser lens setting 4.01; objective lens setting 3.83; ion current density 15 microamps/cm^2) prior to analysis with 5 keV electrons (raster size 1.4 mm x 1.4 mm).

Hydrolysis of TEOS: A solution containing TEOS (61 mL, 273 mmol of Si), ethanol (43 mL), doubly distilled water (5 mL) and aq HCl (0.2 mL of 1 M acid) was heated at 60 °C for 1.5 h. After cooling the solution to room temperature, an additional 4.0 mL of doubly-distilled water and 12 mL of HCl were added to a 100-mL aliquot of the TEOS solution, and the mixture was stored in a freezer (-8 °C), where it was stable (did not gel) for several months. For coating, the solution was diluted by a factor of three with ethanol (0.62 mmol of Si/mL).[9]

Procedure for Doping TEOS with Salt: A solution of NaI in doubly distilled water (0.5 mL, 0.08 mM) was added to

Figure 19: Representative RBS spectrum obtained for a coating of LiI-doped SiO_2 on a silicon substrate.

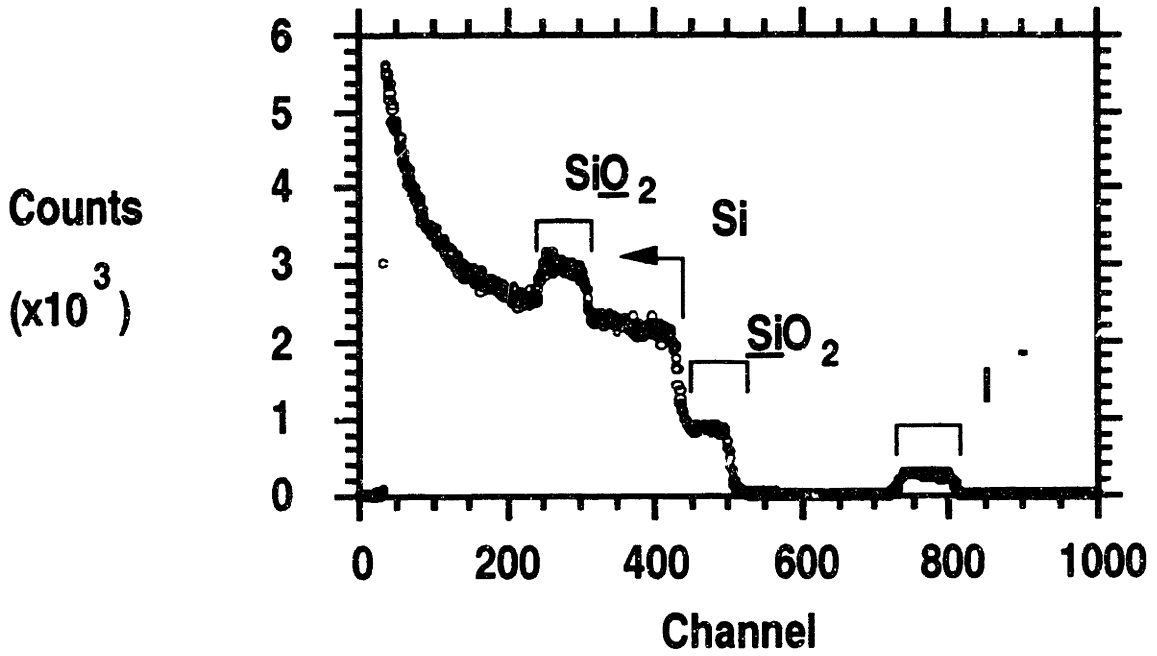
Counts
(x10 3)
6
5
4
3
2
1
0
SiO 2
Si
SiO 2
I -
0
200
400
600
800
1000
Channel

the previously hydrolyzed TEOS (3.10 mM of Si, 5 mL) solution. We coated the sample immediately.

Preparation Of Samples: We coated a silicon <100> wafer using a four-step procedure: first, rinsing the wafer with two 2-mL aliquots each of hexane and ethanol; second, spinning the sample dry on the spin coater (Headway Model PWM 101ECR790) after addition of each aliquot; third, pipetting 2-mL aliquots of halide-doped TEOS solution onto the silicon substrate; fourth, spinning the substrate at 1500 rpm for 2 min. The addition of salts to the TEOS solution affected the viscosity of the solution to various degrees. Because the viscosity of the solution affects the thickness of the coating in spin-coating, the thicknesses of the coatings varied depending on which salt was added. Samples were heated in a Fisher Scientific Isotemp Programmable Ashing Furnace Model 497 at 1 °C/min, held for 3 h at the desired temperature, and cooled to room temperature at 1 °C/min. Samples were analyzed by RBS and returned to the ashing furnace for the subsequent thermal treatment.

Organic Modification of Sol-Gel Materials: An Overview of the Literature

I. Introduction

Sol-gel derived materials, modified by incorporation of organic compounds, have the potential to combine properties of both the inorganic (the metal alkoxide-derived matrix) and the organic components. The high temperatures necessary for the processing of conventional glass -- temperatures at which organic compounds are not thermally stable -- are not necessary for the synthesis of sol-gels because they densify at relatively low temperatures. Thus, the desirable properties of the organic components remain intact throughout processing.

Researchers are only now beginning to explore applications of these hybrid materials. Most research efforts have focused on the synthesis and properties of these hybrid materials, and some structure/property relationships have evolved from these studies.

I.a. Sol-Gel Chemistry

The formation of the inorganic network is a step-growth polymerization process consisting of hydrolysis of the metal alkoxide, with an acid or base catalyst, (equation 1), and subsequent condensation of the metal hydroxide with either another hydroxide (equation 2) or an alkoxide (equation 3). Equations 1-3 show these reactions for silicon alkoxide. They are, however appicable to many metal alkoxides.

$$Si(OR)_4 + H_2O \xrightarrow{H^+} HO\text{-}Si(OR)_3 + ROH \quad (1)$$

$$2\ (RO)_3Si\text{-}OH \longrightarrow (RO)_3Si\text{-}O\text{-}Si(OR)_3 + H_2O \quad (2)$$

$$(RO)_3Si\text{-}OH + Si(OR)_4 \longrightarrow (RO)_3Si\text{-}O\text{-}Si(OR)_3 + ROH \quad (3)$$

Organic moieties can be incorporated into sol-gel networks by at least three general routes. First, addition of telechelic (with functionality at each terminus of the polymer chain) oligomers or polymers containing functionality that is compatible with sol-gel chemistry (Si-OH, Si-OR, or C-OH groups) allows their incorporation by co-condensation with metal alkoxides. Second, addition of organo-metal alkoxides, R'Si(OR)3, hydrolyzed either alone or with unmodified-metal alkoxides, incorporates the R' functionality directly into the network via hydrolytically stable C-Si bonds. Third, physical incorporation of the organic component into the gel by either adding the organic to the metal alkoxide monomer solution or infiltrating the organic into the pores of a preformed, dried, inorganic gel with the organic component incorporates organics into the gel without chemically linking them to the inorganic network. These approaches are summarized in Scheme 1.

II. The Incorporation of Telechelic Polymers and Oligomers

In general, the incorporation of elastomeric oligomers or polymers into the gel network contributes flexibility and relaxation, allowing for the formation of crack-free, hybrid monoliths. The chemical incorporation of elastomers therefore improves processability over those of purely inorganic gels.

II.a. Incorporation of Hydroxy Terminated Polydimethylsiloxane (PDMS) Polymers and Oligomers

Elastomeric, hydroxy-terminated, polydimethysiloxanes (Tg ~ -100°C to -80°C depending on molecular weight) can incorporate directly into the sol-gel network through condensation reactions of the polymer's terminal SiOH groups with those of TEOS. The commercial availability of telechelic PDMS in a range of molecular weights (550 to 36,000) allowed for the study of the effect of molecular weight on the hybrid glass properties.

II.b. Incorporation of PDMS Into SiO_2

The incorporation of polydimethysiloxane (550 and 1700 mwt) into the SiO_2 network derived from tetraethylorthosilicate (TEOS) resulted in the formation

Scheme 1: Modes of Incorporation of Organic Components into Sol-Gels

1) Telechelic Oligomers and Polymers

$xHO\text{-}(R')_x\text{-}OH + ySi(OR)_4 + H_2O \longrightarrow (SiO2)y(R'O\text{-})x + ROH$

$R' = -Si(CH_3)_2\text{-}[OSi(CH_3)_2]_x\text{-}OSi(CH_3)_2\text{-}$ or $-(CH_2)_4\text{-}[O(CH_2)_4]_x\text{-}$

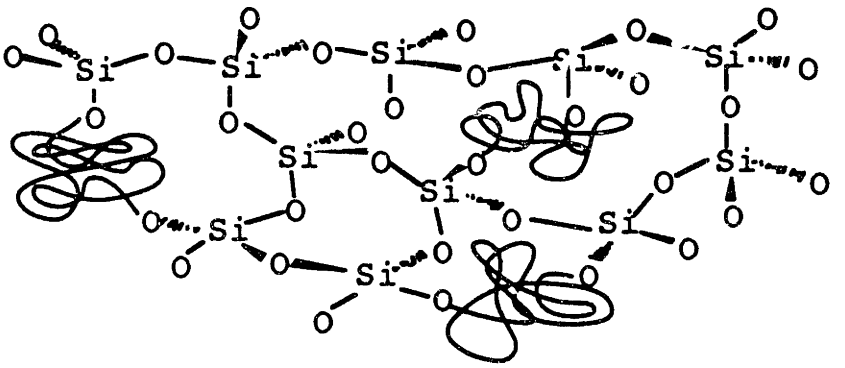

2) Chemically-Modified Metal Alkoxides

$xR'Si(OR)_3 + ySi(OR)_4 + H_2O \longrightarrow (SiO_2)y(R'SiO_{3/2})x + ROH$

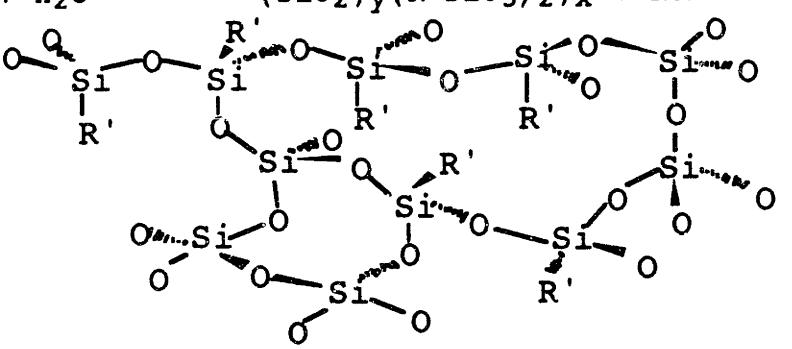

3) Physical Incorporation

$xR' + ySi(OR)_4 + H_2O \longrightarrow (SiO_2)y(R')x + ROH$

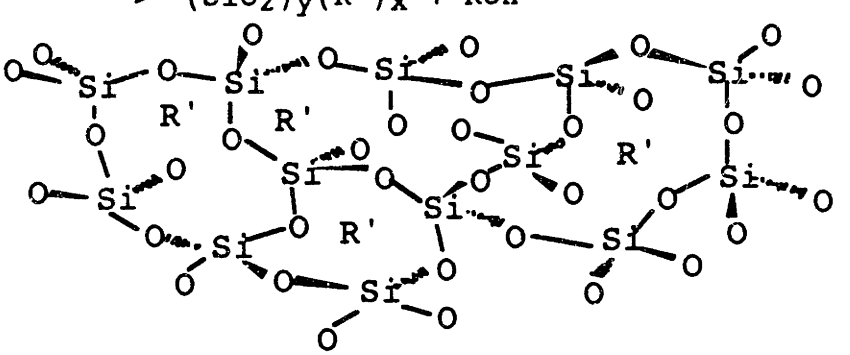

of clear monoliths with considerably more flexibility than purely inorganic gels. In all samples, PDMS existed in two environments, as seen by two tan δ maxima (Tg's) from dynamic mechanical analysis (DMA).[60] These multiple and broad Tg's indicated multiple environments for the polymer. The phase with the lower Tg had the more polymer-rich, less restrictive environment compared with the phase with the higher Tg. These phases must either have been very small, less than the wavelength of visible light, or the phases must have had similar indices of refraction, because the samples were clear and did not scatter light.

Structure - property investigations of this system showed that, in general, polymers were incorporated into the network more homogeneously with a higher acid-catalyst content, a higher TEOS content (48 to 70 weight %), and a lower oligomeric molecular weight (550 vs 1700 mwt).[60] Results of small angle x-ray analyses (SAXS) indicated a decrease in the mean square electron density for samples with higher acid catalyst content, which was consistent with an increase in the homogeneity of the samples.[60] As the content of the acid catalyst increased, Young's modulus decreased, and elongation at break increased. Likewise, as the TEOS content increased, Young's modulus increased and the maximum for the higher tan δ peak -- the Tg for the polymer phase that is more homogeneously incorporated -- increased.[60,61] Raman spectroscopic analyses of these hybrid gels showed broadening but no shift of the Si-O absorbance at 800 cm^{-1} as the network formed. The CH bending mode at 1460-1480 cm^{-1} (from the alkyl group in the alkoxide) decreased in intensity as hydrolysis proceeded. It did

not disappear, however, indicating either incomplete hydrolysis of the alkoxide or incomplete loss of organics from the sample.[62]

II.c. Incorporation of PDMS into SiO_2/TiO_2

The incorporation of polymeric and oligomeric PDMS into silicon-titanates also resulted in clear monoliths with multiple and broad Tg's, as measured by DSC[63] and DMA[64] indicating multiple environments for the polymer. The order of addition was found to be important in the successful synthesis of clear pieces. It was necessary for the "free" water to be incorporated in hydrolysis reactions with the silicon alkoxides before the titanium alkoxide was added. Otherwise, the titanium alkoxide hydrolyzed immediately to TiO/OH particulates that precipitated. Samples that were optically clear, and made from the 36,000 molecular weight PDMS precursor, did not crystallize during the DSC experiment, whereas the starting material did (Tm ~ -40 °C). This reduction in mobility to crystallize was consistent with a model in which the polymer was incorporated into the network,[65] and not with a model in which the polymer was physically mixed with inorganic particulates. Purely physical mixing would lead to an increase, rather than the observed decrease, in the rate of crystallization of PDMS, presumably by heterogeneous nucleation.[65]

Characterization of the mechanical properties of these samples showed a higher Young's modulus and greater toughness based on inorganic content of starting material compared with the PDMS/SiO_2 system.[66]

II.d. Incorporation of Triethoxysilyl Terminated Oligomeric Tetramethyleneoxide (PTMO)

Polytetramethyleneoxide (PTMO) contributes relaxation characteristics to the gel network, thus allowing for the formation of crack-free monoliths as did PDMS. Some major differences exist between PDMS and PTMO: PTMO is soluble in water and PDMS is not; PTMO incorporates into the network through triethoxysilyl end-groups (with three alkoxide groups at each polymer chain end) whereas hydroxy-terminated PDMS has only one reactive moiety (Si-OH).

II.e. Incorporation of PTMO into SiO_2

The incorporation of triethoxysilyl-terminated poly(tetramethylene oxide) into TEOS derived SiO_2 gels resulted in clear monoliths which exhibited higher extensibility (105 % for 50 % TEOS/PTMO - mwt 2,000 precursor compared to 8 % for 50 % TEOS/PDMS - 1700 mwt precursor), higher tensile strength, and lower Young's modulus (2.4 MPa vs 12 MPa) than hybrid gels made from PDMS and TEOS.[66] Dynamic mechanical analyses indicated only one Tg, compared with two for the PDMS system,[66] however some local phase separation still existed.

As the molecular weight of the PTMO precursor was increased, from 650 to 2,000 mwt, Young's modulus decreased.[67] No apparent trend in elongation at break based on molecular weight of the polymer precursor was evident. DMA studies revealed one broad tan δ maximum for each sample, compared to multiple maxima for the SiO_2/PDMS series of samples. The maximum of the tan δ peak was

higher for the sample made with 650 mwt PTMO than for those made from 1,000 or 2,000 mwt PTMO. These results were consistent with a single polymer environment.

SAXS experiments revealed maxima, shifting to smaller angle as the molecular weight increased, in the scattering intensities of PTMO/SiO_2 samples. These results contrasted with the monotonically decreasing scattering intensity profiles from the PDMS/SiO_2 samples. A maximum in the scattering intensity in the SAXS data suggested a "correlation length" relating to the molecular weight of the polymer starting material, presumably due to microphase separation.[66]

As the TEOS content increased (50 to 70 wt % TEOS content with 2,000 mwt PTMO starting material), Young's modulus increased, ultimate strength increased (2.1 MPa for 50 wt % TEOS to 30.4 MPa for 70 wt % TEOS), and DMA studies showed an increase in Tg from 0 °C for the 50 weight % sample to broad, bimodal maxima in tan δ at 30 °C and 80 °C.[66] Apparently the sample with 70 weight % TEOS contained two polymer environments.

Aging effects on the properties of the samples suggested that further diffusion-controlled condensation occurred over time in these samples.[66]

II.f. Incorporation of PTMO Into SiO_2/TiO_2

Compared to samples containing PTMO/SiO_2, incorporation of PTMO into SiO_2/TiO_2 using TEOS and Ti (IV) isopropoxide resulted in samples with higher stress at break, lower elongation at break, and higher Young's modulus, as a function of content of titanium

alkoxide starting material.[66] SAXS experiments revealed that the PTMO/SiO_2/TiO_2 samples had a higher scattering intensity compared to that of PTMO/SiO_2. They also showed maxima in their scattering intensities that were similar to those for PTMO/SiO_2 samples. The shift in the maxima, however, depended on the synthetic procedure used.[66]

DMA experimental results on these samples showed a broader range for Tg centered at lower temperatures than for samples containing no titanium.[67] This result indicated that the incorporation of PTMO into SiO_2/TiO_2 results in an environment (lower Tg - less homogeneously incorporated) which is different from that of SiO_2 (higher Tg - more restrictive).

II.i. Synthesis of Oligomers (siloxanes polyimides, etherketones, and polysilsesquioxanes) for Incorporation into Sol-Gels

The synthesis of oligomeric precursors with controlled molecular weight for incorporation into sol-gels included trimethoxysilylpolydimethylsiloxanes, methoxy-terminated polyarylketones, and derivatized polyimide precursors.[68] The synthesis and incorporation of aryl-bridged polyselsesquioxanes (phenyl, biphenyl, and terphenyls with triethoxysilyl and trichlorosilyl endgroups) into an SiO_2-like network as microporous materials resulted in clear pieces with a high surface area (750-800 m^2/g with mean pore diameter less than 2 nm, as measured by nitrogen adsorption.[69] Studies of hydrolysis using ^{13}C NMR CP/MAS to measure bound ethoxy groups showed that they decreased to $\leq$ 10

% upon acidic hydrolysis and that they disappeared completely upon basic hydrolysis. No Q4 (silicon with four oxygens attached) resonances existed in the ^{29}Si CP/MAS NMR spectra for either method of catalysis, indicating that no aryl-silicon bond cleavage occurred. The degree of condensation was approximately 60-70 % under acidic conditions and 75-85 % under basic conditions, as measured by integration of the T^1 ($ArSi(OH)_2(OSi)$), T^2 ($ArSi(OH)_1(OSi)_2$), and T^3 ($ArSi(OSi)_3$) peaks in the ^{29}Si NMR.

III. Incorporation of $RSi(OR)_3$ with $Si(OR)_4$ or $M(OR)_n$

The relative reactivities of alkyl,alkoxysilanes alkoxides, $(CH_3)_nSi(OEt)_{4-n}$, depended on the degree of substitution and the catalytic conditions (acidic or basic). The relative rates of hydrolysis for methyl-substituted silicon alkoxides were $n = 3 \geq n = 2 > n = 1 >> n = 0$ under acidic catalysis. These relative rates were reversed under basic hydrolysis conditions.[70] These differences in relative reactivities are significant for the formation of homogeneous materials made by mixing substituted and non-substituted alkoxides, however, very few microscopic structure/macroscopic property relationship have been recognized for these materials. This situation is more complicated for systems where organic monomers are added to form an interpenetrating network with the inorganic gel. Nevertheless, several materials made by this approach have useful properties. These materials include: water-wettable, and dioxygen-permeable contact lenses, formed by the reaction of $(RO)_3Si(CH_2)_3OC_2H_5$, $Ti(OR)_4$, and $CH_2=C(CH_3)COOR'$;[71] scratch resistant coatings made

from $Ti(OR)_4$, $Si(OR)_4$, and $(RO)_3Si(CH_2)_3OC_2H_5$,[72] or $Zr(OR)_4$, $Si(OR)_4$, and $(RO)_3Si(CH_2)_4CHOCH$;[73] selective absorbers and membranes from either $(CH_3)_2Si(OR)_2$ or $(Ph_2)Si(OR)_2$ and $Si(OR)_4$;[74] coatings with chemical functional groups at surfaces from $(CH_3)_2Si(OR)_2$, $(RO)_3Si(CH_2)_3NH_2$, and $(RO)_4Si$;[75] abrasive coatings from $(CH_3)_2Si(OR)_2$ and $(RO)_4Si$;[76] and heat-seal substrates that show good resistance to moisture and good adhesion from $(Ph)_2SiCl_2$ and $(RO)_4Si$.[77]

One structure/property study of these $R'Si(OR)_3/Si(OR)_4$ systems showed trends in their properties based on composition of starting materials. Relative differences in the polar and dispersive contributions of surface free energy, characterized by measurements of contact angles of water and methylene iodide, showed that the polar contribution to surface energy decreased with the addition of organic modified monomers (phenyl, methyl, and n-octyl) into sol-gel SiO_2, TiO_2, or Al_2O_3 films.[78] The polar contribution of surface free energy increased as a function of temperature of thermal treatment, indicating pyrolysis of organic functionality. The thermal expansion coefficient of these samples increased with organic modification, most drastically for the n-octyl modified sample (22.0×10^{-6} °C^{-1} versus 0.94×10^{-6} °C^{-1} for the SiO_2 film). These samples also showed, as expected, a dependence of monomer composition on their indices of refraction.

IV. Physical Incorporation of Monomers (Methyl methacrylate) and Dyes into Sol-Gels

Monomers, incorporated into previously dried, porous gels, infiltrate gel pores and polymerize under thermal treatment. Polymethylmethacrylate (PMMA)/SiO_2 samples made in this manner have mechanical properties -- densities, moduli of rupture (MOR), compressive strengths, Vicker's hardnesses, abrasion resistances, and elastic moduli (in compression) -- that are linearly related to the mole fraction of PMMA used in their preparation.[79] Also, a non-linear relationship exists between the index of refraction and the volume fraction of polymer that agrees well with theory.[79]

Sol-gel derived matrices have the potential as useful hosts for non-linear optical materials because they are optically transparent and chemically stabile. By filling the pores with dye-doped methylmethacrylate, optical losses due to Rayliegh scattering decreased. The flexibility of processing of these materials allowed for the introduction of non-linear optical dyes either by addition of the monomers in the precursor solution, or by absorption into the pores of a preformed gel-host.[80]

Measurements of the DC Kerr effect, the change in the index of refraction of a medium due to the interaction of the dipole moment of the dye with an applied electric field, for 2-methyl-4-nitroaniline in a gel derived from a PMMA/SiO_2 composite showed that the dye was slightly more mobile in the glass-polymer host than in a pure PMMA host.[81] The dye was less mobile in both solid hosts than in a solution of dioxane. The PMMA/SiO_2 host also improved the oxidative stability of the dye.

Applications of dye-doped SiO_2 gels included: optical data storage using 1,4 dihydroxyanthraquinone;[82] dye lasers using

rhodamine 6G,[83-87] rhodamine B,[84-86] coumarin,[86,88] and 4-methylembelliferone;[88] fluoresence probes using pyrene,[86,88-91] and acridine;[86] photoconductors using bixin;[86] and luminescent probes using $ReCl(CO)_3L$ (L = bidentate diimine);[87] and non-linear optical materials using 2-methy-4-nitraniline.[88]

Conclusions

Many synthetic approaches are available for the formation of organic-modified, sol-gel materials. Studies on the structure/property and composition/property relationships allow for the rational syntheses of polymer incorporated gels, and further investigations along these areas are needed. The products of this approach are certainly unique materials. The advantage of these products over materials made from more conventional processes must, however, be demonstrated.

The Thermal and Oxidative Stability of 2,4-Dinitroaniline in Sol-Gel Derived Coatings[†]

Abstract: The relative thermal and oxidative stabilities of N-[3-(triethoxysilyl)propyl]2,4-dinitroaniline (1), incorporated covalently into sol-gel coatings and of 2,4-dinitroaniline, incorporated non-covalently into similar coatings, was monitored by measuring their UV-VIS spectra as a function of temperature of thermal treatment. The relative thermal stability of this chromophore in sol-gel derived films was unchanged under several conditions: with no overcoat of SiO2; with a dense sol-gel derived overcoat of SiO2; with a porous overcoat of SiO2; over a porous, high-surface area coating of SiO2; and copolymerized with or physically incorporated into dense and porous SiO2 films derived from tetraethylorthosilicate (TEOS).

Introduction: Modification of sol-gels, by covalent or non-covalent incorporation of organic components, results in materials that combine the properties of the organic and inorganic

---

[†] (1) Supported in part by the National Science Foundation (CHE-88-12709). The Cambridge Accelerator for Materials Science was purchased and supported (in part) through a DARPA/URI grant and is housed in the Harvard University Materials Science Research Laboratory, an NSF-funded facility (DMR-86-14003)

components.‡ Organic components have been incorporated covalently by hydrolyzing a mixture of silicate esters (for example $Si(OEt)_4$

---

‡ Some of these applications include: gas permeable contact lenses (Phillipp, G.; Schmidt, H. *J. of Non-Crystalline Solids*, **1984**, *63*, 283-291.), substrates for heat sealing (Schmidt, H.; Scholze, H.; Tunker, G. *J. of Non-Crystalline Solids*, **1986**, *80*, 557-563.), laser dye-doped gels (Dunn, B.; Knobbe, E.; McKiernan, J.M.; Pouxviel, J.C.; Zink, J.I., in *Better Ceramics Through Chemistry III* Materials Research Society Symposium Proceedings volume 121; Brinker, C.J.; Clark, D.E.; Ulrich, D.R., Eds.; Materials Research Society: Pittsburgh, Pennsylvania, 1988, 331-342.), coatings with variable indices of refraction (Melpolder, S. M.; Coltrain, B. K., in *Better Ceramics Through Chemistry III* Materials Research Society Symposium Proceedings volume 121; Brinker, C.J.; Clark, D.E.; Ulrich, D.R., Eds.; Materials Research Society: Pittsburgh, Pennsylvania, 1988, 811-816.), scratch-resistant eyeglass coatings for plastic lenses (Schmidt, H.; Seiferling, B; Philipp, G.; Deichmann,K., in *Ultrastructure Processing of Advanced Ceramics*; Mackenzie, J,D.; Ulrich, D.R., Eds.; Wiley-Interscience Publications, John Wiley and Sons: New York, New York, 1988, 651-660.), and composites with high strength and ductility (Pope, E.J.A.; Mackenzie, J.D., in *Better Ceramics Through Chemistry II* Materials Research Society Symposium Proceedings volume 73; Brinker, C.J.; Clark, D.E.; Ulrich, D.R., Eds.; Materials Research Society: Pittsburgh, Pennsylvania,1986,

and $R'Si(OR)_3$). The formation of the silica sol-gel network is a step-growth polymerization consisting of hydrolysis of the silicon alkoxide, and condensation of the resulting hydroxyl group with hydroxyl or alkoxide groups (eq 1-3; R = alkyl, alkoxyl, R' = alkyl).[92]

$$RSi(OR')_3 + H_2O \xrightarrow{H^+ \text{ or } OH^-} RSi(OR')_2OH + R'OH \qquad (1)$$

$$2\ RSi(OR')_2OH \longrightarrow R(R'O)_2Si\text{-}O\text{-}Si(OR')_2R + H_2O \qquad (2)$$

$$R(R'O)_2Si\text{-}OH + RSi(OR')_3 \longrightarrow R(R'O)_2Si\text{-}O\text{-}Si(OR')_2R + R'OH \qquad (3)$$

The low temperatures that are typical of sol-gel processing allow the desirable properties of organic dopants to be preserved. The inorganic networks, in turn, provide hard, chemically resistant matrices for the organic component.

A sol-gel network might, in principle, help to stabilize the organic component against thermal or oxidative decomposition at high temperatures. The diffusion coefficient of dioxygen through fully densified sol-gel-derived SiO_2 coatings on Si and on SiC ($D_{O_2} < 10^{-14}$ cm^2/sec at 750°C)[93] is indistinguishable from that through thermally grown SiO_2. Oxidation of silicon or of silicon

---

809-814 and Pope, E. J.; Asami, M.; Makenzie, J. D. *J. Mat. Res.*, **1989**, *4*, 1018-1026).

carbide coated with a sol-gel-derived SiO_2 film is limited by the diffusion of oxygen through this film.[94,95] If oxidative degradation of organic molecules included in sol-gel matrices is similarly limited by mass transport of oxygen through the matrix, then a coating of SiO_2 should retard degradation of the organic dopants by serving as a barrier to diffusion of oxygen.

The purpose of this work was to evaluate the capability of a sol-gel derived silica (SiO_2) network to improve the thermal or oxidative stability of organic components included in it. We incorporated the organic chromophore 2,4-dinitroaniline into sol-gel derived matrices by three procedures (Figure 20): first, by hydrolyzing the derivatized chromophore 1 alone, to form arylsiloxane polymers (eq 4); second, by copolymerizing it into a matrix by hydrolyzing a mixture of 1 with tetraethylorthosilicate (TEOS)(eq 5); third, by mixing underivatized 2,4-dinitroaniline with hydrolyzed TEOS (eq 6). Monitoring the UV-VIS absorption of the chromophore as a function of temperature of thermal treatment under air and under argon measured the relative thermal/oxidative stability of the 2,4-dinitroaniline moiety in these environments. We chose 2,4-dinitroaniline as a test material because its UV absorption at 350 nm can be measured with minimal interference from either the silicate matrix/coating or the sapphire substrate, and because it it easily prepared. This chromophore is representative of those that might be considered for application in optical materials.

We prepared samples of the types illustrated schematically in Figure 20 and examined the stability of the chromophore included

in them, both under argon and under air over the temperature range from 100 to 700 °C.

$$ArNH(CH_2)_3Si(OEt)_3 + H_2O \xrightarrow[THF]{H^+} (ArNH(CH_2)_3SiO_{3/2})_n \qquad (4)$$

$$n\ ArNH(CH_2)_3Si(OEt)_3 + m\ Si(OEt)_4 + H_2O \xrightarrow[THF]{H^+} (ArNH(CH_2)_3SiO_{3/2})_n(SiO_2)_m \qquad (5)$$

$$x\ ArNH_2 + m\ Si(OEt)_4 + H_2O \xrightarrow[THF]{H^+} ArNH_2 \text{ in } (SiO_2)_m \qquad (6)$$

$ArNH(CH_2)_3Si(OEt)_3$ =

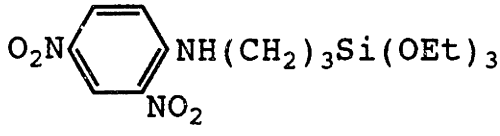

1

The thermal stability of $(ArNH(CH_2)_3SiO_{3/2})_n$ alone (Figure 20, Structure A - the condition with the highest organic content and the lowest expected thermal/oxidative stability) served as a standard against which to test the other structures. We hypothesized that the placement of a barrier to oxygen diffusion -- the coating of dense and of porous SiO_2[9,52] (Figure 20,

Structures B and C) over the $(ArNH(CH_2)_3SiO_{3/2})_n$ layer -- might improve the oxidative stability by limiting the diffusion of oxygen.[93-95] Preparation of these dense and porous layers followed literature procedures.[9,52†]

Coating a layer of high surface-area SiO_2 with $(ArNH(CH_2)_3SiO_{3/2})_n$ allowed us to test whether the increased surface areas at the $(ArNH(CH_2)_3SiO_{3/2})_n$/air and $SiO_2/(ArNH(CH_2)_3SiO_{3/2})_n$ interfaces affected the stability of the chromophore (Figure 20, Structure D).

The stability of the chromophore in the gel, made by copolymerizing $(ArNH(CH_2)_3SiO_{3/2})_n$ with TEOS (Figure 20, Structures E and F) reflected both the effects of reduced oxygen diffusion to the chromophore and of intimate incorporation of the chromophore with the inorganic matrix.

Dissolving 2,4-dinitroaniline in TEOS formed a precursor for both dense and porous coatings incorporating the chromophore non-covalently (Figure 20, Structures E and F). By comparing the differences in stability between covalently and non-covalently incorporated chromophore, we expected to test whether covalent incorporation of the chromophore had any effect on its stability.

---

† These preparations for dense and porous SiO_2 result in SiO_2 coatings with reported indices of refraction of 1.42-1.43 and 1.21-1.24 respectively, when made by dip-coating (see refs. 9 and 52).

Figure 20: Schematic illustrations of structures that incorporate the arylsiloxane moiety into (or onto) a silicate matrix. The material indicated by ▬ was prepared by hydrolysis of 1. The material indicated by ▭ was prepared by cohydrolysis of 1 and TEOS or by physically mixing 2,4-dinitroaniline with previously hydrolyzed TEOS (mole ratio 1:144 for formulations forming dense SiO_2, 1:31 for porous SiO_2). ▭ is unmodified SiO_2, prepared from TEOS alone, and ▭ is the sapphire substrate (crystalline Al_2O_3). The porous coating of SiO_2 consists of spherical silica particles.[92]

A

Chromophore-modified coating on sapphire: alone,

B

under a dense SiO_2 coating,

C 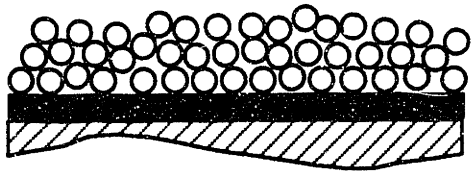

under a porous SiO_2 coating,

D 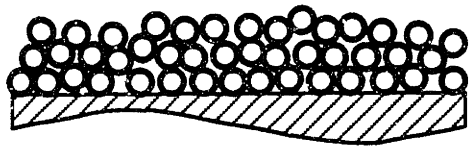

over a porous, high surface area coating,

E 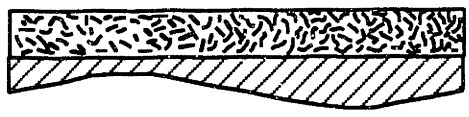

copolymerized or physically incorporated into a dense SiO_2 coating,

F 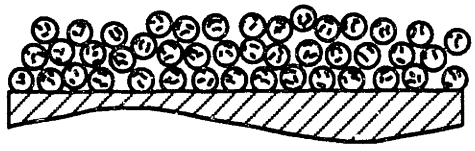

and copolymerized or physically incorporated into a porous SiO_2 coating.

Experimental

Materials: N-[3-(triethoxysilyl)propyl]2,4-dinitroaniline (1) (Petrarch), 2,4-dinitroaniline (Aldrich), tetraethylorthosilicate (Alfa), ammonium hydroxide (Mallinckrodt), and absolute ethanol (USI) were used as received. Hydrochloric acid (Mallinckrodt) was diluted with doubly distilled water. The sapphire substrates were optical quality single crystals (2.00" long ± 0.02 x 0.500" wide ± 0.015 x 0.018" thick ± 0.003), purchased from Saphikon, Inc. Milford N.H.

General Procedure: Treatment of 1 with acidified water in THF and stirring overnight converted it to a yellow sol of $(ArNH(CH_2)_3SiO_{3/2})_n$. This sol was used in coating the substrate. An optical quality single crystal of sapphire (α-Al_2O_3) was coated with the gel by dipping half of it into the prehydrolyzed, chromophore-modified, sol-gel solution. The coated crystal was air dried, heated at 5 °C/min to 100°C, held at 100 °C for 5 min, cooled at 5 °C/min to 25 °C, and placed directly into the spectrophotometer with the dip-coated side in the bottom end of the sample holder. The UV-VIS spectrum of the film was measured directly in transmission mode. Sapphire was an appropriate substrate for our study, because it is thermally stable in the temperature range of interest ($\leq$ 700 °C), it is optically transparent in that part of the UV-VIS spectrum where the chromophore absorbs (350 nm), and it was available in a size appropriate for our sample holder.

These samples were heated without further modification and served as controls in studies of stability. They corresponded to the type of sample indicated by A in Figure 20.

The surfaces of samples prepared by this procedure -- $(ArNH(CH_2)_3SiO_{3/2})_n$ -- were hydrophobic and were not wetted by the sol-gel solutions applied subsequently to provide SiO_2 overcoats. To improve wetting and adhesion, samples (Structure A) were treated briefly with an oxygen plasma. This surface-oxidized sample, when dipped into the appropriate hydrolyzed solution of TEOS, formed a dense[9] or porous[52] SiO_2 coating over the chromophore-containing layer (Figure 20, Structures B and C) after being air dried, heated at 5 °C/min to 100°C for 5 min, and cooled at 5 °C/min to 25 °C. As an alternative method of preparing a porous sample, the sapphire substrate (without the layer containing the chromophore) was first dip-coated with a sol-gel suspension that formed a porous silica.[52] Heating this sample at 200 °C for 5 min consolidated the porous SiO_2 coating. Subsequently, it was coated with the arylsilicate solution, air dried, heated at 5 °C/min to 100 °C for 5 min, and cooled to 25 °C at 5 °C/min (Figure 20, D). The porous SiO_2 surface was hydrophilic enough for the chromophore-modified solution to wet and adhere to it; a surface treatment with oxygen plasma was unnecessary for this sample.

Cohydrolysis of compound 1 with TEOS (mole ratio 1:144, 1:TEOS, for the dense formulation and 1:31 for the porous formulation) formed "composite" materials with 1 intimately and covalently incorporated into the inorganic gel for both dense and porous SiO_2

formulations (Figure 20, Structures E and F). Alternatively, the addition of 2,4-dinitroaniline to TEOS (mole ratio 1:144, chromophore to TEOS, for the dense formulation and 1:33 for the porous formulation) before the hydrolysis step for both formulations resulted in non-covalently incorporated 2,4-dinitroaniline in dense and porous SiO_2 (Figure 20, Structures E and F). Samples made according to coating structures E and F, with both covalently and non-covalently incorporated chromophore, were dip-coated onto sapphire substrates and initially heated to 100 °C for 5 min and cooled at a rate of 5 °C/min prior to the initial UV-VIS measurement.

Procedure for Thermal Treatment: Samples were heated in air or argon at a rate of 1 °C/min to 200 °C, held at that temperature for two hours, and cooled at a rate of 1 °C/min to 25 °C. The UV-VIS spectrum was measured in transmission mode. The samples were returned to the furnace and heated to a higher temperature using the same heating cycle and heating rate. The temperatures for thermal treatment ranged from 200 to 700°C in 100 °C intervals.

Hydrolysis of TEOS Coatings of Dense SiO_2: A solution containing TEOS (61 mL, 273 mmol of Si), ethanol (43 mL), doubly distilled water (5 mL) and aq HCl (0.2 mL of 1 M acid) was heated at 60 °C for 1.5 h. After cooling the solution to room temperature, an additional 4.0 mL of doubly-distilled water and 12 mL of HCl were added to a 100-mL aliquot of the TEOS solution, and the mixture was stored in a freezer (-8 °C), where it was stable (did not gel) for several months.[9]

Hydrolysis of TEOS Coatings of Porous SiO_2: To a solution containing ethanol (328 mL) and NH_4OH (10.7 mL of reagent grade), stirred vigorously with a 1/4" Teflon-coated magnetic stirrer, was added TEOS (33.8 mL, 151 mmol of Si) dropwise over approximately 20 min at room temperature (25 °C). The solution was stirred overnight and stored in a freezer (-8 °C).[8]

Hydrolysis of N-[3-(triethoxysilyl)propyl]2,4-dinitroaniline (1): To a solution of (1) (0.1 g, 0.26 mmol) in THF (20 mL) was added HCl (0.02 mL of a 1N solution, 1.1 mmol of H_2O). The mixture was stirred overnight at room temperature.

Copolymerization of 1 with TEOS Formulations for Coatings of Dense SiO_2: To a solution containing previously hydrolyzed TEOS (10 mL, 18.6mmol) and ethanol (90 mL) was added 1 (0.05 g, 0.13 mM). The solution was stirred overnight and stored in a freezer (-8 °C).

Copolymerization of 1 with TEOS Formulations for Coatings of Porous SiO_2: To a solution in a 25 mL round-bottomed flask containing ethanol (13.6 mL), ammonium hydroxide (0.44mL, 29.9 weight %), and 1 (0.08g, 0.2mmol) was added TEOS (1.4 mL, 6.3 mmol) dropwise while the solution was stirred vigorously with a 1/4" Teflon-coated magnetic stirrer. The solution was stirred overnight at room temperature (24 °C) and subsequently stored in a freezer (-8 °C).

Incorporating 2,4-Dinitroaniline Non-Covalently into a Sol for Coatings of Dense SiO_2: To a solution of ethanol (10 mL) and previously hydrolyzed TEOS (10 mL, 18.6 mmol) was added

2,4-dinitroaniline (0.02 g, 0.13 mmol). The solution was stored in a freezer (-8 °C).

Incorporating 2,4-Dinitroaniline Non-Covalently into a Sol for Coatings of Porous SiO_2: To a solution in a 25 mL round-bottomed flask containing ethanol (13.6 mL), ammonium hydroxide (0.44 mL, 29.9 weight %), and 2,4-dinitroaniline (0.035 g, 0.19mmol) was added TEOS (1.4 mL, 6.3 mmol) dropwise while the solution was stirred vigorously with a 1/4" Teflon-coated magnetic stirrer. The solution was stirred overnight at room temperature (24 °C). The solution was stored in a freezer (-8 °C).

RBS Analysis: The depth profiles of cesium were obtained using the Cambridge Accelerator for Materials Science with a 2 MeV He^+ beam.

Results and Discussion

Characterization of the Chromophore-Modified Coatings and SiO_2 overcoats: Sample characterization consisted of measuring both the thicknesses of coatings, by Rutherford Backscattering Spectroscopy (RBS), and the UV-VIS spectra of the chromophore. The measurements of thickness were necessary to verify of the presence of the SiO_2 overcoats.

Measurement of Coating Thicknesses: We determined the thickness of all coating by RBS. These experiments were carried out using Si <100> wafers as substrates. Measurement of the thicknesses could not be measured on sapphire because the oxygen signals from SiO_2 and α-Al_2O_3 could not be differentiated. Figure

21 shows representative spectra.† The thickness of the chromophore-modified coatings was 300 ± 200 Å. The thickness of the dense SiO_2 overcoatings was 6,700 ± 200 Å, and of the porous SiO_2 overcoating 4,200 ± 200 Å.

UV-VIS Spectra of the Chromophores in Sol-Gel Derived Coatings: Figure 22 shows survey transmission UV-VIS spectra. These spectra include "initial" spectra taken before significant heating and after heating to the highest temperatures used (700 °C), both in air and under argon.

Figure 23 presents the UV-VIS spectra and a plot of relative absorbance at 350 nm of a film derived from 1 alone (Figure 20, Structure A) as a function of temperature of thermal treatment, before significant heating and after heating in air to temperatures in 100 °C steps from 200 °C to 700 °C. The relative absorbance is the ratio of the measured absorbance to that after an initial treatment at 100 °C for 5 min.

---

† In contrast to the relatively narrow oxygen signal (~ 100 channels) in the SiO_2/Si spectrum, the signal for oxygen in the Al_2O_3 sample continues throughout the spectrum. This spectrum establishes that the signal for oxygen in an SiO_2 coating on Al_2O_3 could not be differentiated from that of the signal from the sapphire substrate.

Figure 21: Representative RBS spectra of: the silicon substrate alone; an SiO_2 coating on the silicon substrate; and the sapphire (α-Al_2O_3) substrate alone.

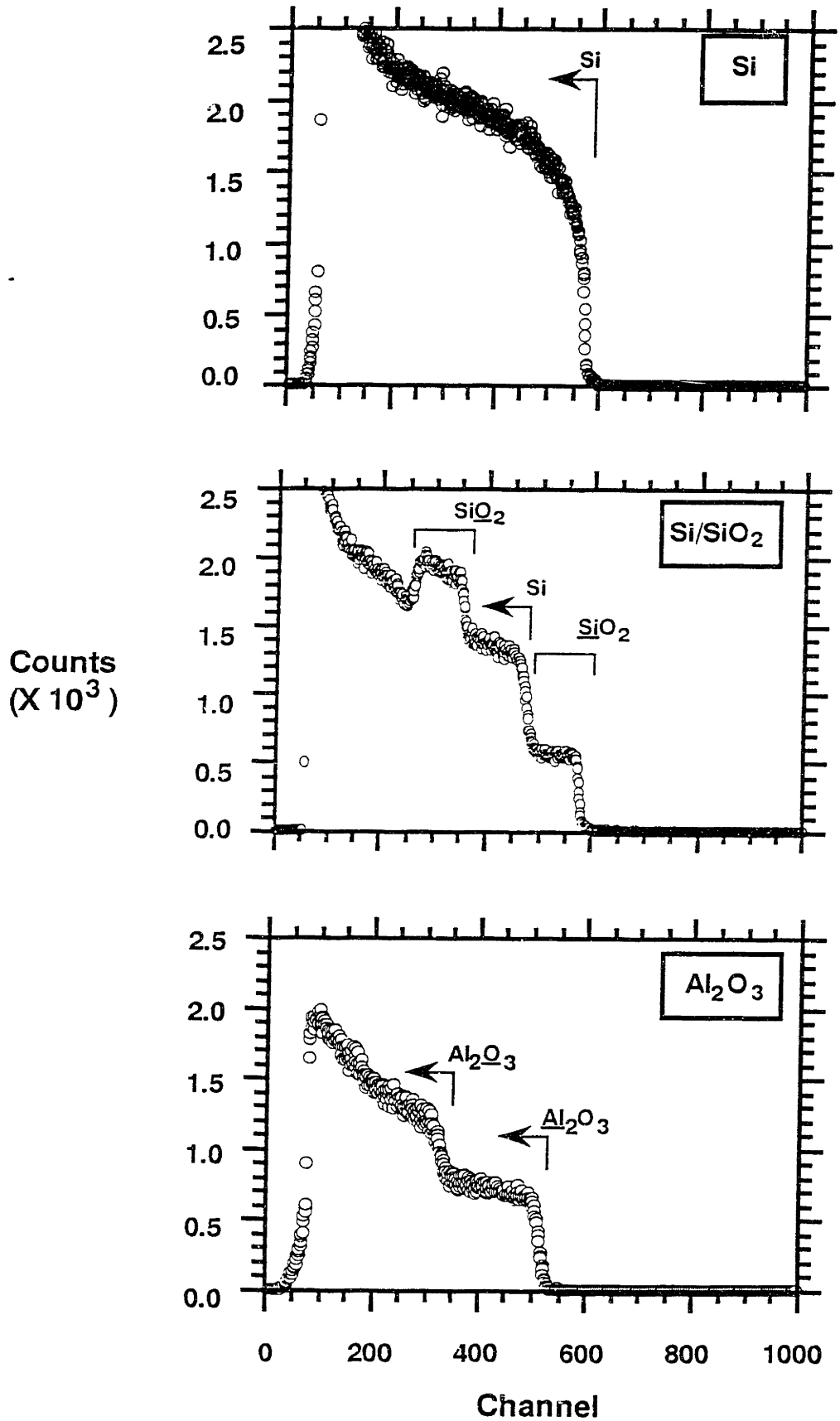
Si
Si
Si/SiO2
SiO2
Si
SiO2
Al2O3
Al2O3
Al2O3
Counts
(X 10^3)
Channel
0
200
400
600
800
1000
0.0
0.5
1.0
1.5
2.0
2.5

Relative Chromophore Stability as a Function of Thermal Treatment: Figure 24 illustrates the absorbances of the 2,4-dinitroaniline group at 350 nm as a function of the temperature of the most recent thermal treatment under air and under argon.

Conclusions: The relative oxidative and/or thermal stability of the 2,4-dinitroaniline group seems not to be significantly improved by inclusion in the sol-gel matrix. The process that limits degradation of this chromophore appears to be thermal rather than oxidative, based on the observation that the stability under argon is indistinguishable from than under air. Adding a SiO_2 overcoating, which should serve as a barrier to diffusion of oxygen, also had no effect on the stability of the chromophore.

There was no significant difference between the relative rate of disappearance of covalently and non-covalently incorporated chromophores, or when coated on a high surface-area silica compared with a flat substrate.

Figure 22: Survey transmission UV-VIS spectra of the alumina substrate, the alumina substrate with SiO_2 coatings not containing chromophore, and alumina substrates bearing the chromophore in the configurations shown in Figure 20.

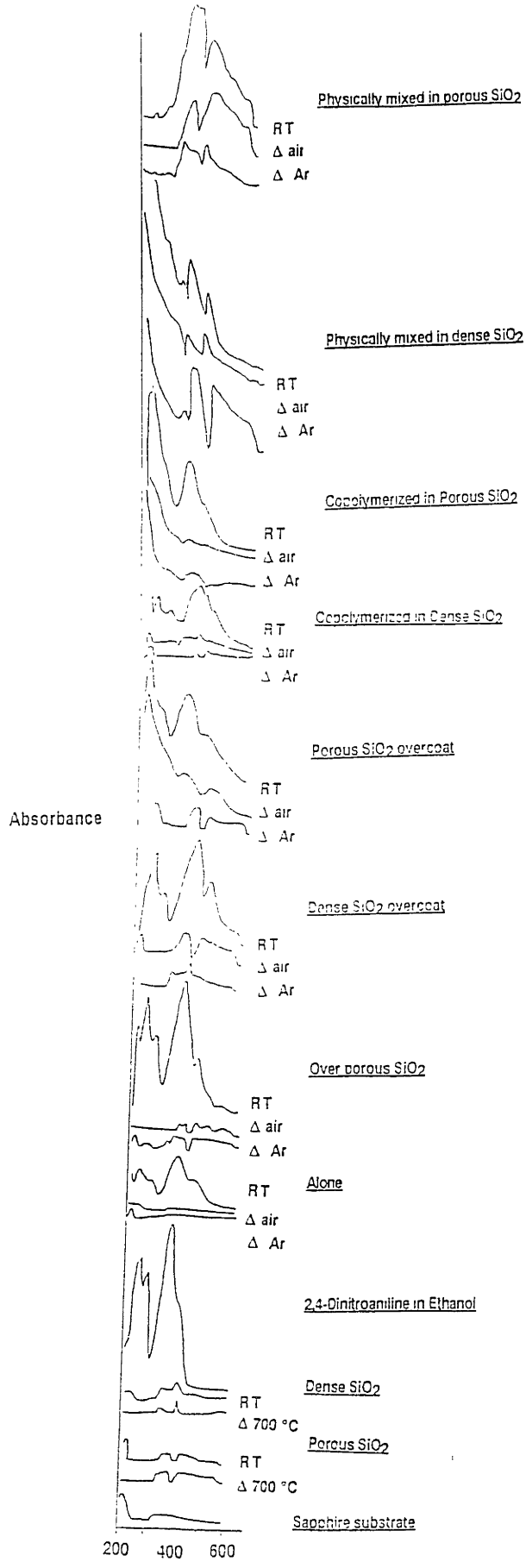
Physically mixed in porous SiO2
RT
Δ air
Δ Ar
Physically mixed in dense SiO2
RT
Δ air
Δ Ar
Copolymerized in Porous SiO2
RT
Δ air
Δ Ar
Copolymerized in Dense SiO2
RT
Δ air
Δ Ar
Porous SiO2 overcoat
RT
Δ air
Δ Ar
Absorbance
Dense SiO2 overcoat
RT
Δ air
Δ Ar
Over porous SiO2
RT
Δ air
Δ Ar
Alone
RT
Δ air
Δ Ar
2,4-Dinitroaniline in Ethanol
Dense SiO2
RT
Δ 700 °C
Porous SiO2
RT
Δ 700 °C
Sapphire substrate
200
400
600
nm

Figure 23: UV-VIS spectra and a plot of relative absorbance of 1 (Figure 20, Structure A) as a function of temperature of thermal treatment in air.

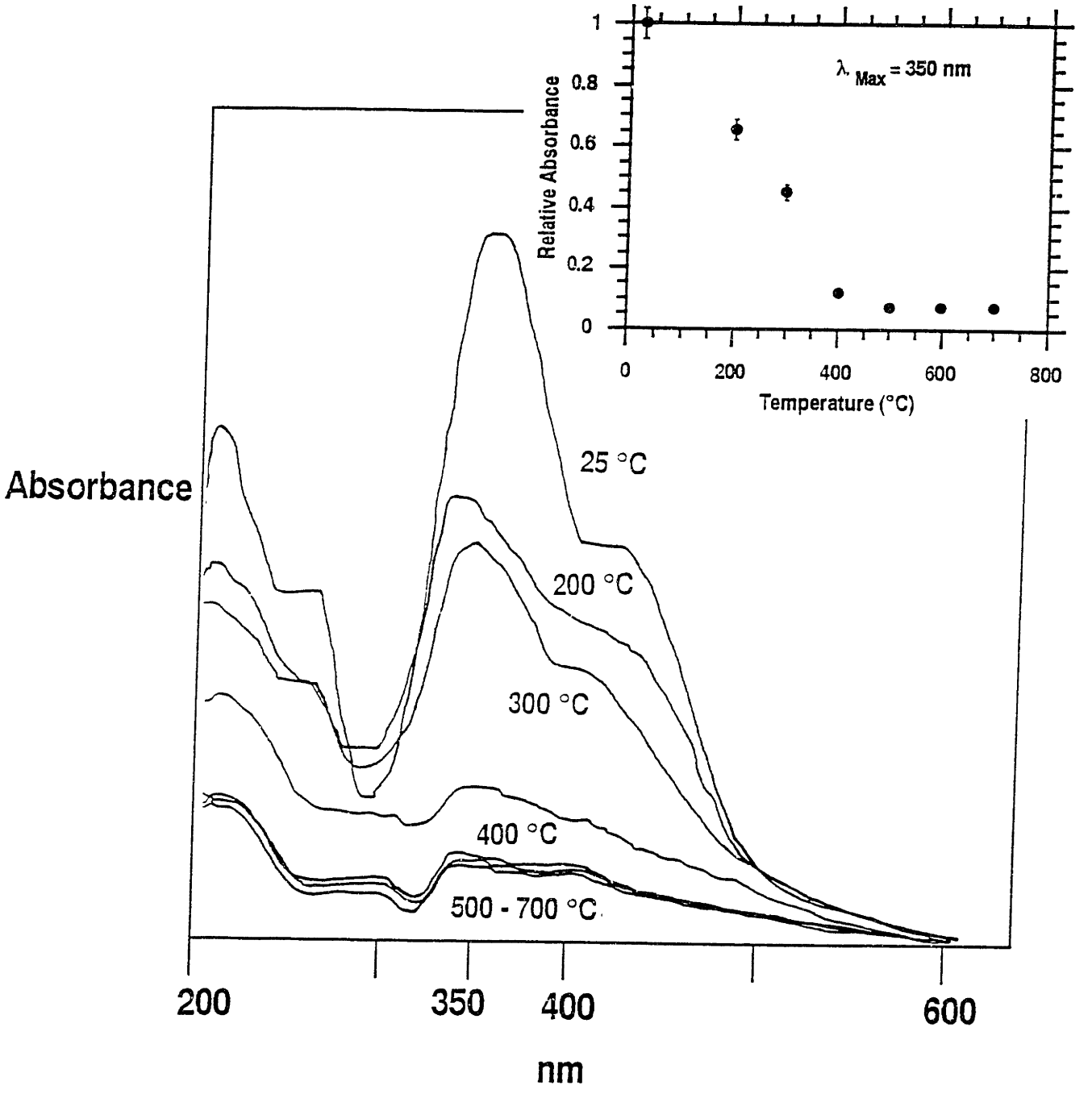
Relative Absorbance
1
0.8
0.6
0.4
0.2
0
0
200
400
600
800
Temperature (°C)
λ Max = 350 nm
Absorbance
25 °C
200 °C
300 °C
400 °C
500 - 700 °C
200
350
400
600
nm

Figure 24: Relative absorbance at 350 nm of incorporated 2,4-dinitroaniline in sol-gel coatings as a function of temperature of thermal treatment in air and under argon. Samples were held at each temperature for 2 hours. The relative absorbance is the ratio of the measured absorbance to that after an initial treatment at 100°C for 5 min. The symbols denote chromophore: alone (○), over porous SiO_2 (●), with a dense SiO_2 overcoat (△), with a porous SiO_2 overcoat (▲), copolymerized in dense SiO_2 (□), copolymerized in porous SiO_2 (■), physically mixed in dense SiO_2 (◇), and physically mixed in porous SiO_2 (◆). The points are shown displaced from the nominal temperatures to avoid overlap. The data points represent the average measurement of two samples, the error bars their range.

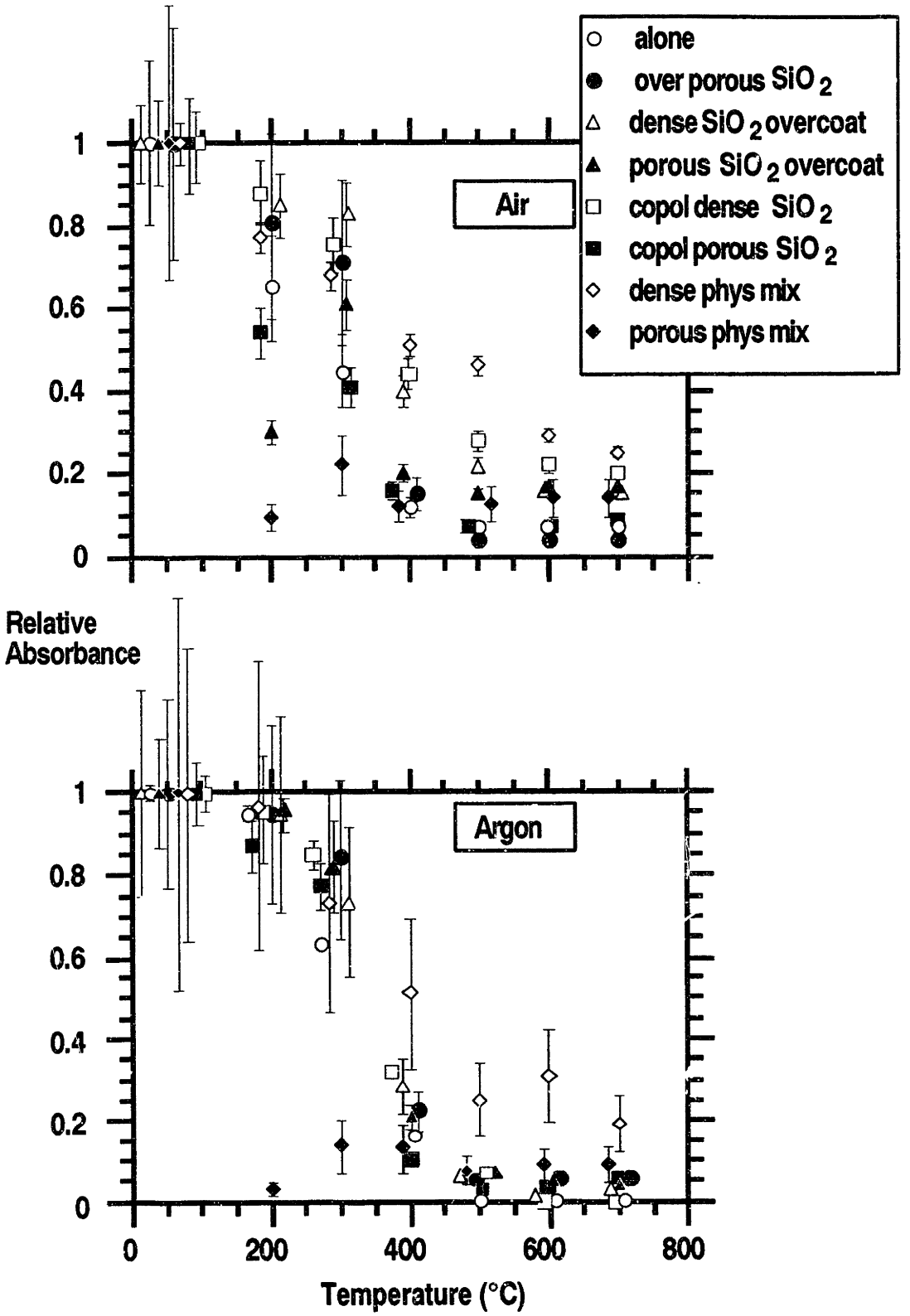
alone
over porous SiO 2
dense SiO 2 overcoat
porous SiO 2 overcoat
copol dense SiO 2
copol porous SiO 2
dense phys mix
porous phys mix
Air
Argon
Relative Absorbance
1
0.8
0.6
0.4
0.2
0
0
200
400
600
800
Temperature (°C)

Appendix 1

Measurement of indices of refraction and thicknesses of SiO_2 gel coatings by optical ellipsometry: We calculated the indices of refraction and thicknesses of the SiO_2 gels using "A FORTRAN Program for Analysis of Ellipsometer Measurements", written by Frank L. McCrackin, NBS, Washington, D.C.

1) Calculation of Δ and Ψ from Polarizer (P), Analyzer (A), and Compensator (Q) values. The wave of light is characterized by the electric field vector, P_C.

$$P_C = T_C\exp(-i\Delta_C) = T_C\cos\Delta_C - iT_C\sin\Delta_C \qquad (1)$$

T_C and Δ_C are obtained from two sets of P, A, and Q values, with Q at a constant setting. T_C is the ratio of the rates of speed along the fast and slow axes, and Δ_C is the relative phase retardation along the axis.

The surface is characterized by

$$p = R_p/R_s = \tan\Psi\exp(i\Delta) \qquad (2)$$

R_p is the complex reflection coefficient parallel to the surface; R_s, perpendicular to the surface. The value of p can also be expressed

$$p = \frac{\tan A\,[\tan Q + p_c\tan(P-Q)]}{p_c\tan Q\tan(P-Q) - 1} \qquad (3)$$

We calculated Δ and Ψ by inserting the P, A, Q, and p_c values into equation (3) and solving for them in equation (2).

2) Calculations of the film thickness, d_2. The total reflection coefficients, R^p parallel to the surface and R^n, normal, are

$$R^p = \frac{r^p_{12} + r^p_{23}y}{1 + r^p_{12}r^p_{23}y} \qquad (4)$$

and

$$R^n = \frac{r^n_{12} + r^n_{23}y}{1 + r^n_{12}r^n_{23}y} \qquad (5)$$

with

r^p_{12}, r^n_{12}, r^p_{23}, and r^n_{23} reflection coefficients parallel, p, and normal, n, to the surface for the medium and the film (1 and 2) and the film and the substrate (2 and 3).

$$y = \exp\left[\frac{-4\pi i n_2 \cos\varphi_2 d_2}{\lambda}\right] \qquad (6)$$

The index of refraction of the film is n_2, the thickness of the film, d_2, and the angle between the light, sample, and detector, $\varphi 2$.

From the ellipsometric readings, we calculated p from equation (2). To obtain d_2, the thickness of the film (and n_2, the index of refraction of the film) we solved the Fresnel reflection equations.[96]

$$EY^2 + BY + C = 0 \qquad (7)$$

with

$$E = pr^{p}_{21}r^{p}_{32}r^{n}_{32} - r^{n}_{21}r^{p}_{32}r^{n}_{32} \qquad (8),$$

$$B = p(r^{n}_{32} + r^{p}_{21}r^{n}_{21}r^{p}_{32}) - r^{p}_{32} - r^{p}_{21}r^{n}_{21}r^{n}_{32} \qquad (9),$$

and

$$C = pr^{n}_{21} - r^{p}_{21} \qquad (10).$$

The two solutions, Y_1 and Y_2, are

$$Y_1 = \frac{\left[-B + \sqrt{(B^2 - 4EC)}\right]}{2E} \qquad (11)$$

and

$$Y_2 = \frac{\left[-B - \sqrt{(B^2 - 4EC)}\right]}{2E} \qquad (12).$$

From these solutions, we solve for the complex value of the film thickness, d_2. The imaginary part reflects the error in either the ellipsometric readings or the n values. For an accurate value of d_2, the imaginary part of the d_2 value must be minimized.

3) Calculation of n_2 and d_2. First, we need to set limits on possible n_2 values where $n_2' < n_2''$. When the correct n_2 value is

used in the calculation for d_2, the error goes to zero. At either side of the correct n_2, the imaginary part of the d_2 solution changes signs, from >0 to <0, for example. The program computes d_2 from the series of n_2 values provided, and, when it finds a sign change in the imaginary part of the calculated d_2 values, it redefines n_2' and n_2'' to minimize the error. To test for a sufficient solution, the program calculates Δ and Ψ from the real part of the d_2 solution and the corresponding n_2. If Δ and Ψ are within 0.005 ° of the experimental values (less than measurement error), the solution is sufficient.

4) Procedure for determining n_2 and d_2 for the SiO_2 gel coatings. First, we made a series of coatings of different thicknesses. These coatings were heated under the same conditions as described in Figure 5. A minimum of three ellipsometric measurements were made on each sample. Only results on samples whose thicknesses were well away from the cycle thickness were used to calculate an average index of refraction.

We fixed the indices of refraction (at the average value calculated) for the sample coatings through which we were to study cesium diffusion, and calculated d_2 of these coatings for each of the temperatures of thermal treatment. These results are plotted in Figure 6.

Appendix 2

Calculation of the Apparent Diffusion Coefficient of Cesium in SiO_2 Gels.

Fick's second law of diffusion relates the change of concentration, c, as a function of time, t, to the gradient of the flux: a function of the diffusion coefficient, D, times the concentration gradient, dc/dx.

$$\frac{\partial c}{\partial t} = \frac{\partial}{\partial x}\left(D\frac{\partial c}{\partial x}\right) \qquad (1)$$

The assumption that the concentration gradient is equivalent to the chemical potential gradient, the true driving force in diffusion, is implicit in Fick's second law. We assume further that D is constant, independent of concentration and position. Equation 1 simplifies to relate the change in concentration as a function of time to the the product of the diffusion coefficient times the Laplacian of c. For a non-steady-state solution in one dimension, as in a film, equation 1 reduces to

$$\frac{\partial c}{\partial t} = \frac{\partial}{\partial x} D\frac{\partial^2 c}{\partial x^2} \qquad (2)$$

For a film with a quantity of solute, α, diffusing from a surface into a material, the thin film solution[97] is

$$c = \frac{\alpha}{\sqrt{\pi D t}}\exp\left(\frac{-x^2}{4Dt}\right) \qquad (3).$$

To extract the diffusion coefficient, D, ln(c) is plotted versus x^2. The slope of the line is $)t)^{-1}$. The thin-film solution is valid for diffusion into an undoped gel, provided that the gel can be considered infinite; no loss of material occurs through the other side of the film at the SiO_2 gel/Si interface.

The thin film solution is a reasonable assumption for the estimation of an apparent diffusion coefficient for our system, where a thin film of solute is placed on a "semi-infinite" and solute-free medium. The boundary condition that the flux at the surface is zero (dc/dx = 0 at x = 0) satisfies the thin film solution. The SiO_2 coating can be considered as an infinite medium only if it passes the "leak test". Following Shewmon: "a short bar can be considered infinite if the quantity of solute which would lie outside its length in a truly infinite bar is an insignificant portion of the total solute present".[98] With 0.1% as the insignificant portion of material to "leak" out, equation (1) is the ratio of the solute which has diffused beyond the distance x' to the total content of solute in the bar where D is the diffusion coefficient (cm^2/sec), t is time (seconds), and x is distance (cm).

$$10^{-3} = \frac{\int_{x'}^{\infty} e^{-\frac{x^2}{4Dt}} dx}{\int_{0}^{\infty} e^{-\frac{x^2}{4Dt}} dx} \qquad (1)$$

The solution of x' is $x' = 4\sqrt{Dt}$. For our system, with an apparent diffusion coefficient of 1.4×10^{-14} cm^2/sec at an anneal time of

7200 seconds, there is less than 0.1% diffusion beyond ~ 4.2×10^{-5} cm or 4,200Å. Our SiO_2 films extends to approximately 5,000Å from the surface (longer than the minimum length for an "infinite" medium for the given diffusion coefficient and annealing timing), and the assumptions that the thin film solution holds are correct. One can also see qualtivatively that there is little or no diffusion of cesium into silicon by comparing the depth profiles of cesium with those of oxygen.

The Si/SiO_2 interface is fixed - no detectable oxidation occurs. Samples were heated in an oxygen-free atmosphere - argon - to effect diffusion of the cesium at elevated temperatures. There is no significant detectable increase in the depth profiles of oxygen of the films after thermal treatment.

Since cesium is a charged species, it must either ion exchange with another cationic species, for example H^+ on Si-$\overline{OH}$, or diffuse with an anion. Here we cannot solve for interdiffusion of cesium with another cation because we cannot measure an interdiffusing species in this system (most likely H^+) by RBS. We present the calculated diffusion coefficient as the apparent D. Our purpose in calculating an apparent diffusion coefficient for cesium is to compare the rates of movements of cesium in different samples as a function of their thermal history, rather than to report an absolute value of the D_{Cs}.

Representative data for the calculation of the diffusion coefficient are presented in Figure 25. The slope is $(4Dt)^{-1}$; we assume that t = time at the holding temperature, ignoring the time involved in ramping, therefore t = 120 min = 7,200 sec. The

range of depth is 0 to 2.8 x 10^{-10} cm^2 (0 to 1670 Å). The slope, -10 x 10^9 cm^2, yields a diffusion coefficient, D_{Cs}, of 3.5 x 10^{-15} ± 1.2 x 10^{-15} cm^2/sec.

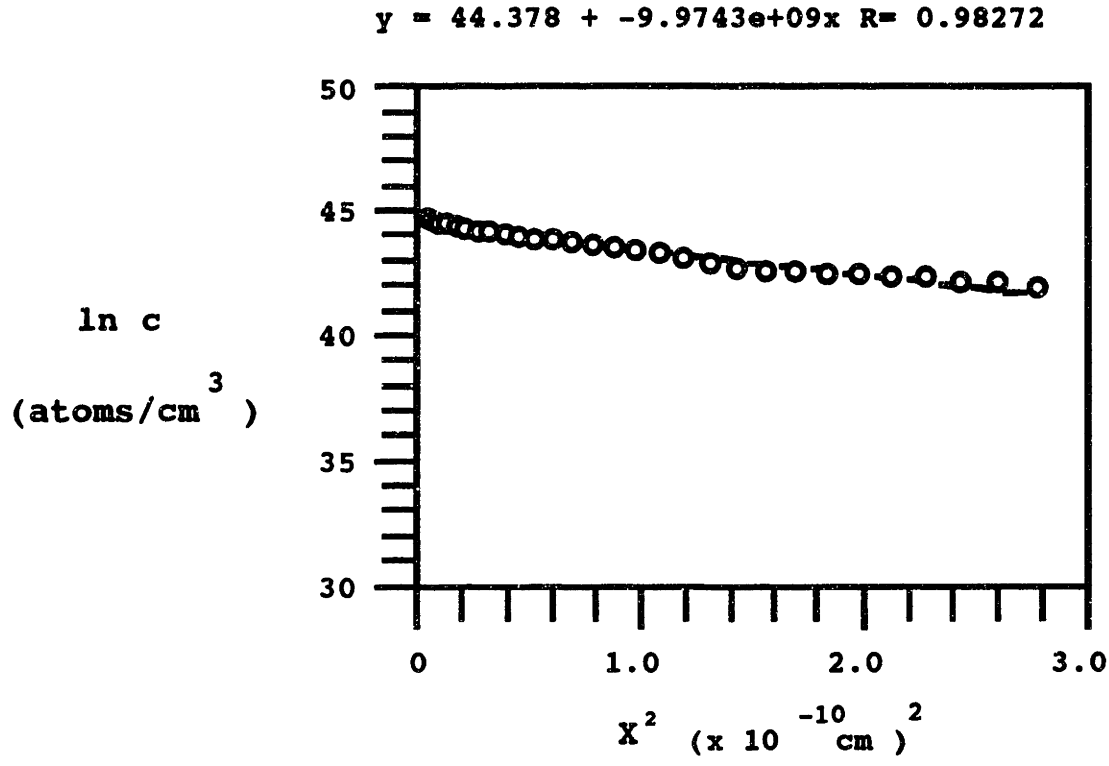

Figure 25: Plot of ln of concentration (atoms/cm^3) versus x^2 (cm^2) for a gel preheated to 800 °C and heated to 750 °C after Cs was applied.

Bibliography:

(1) Thomas, Ian. M. *Opt. News* 1986, *12*, 18.

(2) *Multilayer Ceramic Devices, Advances in Ceramics, volume 19*, Blum, John B.; Cannon, W. Roger, Eds.; The American Ceramics Society, Inc. Westerville, Ohio, 1986.

(3) Brinker, C. J.; Hurd, A. J.; Ward, K. J. *Ultrastructure Processing of Advanced Ceramics*; Mackenzie, John, D.; Ulrich, Donald R., Eds.; John Wiley and Sons: New York, New York, 1988; pp. 223-240.

(4) Schroeder, H. *Phys. Thin Films* **1969**, *5*, 87-141.

(5) Dislich, H.; Hassmann, E. *Thin Solid Films* **1981**, *77*, 129-139.

(6) Dislich, H. *J. Non-Cryst. Solids* **1983**, *57*, 371-388.

(7) Sakka, S.; Kamiya, K.; Makita, K.; Yamamoto, Y. *J. Non-Cryst. Solids* **1984**, *63*, 223-235.

(8) Orgaz, F.; Rawson, R. *J. Non-Cryst. Solids* **1986**, *82*, 378-390.

(9) Brinker, C.J.; Keefer, K.D.; Schaefer, D.W.; Assink, R.A.; Kay, B.D.; Ashley, C. S. *J. Non-Cryst. Solids* **1984**, *63*, 45-59.

(10) Sim, S.M.; Chu, P-Y.; Krabill, R.H.; Clark, D.E. in ed. Mackenzie, John D., Ulrich, Donald R. *Ultrastructure Processing of Advanced Ceramics*, John Wiley and Sons, New York, **1988**, p 995-1010.

(11) Geffcken, W.; Berger, E. Dtsch. Reichspatent 736,411 (1939), US Patent 2366516 (1945)

(12) Schroeder, H. *Opt. Acta* **1962**, *9*, 249-254.

(13) Dislich, H.; Hinz, P. *J. Non-Cryst. Solids* **1982**, *48*, 11-16.

(14) Sokolova, R.S. *Sov. J. Opt. Technol.* **1973**, *40*, 761.

(15) Phillips, R. W.; Dodds, J.W. *Appl. Opt.* **1981**, *20*, 40-47.

(16) P. Biswas, D. Kundu, D. Ganguli *J. Mat. Sci. Lett.* **1987**, *6*, 1481-1482.

(17) Mohallem, N.D.S.; Aegerter, M.A. *J. Non-Cryst. Solids* **1988**, *100*, 526-530.

(18) Thomas, Ian M. *Appl. Opt.* **1987**, *26*, 4688-4691.

(19) Wrighton, Mark S.; Palazzotto, Michael C.; Bocarsly, Andrew B.; Bolts, Jeffrey M.; Fischer, Alan B.; Nadjo, Louis *J. Am. Chem. Soc.* **1978**, *100*, 7264-7271.

(20) Feldman, Leonard C.; Mayer, James W. *Fundamentals of Surface and Thin Film Analysis*, North-Holland, New York, 1986, pp 13-68.

(21) Wang, P. W.; Feng, Y. P.; Roth, W. L.; Corbett, J. W. *J. of Non-Crystalline Solids* **1988**, *104*, 81-84.

(22) Mayer, J. W. Solar Cells, **1979/80**, 1, 141-4.

(23) Vedam, K.; McMarr, P. J., Narayan, J. *App. Phys. Lett.* **1985**, *47 (4)*, 339-341.

(24) Vedam, K. *MRS Bulletin*, **1987**, *January/February 15*, 21-23.

(25) Yamane, Masayuki; Caldwell, J. Brian; Moore, Duncan T. in *Better Ceramics Through Chemistry II, Materials Research Society Symposium Proceedings*, Brinker, C. Jeffrey; Clark, David E.; Ulrich, Donald R., Eds.; Materials Research Society: Pittsburgh, Pennsylvania, vol 73, 1986, pp.765-768.

(26) Yamane, Masayuki; Kawazoe, Hiroshi; Yasumori, Atsuo; Takahashi, Toshikazu *J. Non-Cryst. Solids* **1988**, *99*, 160-167.

(27) Ref. 20 equation 3.32, p. 58

(28) Winkle, Mark R.; Lansinger, Janet M.; Ronald, Robert C. *J. Chem. Soc., Chem. Commun.* **1980**, *3*, 87-8.
(29) Brauman, J. C.; Anderson, R. M.; McDonald, M. L. Specimen Preparation for Transmission Electron Microscopy of Materials, Materials Research Society Symposium Proceedings, 1988, vol 115.
(30) Klemperer W. G.; Mainz, V. V.; Millar, D. M. *Better Ceramics Through Chemistry II* Materials Science Society Volume 73; Brinker, C. Jeffrey; Clark, David C.; Ulrich, Donald R., Eds.; Materials Research Society: Pittsburgh, Pennsylvania, 1986; pp.3-13 and pp. 15-25.
(31) Streckert, H. H.; Montgomery, F. C.; Tilley, T. Don; Campion, Brian K.; Heyn, Richard H. *Ultrastructure Processing of Advanced Ceramics*; Mackenzie, John, D.; Ulrich, Donald R., Eds.; John Wiley and Sons: New York, New York, 1988; p.963-972.
(32) Covino, J.; Wilson, C. *Ultrastructure Processing of Advanced Ceramics*; Mackenzie, John, D.; Ulrich, Donald R., Eds.; John Wiley and Sons: New York, New York, 1988; p.981-993.
(33) Sim, S. M.; Chu, P-Y.; Krabill, R. H.; Clark, D. E. *Ultrastructure Processing of Advanced Ceramics*; Mackenzie, John, D.; Ulrich, Donald R., Eds.; John Wiley and Sons: New York, New York, 1988; pp.995-1010.
(34) Reed, Scott; Ashley, Carol *Better Ceramics Through Chemistry III* Materials Research Society Symposium Volume 121; Brinker, C. Jeffrey; Clark, David. E.; Ulrich, Donald R., Eds.; Materials Research Society: Pittsburgh, Pennsylvania, 1988; pp.631-634.
(35) Kindred, Douglas S.; Moore, Duncan T. *Applied Optics*, **1988**, *27*, No3, 492-495.
(36) Moore, Duncan T. *Applied Optics*, **1980**, *19*, No 7, 1035-1038.
(37) Bouaziz, J.; Woignier, T.; Bourret, D.; Sempere, R. *J. Non-Crystalline Solids*, **1986**, *82*, 225-231.
(38) Klein, L.; Gallo, T. A.; Garvey, G. J. *J. of Non-Crystalline Solids* **1984**, *63*, 23-33.
(39) Rudolf, F.; Jaccard, C; Chollet, L. *Thin Solid Films* **1980**, *65*, 331-337.
(40) Wang, P. W.; Feng, Y. P.; Roth, W. L.; Corbett, J. W. *J. of Non-Crystalline Solids* **1988**, *104*, 81-84.
(41) Chang, Chin-An; Yee, D. S.; Petkie, R. Appl. Phys. Lett. **1989**, *54*, 2545-2547.
(42) Frischat, G. H. *Glastech. Ber.* **1971**, *44*, 93-98; Frischat, G. H. *J. Am. Ceram. Soc.* **1969**, *53*, 625.
(43) Ehrmann, P.; deBilly, M.; Zarzycki, J. *Verres Refrac.* **1964**, *18*, 164.
(44) Doremus, R. H. *J. Phys. Chem.* **1964**, *68*, 2212-2218.
(45) Johnson, J. R.; Bristow, R. H.; Blau, H. H. *J. Am. Ceram. Soc.* **1951**, *34*, 165-172.
(46) Charles, R. J. *J. Am. Ceram. Soc.* **1962**, *45*, 105-113.
(47) Lengyel, B.; Boksay, Z. *Z. Phys. Chem.* **1954**, *203*, 93-112.
(48) Lengyel, B.; Boksay, Z. *Z. Phys. Chem.* **1955**, *204*, 157-164.
(49) Doremus, Robert H. *Glass Science*; John Wiley and Sons: New York, 1973, p.167-169.
(50) *Handbook of Chemistry and Physics*, 55th edition; Weast, Robert C. Ed.; CRC Press: Cleveland, Ohio; 1974-1975, pp. B-121.

(51) Kingery, W. D.; Bowen, H. K.; Uhlmann, D. R. *Introduction to Ceramics*; John Wiley and Sons: New York, New York; 1976, pp.662.
(52) Frye, Gregory C.; Ricco, Antonio J.; Martin, Stephen J.; Brinker, C. Jeffrey *Better Ceramics Through Chemistry III* Materials Research Society Symposium Volume 121; Brinker, C. Jeffrey; Clark, David. E.; Ulrich, Donald R., Eds.; Materials Research Society: Pittsburgh, Pennsylvania, 1988; p.349-354.
(53) Decottignies, M.; Phalippou, J.; Zarzycki, J. *J. of Mat. Sci.* **1978**, *13*, 2605-2618.
(54) Bertoluzza, Alessandro; Fagnano, Concezio; Morelli, Maria Antonietta *J. of Non-Crystalline Solids* **1982**, *48*, 117-128.
(55) Chu, W. K.; Mayer, J. W.; Nicolet, M. A. *Backscattering Spectrometry*; Academic Press: New York, 1977, pp. 126.
(56) Pope E. J. A.; Mackenzie J. D. *Journal of Non-Crystalline Solids* **1986**, *87*, 185-198
(57) Melpolder, S. M.; Coltrain, B. K.; Salva, J. M. in Proceedings of the Fourth International Conferences on Ultrastructure Processing of Ceramics, Glasses, and Composites, Tucson, Arizona, February, 1989: Uhlmann, D. R.; Ulrich, D. Eds.; to be published.
(58) Ref 50 pp.B-133.
(59) Powell, C. J.; Seah, M. P. *J. Vac. Sci. and Tech. A.* **1990**, *8*, 735-763.
(60) Huang, Hao-Hsin; Orler, Bruce, Wilkes, Garth L., *Macromolecules*, **1987**, *20*, 1322-1330.
(61) Wilkes, Garth L.; Orler, Bruce; Huang, Hao-Hsin, Polymer Preprints (Am. Chem. Soc., Div. Polym. Chem.) 26(2) 300-2 1985.
(62) Glaser, Raymond, Wilkes, Garth L. Polymer Preprints (Am. Chem. Soc., Div. Polym. Chem.) 28(2) 236-7 1987.
(63) Parkhurst, C. S.; Doyle, W. F.; Silverman, L. A.; Singh, S.; Andersen, M. P.; McClurg, D.; Wnek, G. E.; Uhlmann, D. R., in *Better Ceramics Through Chemistry II* Materials Research Society Symposium Volume 73; Brinker, C. Jeffrey; Clark, David. E.; Ulrich, Donald R., Eds.; Materials Research Society: Pittsburgh, Pennsylvania, 1986; p.769-773.
(64) Glasner, Raymond H.; Wilkes, Garth L. *Polym. Bull. (Berlin)*, **1988**, *19(1)*, 51-7.
(65) Andrianov, K. A.; Slonimskii, G. L.; Zndanov, A. A.; Levin, V. Yu.; Godovski, Yu. K.; Moskalenko, V. A. *J. Polymer Sci.* A1, **1972**, 23 - 43.
(66) Huang, Hao Hsin, Glaser, Raymond H.; Wilkes, Garth L., *ACS Symp. Ser., 360 (Inorg. Organomet. Polym.)*, **1988**, 354-76.
(67) Huang, Hao Hsin, Wilkes, Garth L., Polymer Preprints (Am. Chem. Soc., Div. Polym. Chem.) 28(2), **1987**, 244-5.
(68) Spinu, M.; Arnold, C. McGrath, J. E.; Parkhurst, C. L. *Polymer Preprints (Am. Chem. Soc., Div. Polym. Chem.), 30(2)*, **1989**, 125-7.
(69) Shea, Kenneth J.; Loy, Douglas A.; Webster, Owen W., *Chemistry of Materials*, **1989**, *1*, 572-574.
(70) Schmidt, H., *J. Non-Cryst. Solids*, **1985**, *73*, 681-691.
(71) Schmidt, H. et al. *J. Non-Cryst. Solids*, **1984**, *63*, 283 - 292.
(72) Schmidt, H. private communication.

(73) Schmidt, H.; Seiferling, B.; Philipp, G.; Deichmann, K., in Ultrastructure Processing of Advanced Ceramics; Mackenzie, John D.; Ulrich, Donald, R., Eds.; Wiley Interscience: New York, New York, 1988; p.651-660.
(74) Schmidt, H. et al. U. K. Pat. 2015549A Dec 27, 1978.
(75) Schmidt, H. et al. U. K. Pat. 2018803B Dec 27, 1978.
(76) Schmidt, H. et al. U. S. Pat. 4,440,748 April 3, 1984.
(77) Schmidt, H. U. S. Pat. 4,374,696 February 22, 1983.
(78) Melpolder, Sharon M.; Coltrain, Bradley K. in *Better Ceramics Through Chemistry III* Materials Research Society Symposium Volume 121; Brinker, C. Jeffrey; Clark, David. E.; Ulrich, Donald R., Eds.; Materials Research Society: Pittsburgh, Pennsylvania, **1988**; p.811-816.
(79) Pope, E. J. A.; Asami, M. J.; Mackenzie, J. D., *J. Mat. Res.*, Vol4, **1989**, p 1018-1026.
(80) Nasu, Hiroyuki; Mackenzie, John, *Optical Engineering*, February **1987**, *26 (2)*, 102-106.
(81) Che, Tessie M.; Carhey, Raymond V.; Khaharian, Garo, Keosian, Richard A.; Borzo, Marie, *J. of Non-Cryst. Solids*, **1988**, *102*, 280-287.
(82) Tani, T.; Namikawa, H.; Arai, K.; Makashima, A., *J. Appl. Phys.*, **1985**, *58 (9)*, 3559-65.
(83) Avnir, D.; Levy, D.; Reisfeld, R., *J. Phys. Chem.*, **1984**, *88*, 5956-5959.
(84) Avnir, D.; Levy, D., in Proceedings of the 2nd International Conference of Unconventional Photoactive Materials, Scher, H. Ed.; Plenum: 1986.
(85) Avnir, D.; Kaufman, V. R.; Reisfeld, R., *J. Non-Cryst. Solids*, **1985**, *74*, 395-406
(86) Makashima, A.; Tani, T., *J. Am. Ceram. Soc.*, **1986**, *69*, C-72-74.
(87) Dunn, B.; Knobbe, E.; McKiernan, J. M.; Pouxviel, J. C.; Zinc, J. I. in *Better Ceramics Through Chemistry III* Materials Research Society Symposium Volume 121; Brinker, C. Jeffrey; Clark, David. E.; Ulrich, Donald R., Eds.; Materials Research Society: Pittsburgh, Pennsylvania, 1988; 331-342.
(88) Pope, Edward J. A.; Mackenzie, John D., MRS Bulletin, March 17/ May 15, 1987, 29-31.
(89) Kaufmann, D.; Avnir, D., in *Better Ceramics Through Chemistry II* Materials Research Society Symposium Volume 73; Brinker, C. Jeffrey; Clark, David. E.; Ulrich, Donald R., Eds.; Materials Research Society: Pittsburgh, Pennsylvania, 1986; p.145-156.
(90) Kaufman, V. R.; Avnir, D., *Langmuir*, **1986**, *2*, 717-722.
(91) Kaufman, V. R.; Levy, D.; Avnir, D., *J. of Non-Cryst. Solids*, **1985**, *82*, 103-109.
(92) Hench, L. L.; West, Jon K. *Chem. Rev.*, **1990**, 33-72.
(93) Schlichting, J. *J. of Non-Crystalline Solids*, **1984**, *63*, 173-181.
(94) Motzfeld, K. *Acta. Chem. Scand.*, **1964**, *18*, 1596-1606.
(95) Schaeffer, H.A., in *Nitrogen Ceramics*; Rilev, F., Ed.; Noordhoff: Leyden, 1977, 241-255.
(96) Fresnel, A. *Ann. Chim. et Phys*, **1825**, *28*, 147-161.

(97) Crank, J. *The Mathematics of Diffusion*; Clarendon Press: Oxford, England, 1975, pp.11-13.
(98) Shewmon, Paul G. *Diffusion in Solids*; J. Williams Book Company: Jenks, OK, 1983, pp.9

Biographical Note: Carol Lynn Schutte

Institutions Attended:

PhD.

1984-1990 Department of Materials Science and Engineering
Massachusetts Institute of Technology
Cambridge, Mass

M.S.

1978-1980 Department of Chemistry
University of Rochester
Rochester, New York

B.S.

1975-1978 Department of Chemistry
Rensselear Polytechnic Institute
Troy, New York

Awards:

1988-1989 American Association of University Women
Dissertation Fellow

1975 Horace Schiedt Chemistry Prize
Kent School, Kent, Conn.

Professional Experience:

1980-1984 Research Chemist
Eastman Kodak Research Laboratories
Rochester, New York

Summers of 1978 and 1977 Coop Chemist
GE Silicones
Waterford, New York

1978-1980 Teaching Assistant
Department of Chemistry
University of Rochester
Rochester, New York

Publications:

(1) "Analysis of Depth Profiles of Sol-Gel Derived Multilayer Coatings by Rutherford Backscattering Spectrometry and by Cross-Sectional Transmission Electron Microscopy"
Carol L. Schutte, Patrick M. Smith, and George M. Whitesides*
(*Journal of Materials Research*, submitted 1990)

(2) "The Diffusion of Cesium Ion in SiO_2 Films Derived From Sol-Gel Precursors", Carol L. Schutte and Geodrge M. Whitesides*
(*Chem. of. Matls.*, submitted 1990)

(3) "The Loss of Halide from Sol-Gel Films on Heating Does Not Involve Oxidation", Carol L. Schutte and George M. Whitesides*
(*Chem. of. Matls.*, to be submitted 1990)

(4) "The Thermal and Oxidative Stability of 2,4-Dinitroaniline in Sol-Gel Derived Coatings", Carol L. Schutte, Kevin W. Williams, and George M. Whitesides* (*Chem. of. Matls.*, to be submitted 1990)

(5) "Initial Evidence of Si-O-Ti Bonds in Organically Modified A Silicon Titanates by Solid State ^{29}Si Nuclear Magnetic Resonance Spectroscopy", Carol L. Schutte, Joseph R. Fox, Robert D. Boyer, and Donald R.Uhlmann, in Proceedings of the Fourth International Conferences on Ultrastructure Processing of Ceramics, Glasses, and

Composites, Tucson, Arizona, February, 1989: Uhlmann, D. R.; Ulrich, D. Eds.; to be published.
(6) "Siloxane Modified SiO_2-TiO_2 Glasses via Sol-Gel" Carol S. Parkhurst, William F. Doyle, Lee A. Silverman, Sacchi Singh, Michele P. Andersen, David McClurg, Gary E. Wnek, and Donald R. Uhlmann, in Better Ceramics Through Chemistry II, Materials Research Society Symposium Proceedings, Brinker, C.Jeffrey; Clark, David E.; Ulrich, Donald R., Eds.; Materials Research Society: Pittsburgh, Pennsylvania, vol 73, 1986, pp.769-773.
(7) "Alkoxides as Nucleophiles in (π-Allyl)palladium Chemistry. Synthetic and Mechanistic Studies", Susan A. Stanton, Steven W. Felmam, Carol S. Parkhurst, and Stephen A. Godleski*, J. Am. Chem. Soc. 1983, 105, 1964-1969.

Recommendations for Future Work

This thesis demonstrates the preparation of well defined thin-film multilayers ($\leq$ 2000 Å -- thinner than those provided by powder processing techniques that form layers of ~ 25 μm). Future work in this area could include the building of microcapacitors from a sol-gel multilayer system. The use of small lightweight capacitors as power supplies would permit the manufacture of small devices (motors). Once the thicknesses of the layers become small, on the level of angstroms, the system has the potential to exhibit novel polarizations and high ε.[†]

A capacitor consists of 3 layers: two electrically conducting layers separated by a layer that behaves as a dielectric. A sol-gel solution that is a precursor to either a conducting glass (SnO_2) or a non-conducting glass filled with particles of electrically conductive materials (graphite) could serve as the formulation for the conducting layers. Useful studies on a multilayer system consisting of these layers would include the following:

1) A study of the effect of the breakdown voltage (the highest voltage that can be applied before the capacitor shorts out) as a function of thermal pretreatment should reveal the effect of the stage of the gel-to-glass transition on the behavior of the dielectric layer. If the water content is too high, conductivity in the dielectric layer would inhibit the storage of charge in the conducting layers. As the gel loses water through desorption and chemical condensation, the capability of the system to store charge should increase.

2) Once the thermal pretreatment schedule is optimized, a study of the effect of the thickness of the dielectric layer -- varied by changing the concentration of the precursor solution prior to spin-coating -- on the behavior of the capacitor would show the minimum allowable thickness without capacitor breakdown.

3) Finally, the use of a heavy element (heavy enough to be detected by RBS without interference) for a component in the conducting layers could serve as a "tag" with which to follow diffusion that might occur during thermal treatment. A sample whose components exhibit diffusion and intermixing of components of the conducting and the dielectric layers should behave differently from a sample containing sharp interfaces between the layers.

[†] Rosner and Rubner have demonstrated these effects using organic systems.(Rosner, R.; Rubner M. Proceedings of the Materials Research Society, Boston Mass, Fall 1989, Organic Materials Symposium, to be published).